A brainwide atlas of synapses across the mouse life span

A brain-wide atlas of synapses across the mouse lifespan*

Authors:

Mélissa Cizeron[1,2†], Zhen Qiu[1†], Babis Koniaris[1,3], Ragini Gokhale[1], Noboru H. Komiyama[1,4], Erik Fransén[5,6] & Seth G.N. Grant[1,4]

† these authors contributed equally

Correspondence to seth.grant@ed.ac.uk

Affiliations:

[1]Genes to Cognition Program, Centre for Clinical Brain Sciences, Chancellors Building, Edinburgh BioQuarter, 49 Little France Crescent, University of Edinburgh, Edinburgh EH16 4SB, UK

[2]Institut NeuroMyoGène, Université de Lyon, Université Claude Bernard Lyon 1, CNRS UMR-5310, INSERM U-1217, 8 Avenue Rockefeller, 69008 Lyon, France

[3]School of Computing, Edinburgh Napier University, 10 Colinton Road, Edinburgh EH10 5DT, UK

[4]Simons Initiative for the Developing Brain (SIDB), Centre for Discovery Brain Sciences, University of Edinburgh, Hugh Robson Building, George Square, Edinburgh EH8 9XD, UK

[5]Department of Computational Science and Technology, School of Electrical Engineering and Computer Science, KTH Royal Institute of Technology, 10044 Stockholm, Sweden

[6]Science for Life Laboratory, KTH Royal Institute of Technology, SE-171 21 Stockholm, Sweden

One sentence summary: The number and molecular makeup of synapses shifts with age in patterns unique to subregions of the brain.

*This manuscript has been accepted for publication in *Science*. This version has not undergone final editing. Please refer to the complete version of record at http://www.sciencemag.org/.

Abstract

Synapses connect neurons together to form the circuits of the brain and their molecular composition controls innate and learned behavior. We have analyzed the molecular and morphological diversity of five billion excitatory synapses at single-synapse resolution across the mouse brain from birth to old age. A continuum of changes alters synapse composition in all brain regions across the lifespan. Expansion in synapse diversity produces differentiation of brain regions until early adulthood and compositional changes cause dedifferentiation in old age. The spatiotemporal synaptome architecture of the brain potentially accounts for lifespan transitions in intellectual ability, memory, and susceptibility to behavioral disorders.

Excitatory synapses are the main class of brain synapse and their postsynaptic proteins regulate both innate and learned behaviors(*1-6*). Mutations in these proteins cause over 130 brain diseases(*7*), including disorders that characteristically arise in childhood, adolescence, young or elderly adults.

Using synaptome mapping(*8*), we have mapped excitatory synapse diversity and spatiotemporal synaptome architecture in over 100 brain regions from birth until 18 months of age in mice (Fig. S1). Synapses were labelled using fluorescent tags on endogenous PSD95 (PSD95-eGFP) and SAP102 (SAP102-mKO2)(*8*), two postsynaptic scaffold proteins that assemble multiprotein signaling complexes(*9-12*) necessary for synaptic plasticity and innate and learned behaviors(*2, 3, 5-7, 12*). Disrupting the normal expression of these scaffold proteins or their associated proteins results in human neurodevelopmental and psychiatric disorders including autism, schizophrenia and intellectual disability(*6, 7, 9, 12*).

Our findings reveal a spatiotemporal program of synapse diversity across the brain, which we call the lifespan synaptome architecture (LSA). The LSA shows how synapse diversity is generated as brain regions become dissimilar, and how synaptome architecture changes through development to adulthood and old age. The LSA provides a framework for understanding stereotypical lifespan trajectories of behavioral changes and psychological functions(*13-15*) and why gene mutations characteristically result in synaptic pathology in particular brain areas and ages. The Mouse Lifespan Synaptome Atlas and interactive visualization and analysis tools(*16*) provide a community resource for investigation of synapse function across all brain regions and the lifespan.

Lifespan synaptome mapping pipeline and data resource

Para-sagittal brain sections from cohorts of PSD95-eGFP/SAP102-mKO2 male mice were collected at ten postnatal ages: one day (1D), one week (1W), two weeks (2W), three weeks (3W), one month (1M), two months (2M), three months (3M), six months (6M), 12 months (12M) and 18 months (18M) (Figs. 1A, S2, S3). Whole brain sections were imaged at single-synapse resolution(*17*) on a spinning disc confocal microscope (pixel resolution 84 nm and optical resolution ~260 nm) and the density, intensity, size and shape parameters of individual puncta were acquired using computer vision methods as previously described(*8*). Synapses were classified into three types: type 1 express PSD95 only, type 2 express SAP102 only, and type 3 express both PSD95 and SAP102(*8*). Thirty-seven subtypes were defined on the basis of

molecular and morphological features(*8*). Supervised synaptome maps were generated by registering the data to the Allen Reference Atlas(*18*). Data were delineated into 109 anatomical subregions within 12 overarching regions, comprising isocortex, olfactory areas, hippocampal formation, cortical subplate, striatum, pallidum, thalamus, hypothalamus, midbrain, pons, medulla, and cerebellum (Table S1).

All data and analysis tools are available in the Mouse Lifespan Synaptome Atlas(*16*). Synaptome Explorer enables in-depth exploration of raw and processed image data in single sections at single-synapse resolution and the Synaptome Homology Viewer enables comparison of brain regions within and between mice of different ages.

The synaptome continuously changes across the lifespan

Raw images at low and high magnification reveal that each synaptic protein has a distinct spatiotemporal pattern and that the synaptome changes with age (Figs. 1A, S2, S3). To quantify the spatiotemporal differences in the synaptome, the lifespan trajectories of PSD95 and SAP102 puncta density, intensity and size were plotted as graphs and heatmaps revealing characteristic patterns for the whole brain, 12 regions and 109 subregions (Figs. 1B, S4, S5, Table S1). Each parameter continuously changes across the lifespan. Synapse density rapidly increases during the first month in all brain areas, then fluctuates before declining in old age (Figs. 1A-C S3-S5) (adult brain size remained unchanged, Fig. S6), consistent with previous studies of synapse number quantified using electron microscopy in the rat brain(*19-22*). Each brain area undergoes a specific program of synapse development, maturation and ageing. For example, the density of synapses peaks in the brainstem before cerebrum structures, potentially reflecting the requirement for the brainstem in early postnatal functions (Fig. S7). The two synapse proteins showed different spatiotemporal trajectories (Figs. 1B, 1C, S4, S5), with SAP102 puncta density peaking before that of PSD95 in most brain areas (Fig. S7), consistent with previous literature (*23*). Although, together, PSD95 and SAP102 label most excitatory synapses, additional markers would be required for an assessment of total excitatory synapse number in all brain regions and at all developmental stages.

Between 3M and 18M, most brain regions and subregions show significantly ($P < 0.05$, Bayesian test with Benjamini-Hochberg correction) reduced synapse density (Fig. 1C top panel, 70/109 subregions for PSD95; 78/109 for SAP102; Fig. S8) and increased size (Fig. 1C bottom panel, 56/109 subregions for PSD95; 80/109 for SAP102; Fig. S8). Examination of the size distribution

of the synapse populations shows a shift toward larger synapses with age (effect size >0.25 with $P < 0.01$, Kolmogorov-Smirnov test), consistent with previous electron microscopy studies in the ageing macaque dorsolateral prefrontal cortex(*24-26*).

Lifespan changes in the synaptome architecture can be divided into three broad phases. During the first phase (LSA-I), from birth to 1M, numbers of puncta increase rapidly. The second phase (LSA-II) begins as the rate of increase in puncta density slows and is characterized by relative stability until 6M (adulthood). The third phase (LSA-III), late adult life, is characterized by a decline in puncta density and increase in synapse size (Figs. 1C, S8).

Synapse diversity across the lifespan

Each synapse type (Figs. 2A, 2D, S9, S10) and subtype (Figs. 2B, 2C, 2E, S11, S12) has a specific trajectory in each brain region and subregion, reaching their peak values at different ages. Thus, the synapse composition of brain regions continues to change throughout the lifespan and is not restricted to LSA-I when synapse density increases. Moreover, the presence of more than one peak at different ages (e.g. subtype 17 and 18, $P < 0.05$, paired t-test and Kolmogorov-Smirnov test, Cohen's $d > 1.2$, Figs. S10-S12) suggests that shaping synapse composition (through processes such as transcriptional regulation, synapse pruning and growth) is an ongoing process. In LSA-III, some subtypes are reduced ($P < 0.05$, Bayesian test with Benjamini-Hochberg correction) while others increased ($P < 0.05$, Bayesian test with Benjamini-Hochberg correction), with differing specificity to brain regions (Fig. S13). For example, subtypes 2, 27 and 34, which are large synapses, increased in many brain regions (Figs. 2E, S12, S13), whereas subtypes 12, 14-16, which are small synapses, were lost in olfactory areas and thalamus in the old brain (Figs. 2E, S12, S13). Thus, subtypes of excitatory synapses are selectively gained or lost with ageing and different regions of the brain age in distinct ways.

LSA-I is initially dominated by a small subset of synapse types/subtypes, and these are overtaken by expanding populations of other types/subtypes (Figs. 2A-C, S9, S11). For example, type 2 and subtype 16 synapses dominate in the first postnatal week (Cohen's $d > 2$ with $P < 0.01$, two-way ANOVA with post-hoc multiple comparison test) but are reduced by 1M (Cohen's $d < –2$, $P < 0.001$, two-way ANOVA with post-hoc multiple comparison test). We next quantified synapse diversity and found that all regions and subregions show a rapid initial increase in the first three postnatal weeks (Figs. 2F, S14). Brain areas responsible for higher cognitive functions (isocortex, cortical subplate, hippocampus, striatum) continued to expand their excitatory synaptic diversity

as reflected by the markers PSD95 and SAP102 after LSA-I, reaching a peak at 2M, whereas brain areas serving basal neurophysiological functions (midbrain, pons, medulla) peaked at 3W-1M during LSA-I (Figs. 2F, S14). Synapse diversity plateaued from 3M onwards in most brain areas (Fig. 2F). Unsupervised synaptome maps of the mouse brain, which visualize the anatomical distribution of synapse diversity (Fig. 2G, S15), clearly show the increase in diversity in LSA-I, with the emergence of layers in the isocortex and subregional differentiation in the hippocampus.

Synaptome architecture first specializes then dedifferentiates

To reveal how changes in synapse composition might contribute to differences between brain areas, we plotted similarity matrices of brain subregions at each age (Figs. 3A, S16) (matrices were non-random, $P < 0.05$, Cohen's $d > 2$, permutation test). Similarity across all brain areas is highest in the first postnatal week and diminishes until 3M ($P < 0.001$, two-way ANOVA with post-hoc multiple comparison test) (Figs. 3A, 3B, S16). As the brain ages beyond 3M there is a progressive increase in the similarity between brain areas ($P < 0.001$, two-way ANOVA with post-hoc multiple comparison test) (Figs. 3A, 3B, S16). Individual brain regions also showed a reduction in similarity with the rest of the brain (i.e. differentiation) during the first three months ($P < 0.001$, two-way ANOVA with post-hoc multiple comparison test) (Fig. S17) and from 3M-6M onwards all regions except the cerebellum and medulla showed an increase in similarity (i.e. dedifferentiation) ($P < 0.01$, two-way ANOVA with post-hoc multiple comparison test) (Fig. S17).

We asked whether dedifferentiation in LSA-III represents a return to a synaptome resembling that of a young brain or to a distinct, elderly-specific synaptome architecture. Using a hypersimilarity matrix that compares all subregions at all ages we found that the 18M brain, in contrast to the 3M brain, is more similar to the 2W brain (Cohen's $d = 1.5$, $P < 0.01$, Bayesian test) (yellow boxes in Figs. 3C and S18, S19A). The hypersimilarity matrix also reveals three major blocks corresponding to the LSA phases (white boxes in Figs. 3C and S18) with a transition between LSA-I and LSA-II at 3W, which corresponds to the behavioral transition from dependence on maternal care to independent living. The hypersimilarity matrix of hippocampal subregions showed a similar pattern (Cohen's $d = 1.7$, $P < 0.01$, Bayesian test) (Figs. 3D and S19B).

To identify the synapse types and subtypes contributing to the differentiation-dedifferentation trajectory we correlated the abundance of each synapse subtype with the similarity ratio using brain-wide data and regional data (Fig. S20), revealing a role for all three synapse types and a

subset (21/37) of synapse subtypes (r > 0.5 or < –0.5, $P < 0.05$, Mantel test with Benjamini-Hochberg correction).

The functional connectivity between brain areas, measured using resting state functional magnetic resonance imaging, correlates with the topology (small-worldness) of the synaptome network(*8*). Small worldness increased from birth to 3M ($P < 0.001$, two-way ANOVA with post-hoc multiple comparison test) and then declined to 18M ($P < 0.001$, two-way ANOVA with post-hoc multiple comparison test) (Fig. 3E), suggesting that the differentiation-dedifferentation trajectory influences the integrative property of brain circuits.

Lifespan synaptome changes alter functional outputs

To explore how the age-dependent changes in synaptome architecture may cause changes in cognitive functions we focused on the hippocampal formation, which is key for spatial navigation, learning and memory(*27*). In the CA1 stratum radiatum of the adult mouse there are orthogonal (radial and tangential) spatial gradients in PSD95 and SAP102 synaptic parameters that produce a local architecture of molecularly diverse synapses(*8, 28*). Quantification of these gradients at 1W, 3M and 18M showed age-dependent changes for PSD95 intensity in both radial and tangential directions (Figs. 4A, S21). For SAP102 on the other hand, no radial gradient was observed and the tangential gradient was established by 1W and thereafter remained unchanged (Figs. 4A, S21). This shows that these two closely related synaptic proteins undergo distinct spatiotemporal changes within the dendrites of CA1 pyramidal cells, producing a changing two-dimensional synaptome map across the lifespan. Using a computational simulation approach that tests the response (excitatory postsynaptic potential, EPSP) of CA1 synaptome maps to patterns of neural activity(*8*), we found that gamma and theta-burst patterns produced differential responses between 1W-3M and 3M-18M ($P < 0.05$, paired t-test, Kolmogorov-Smirnov test), in contrast to theta trains that produced a stable response at all ages (Figs. 4B, S22). This illustrates how lifespan synaptome changes affect synaptic responses to distinct temporal patterns of neural activity.

Different subregions of the hippocampal formation contribute distinct cognitive functions, which together produce an integrated behavioral output(*27, 29, 30*). This integrated function is exemplified by the trisynaptic circuit in which axons project from neurons in the dentate gyrus to CA3 neurons, which project to CA1 neurons(*27*). Our data show that each subregion in the trisynaptic circuit undergoes a different lifespan trajectory of synaptic subtype composition,

indicating that the memory functions controlled by these hippocampal subregions are highly likely to change with age (Figs. 4C, S23).

Discussion

The dynamic temporal trajectories of excitatory synapse number, protein composition, morphology, type and subtype diversity in over 100 brain areas reveal a lifespan synaptome architecture for the mouse brain. The continuum of changes in the synaptome architecture is divided into three epochs that broadly correspond to childhood/adolescence, early adulthood, and late adulthood. Synapse diversity expands between birth and early adulthood, driving the differentiation of brain regions, before changes in synapse composition progressively dedifferentiate brain regions in old age. These changes alter brain network and hippocampal physiological properties and are potentially relevant to the trajectory of cognitive functions described in lifespan studies of human behavior(*31-34*) and the changes in the behavioral repertoire of animals across the lifespan(*13-15*).

The LSA reveals how factors that modify the expression of synaptic proteins (including genetic mutations, toxic proteins, inflammation and drugs) can target particular synapses and brain regions at different ages and lead to behavioral changes. Expanding our approach to other synaptic proteins labelling greater synapse diversity, examining the synaptome of neuron types and dendritic morphology, and linking these brain-wide synapse-resolution data to transcriptional mechanisms that control brain gene expression across the lifespan(*35*) should enhance the effort to uncover the mechanisms and impacts of brain development, aging and disease. Our highly scalable synaptomic methods and the Lifespan Synaptome Atlas delivered here provide new tools for addressing these issues.

References

1. S. G. Grant *et al.*, Impaired long-term potentiation, spatial learning, and hippocampal development in fyn mutant mice. *Science* **258**, 1903-1910 (1992).
2. N. H. Komiyama *et al.*, SynGAP regulates ERK/MAPK signaling, synaptic plasticity, and learning in the complex with postsynaptic density 95 and NMDA receptor. *J Neurosci* **22**, 9721-9732 (2002).
3. M. Migaud *et al.*, Enhanced long-term potentiation and impaired learning in mice with mutant postsynaptic density-95 protein. *Nature* **396**, 433-439 (1998).
4. A. J. Silva, R. Paylor, J. M. Wehner, S. Tonegawa, Impaired spatial learning in alpha-calcium-calmodulin kinase II mutant mice. *Science* **257**, 206-211 (1992).
5. P. C. Cuthbert *et al.*, Synapse-associated protein 102/dlgh3 couples the NMDA receptor to specific plasticity pathways and learning strategies. *J Neurosci* **27**, 2673-2682 (2007).

6. J. Nithianantharajah *et al.*, Synaptic scaffold evolution generated components of vertebrate cognitive complexity. *Nat Neurosci* **16**, 16-24 (2013).
7. A. Bayes *et al.*, Characterization of the proteome, diseases and evolution of the human postsynaptic density. *Nat Neurosci* **14**, 19-21 (2011).
8. F. Zhu *et al.*, Architecture of the mouse brain synaptome. *Neuron* **99**, 781-799 e710 (2018).
9. E. Fernandez *et al.*, Targeted tandem affinity purification of PSD-95 recovers core postsynaptic complexes and schizophrenia susceptibility proteins. *Mol Syst Biol* **5**, 269 (2009).
10. R. A. Frank *et al.*, NMDA receptors are selectively partitioned into complexes and supercomplexes during synapse maturation. *Nat Commun* **7**, 11264 (2016).
11. R. A. W. Frank, F. Zhu, N. H. Komiyama, S. G. N. Grant, Hierarchical organization and genetically separable subfamilies of PSD95 postsynaptic supercomplexes. *J Neurochem* **142**, 504-511 (2017).
12. H. Husi, M. A. Ward, J. S. Choudhary, W. P. Blackstock, S. G. Grant, Proteomic analysis of NMDA receptor-adhesion protein signaling complexes. *Nat Neurosci* **3**, 661-669 (2000).
13. C. Darwin, *The expression of the emotions in man and animals*. (Murray, [S.l.], 1872).
14. W. James, *The principles of psychology*. (H. Holt and Company, New York, 1890).
15. N. Tinbergen, *The study of instinct*. (Clarendon Press, Oxford Eng., 1951).
16. Gokhale, R., Qiu, Z., Koniaris, B., Grant, S.G.N. *The Mouse Lifespan Synaptome Atlas*. (2020). www.brain-synaptome.org
17. X. Chen *et al.*, Mass of the postsynaptic density and enumeration of three key molecules. *Proc Natl Acad Sci USA* **102**, 11551-11556 (2005).
18. H.-W. Dong, *Allen reference atlas : a digital color brain atlas of the C57black/6J male mouse*. (Wiley [Chichester : John Wiley, distributor], Hoboken, N.J., 2008).
19. I. Adams, D. G. Jones, Synaptic remodelling and astrocytic hypertrophy in rat cerebral cortex from early to late adulthood. *Neurobiol Aging* **3**, 179-186 (1982).
20. G. K. Aghajanian, F. E. Bloom, The formation of synaptic junctions in developing rat brain: a quantitative electron microscopic study. *Brain Res* **6**, 716-727 (1967).
21. K. D. Micheva, C. Beaulieu, Quantitative aspects of synaptogenesis in the rat barrel field cortex with special reference to GABA circuitry. *J Comp Neurol* **373**, 340-354 (1996).
22. B. Crain, C. Cotman, D. Taylor, G. Lynch, A quantitative electron microscopic study of synaptogenesis in the dentate gyrus of the rat. *Brain Res* **63**, 195-204 (1973).
23. G. Elias, P. Apostolides, A. Kriegstein, R. Nicoll, Differential trafficking of AMPA and NMDA receptors by SAP102 and PSD-95 underlies synapse development. *Proceedings of the National Academy of Sciences* **105**, 20953-20958 (2008).
24. D. Dumitriu *et al.*, Selective changes in thin spine density and morphology in monkey prefrontal cortex correlate with aging-related cognitive impairment. *J Neurosci* **30**, 7507-7515 (2010).
25. J. H. Morrison, M. G. Baxter, The ageing cortical synapse: hallmarks and implications for cognitive decline. *Nat Rev Neurosci* **13**, 240-250 (2012).
26. A. Peters, C. Sethares, J. I. Luebke, Synapses are lost during aging in the primate prefrontal cortex. *Neuroscience* **152**, 970-981 (2008).
27. J. Basu, S. A. Siegelbaum, The corticohippocampal circuit, synaptic plasticity, and memory. *Cold Spring Harb Perspect Biol* **7**, (2015).
28. M. J. Broadhead *et al.*, PSD95 nanoclusters are postsynaptic building blocks in hippocampus circuits. *Sci Rep* **6**, 24626 (2016).
29. D. M. Bannerman *et al.*, Hippocampal synaptic plasticity, spatial memory and anxiety. *Nat Rev Neurosci* **15**, 181-192 (2014).
30. I. Soltesz, A. Losonczy, CA1 pyramidal cell diversity enabling parallel information processing in the hippocampus. *Nat Neurosci* **21**, 484-493 (2018).

31. P. B. Baltes, S. W. Cornelius, A. Spiro, J. R. Nesselroade, S. L. Willis, Integration versus differentiation of fluid/crytallized intelligence in old age. *Dev. Psychol.* **16**, 625 (1980).
32. S. C. Li *et al.*, Transformations in the couplings among intellectual abilities and constituent cognitive processes across the life span. *Psychol Sci* **15**, 155-163 (2004).
33. G. Reinert, in *Life-span developmental psychology*. (Elsevier, 1970), pp. 467-484.
34. E. M. Tucker-Drob, Differentiation of cognitive abilities across the life span. *Dev Psychol* **45**, 1097-1118 (2009).
35. N. G. Skene, M. Roy, S. G. Grant, A genomic lifespan program that reorganises the young adult brain is targeted in schizophrenia. *Elife* **6**, e17915 (2017).
36. Cizeron, M., Qiu, Z., Koniaris, B., Gokhale, R., Komiyama, N., Fransén, E., Grant, S.G.N. (2020). Mouse Lifespan Synaptome Atlas dataset https://doi.org/10.7488/ds/2796
37. Qiu, Z., Grant, S.G.N. (2020). Mouse Lifespan Synaptome Atlas code repository https://doi.org/10.5281/zenodo.3825214
38. M. H. Ullman-Cullere, C. J. Foltz, Body condition scoring: a rapid and accurate method for assessing health status in mice. *Laboratory Animal Science* **49**, 319-323 (1999).
39. B. Efron, R. J. Tibshirani, *An introduction to the bootstrap*. (CRC press, 1994).
40. N. Chenouard *et al.*, Objective comparison of particle tracking methods. *Nat Methods* **11**, 281 (2014).
41. J. K. Kruschke, Bayesian estimation supersedes the t test. *J Exp Psychol Gen* **142**, 573-603 (2013).
42. E. Bullmore, O. Sporns, Complex brain networks: graph theoretical analysis of structural and functional systems. *Nat Rev Neuroscience* **10**, 186 (2009).
43. NVIDIA GameWorks (2019). https://developer.nvidia.com/opengl-driver. Accessed 11 May 2020.

Acknowledgements: C. McLaughlin and K. Elsegood for mouse colony and lab management, D. Kerrigan and D. Fricker for genotyping; N. G. Skene for statistical advice; S. Munni, O. Kealy, H. Taczynski for image calibration; D. Maizels for artwork; C. Davey for editing. **Funding**: Wellcome Trust (Technology Development Grant 202932), the European Research Council (ERC) under the European Union's Horizon 2020 Research and Innovation Programme (695568 SYNNOVATE), Simons Foundation for Autism Research Initiative (529085). **Author Contributions:** MC, design of animal cohort; collection, preparation and imaging of brain samples; delineation of brain regions/subregions; calibration of synapse detection; analysis of synapse parameters; analysis of hippocampal gradients; data interpretation; ZQ, methodology development and optimization of lifespan SYNMAP pipeline; data analysis of the whole lifespan mouse cohort: image segmentation and puncta quantification, classification, unsupervised and supervised mapping of synapse parameters, types and subtypes, diversity and network topology analysis; EF, statistical analysis and computational modelling of synaptome physiology; BK, construction of Synaptome Explorer and Synaptome Homology Viewer; RG, construction of website; NHK, advice and supervision; SGNG, conception, analysis, supervision and writing. **Competing interests:** The authors declare no competing interests. **Data and materials**

availability: all data are available at the Mouse Synaptome Atlas(*16*) and Edinburgh DataShare(*36*) and code at (*37*). Requests for materials should be addressed to S.G.N.G.

List of Supplementary Materials:

Materials and Methods

Figures S1-S23

Table S1

References *(38-43)*

Figure Legends

Figure 1. Lifespan trajectories of synapse parameters

A. PSD95-eGFP (green) and SAP102-mKO2 (magenta) expression acquired at low (20X, i and ii) and high (100X, iii) magnification in the whole brain (i), hippocampus (ii), and molecular layer of the dentate gyrus (iii) at ten ages across the mouse postnatal lifespan. Scale bars: i, 4 mm; ii, 500 μm; iii, 3.5 μm. D, day; W, week; M, month.

B. Lifespan trajectories of synapse density, intensity (normalized to the mean intensity, arbitrary units: AU) and size in the whole brain. PSD95-eGFP (green) and SAP102-mKO2 (magenta). Points represent individual mice, with beta-spline smoothed curve of mean values and standard error of the mean.

C. Differences (Cohen's *d*) in synapse parameters between 3M and 18M in brain subregions (numbered, see Table S1). $*P < 0.05$, Bayesian test with Benjamini-Hochberg correction. CB: cerebellum, CTXsp: cortical subplate, HPF: hippocampal formation, HY: hypothalamus, MB: midbrain, MY: medulla, OLF: olfactory areas, P: pons, PAL: pallidum, STR: striatum, TH: thalamus.

Figure 2. Lifespan trajectories of synapse types, subtypes and diversity

A. Stacked bar plot of percentage of synapse type density (type 1, PSD95 only; type 2, SAP102 only; type 3, colocalized PSD95+SAP102) in the whole brain across the lifespan.

B. Percentage of synapse subtype density in the whole brain across the lifespan. Key: synapse subtypes (1-37).

C. Percentage of synapse subtype density in hippocampus and cerebellum across the lifespan.

D. Lifespan trajectories of synapse type (normalized) density in 12 regions and 109 subregions (rows, see Table S1). Density in each subregion was normalized (0-1) to its maximal density across the lifespan (columns). Twelve brain regions are shown (abbreviations as Fig. 1C).

E. Lifespan trajectories of three representative synapse subtypes (2, 16, 31) in each of 109 subregions (rows) (see Table S1). Density in each subregion was normalized (0-1) to its maximal density across the lifespan (columns).

F. Lifespan trajectories of synapse diversity (Shannon entropy) for whole brain (top) and main regions from the cerebrum (middle) and brainstem and cerebellum (bottom). Beta-spline smoothed curve of mean and standard error of the mean are shown.

G. Unsupervised synaptome maps showing the spatial patterning of synapse diversity (Shannon entropy) per area (pixel size 21.5 µm x 21.5 µm) in representative para-sagittal sections (all ages available in Fig. S15 and website(*8*)).

Figure 3. Lifespan synaptome architecture

A. Matrix of similarities between pairs of subregions (rows and columns) at 1W, 3M and 18M (see Fig. S16 for all ages). Small white boxes indicate the subregions that belong to the same main brain region (see color code, left and top) and larger white boxes indicate main clusters: cerebrum, brainstem, cerebellum. Note reduction in similarity from 1W to 3M and increase to 18M. Iso, isocortex; other abbreviations as Fig. 1C.

B. Similarity ratio compares the relative similarity of the synaptome in each main brain region with that of every other region(*8*). See Materials and Methods for details. Significant differences of ratio between 3M and other ages: $^{**}P < 0.01$, $^{***}P < 0.001$; two-way ANOVA with post-hoc multiple comparison test.

C. Whole-brain hypersimilarity matrix showing the similarity between pairs of subregions at all ages. White boxes indicate the three main clusters, which correspond to LSA-I, -II and -III. Yellow box shows increased similarity of the old brain with the young brain.

D. Hippocampus hypersimilarity matrix showing the similarity of pairs of hippocampal subregions at all ages (higher magnification image in Fig. S18). White boxes indicate the three main clusters corresponding to LSA-I, -II and -III. Yellow box shows the increased similarity of the old brain with the young brain.

E. Average small worldness across the lifespan. Scatter plots indicate the average small worldness per mouse brain section at different ages. Significant differences of small worldness between 3M and other ages: $^{*}P < 0.05$, $^{**}P < 0.01$, $^{***}P < 0.001$; two-way ANOVA with post-hoc multiple comparison test.

Figure 4. Lifespan changes in hippocampus architecture and electrophysiological properties

A. Schematics of hippocampus showing radial and tangential gradients in CA1sr subfields. Graphs show gradients of normalized synapse intensity (AU) of PSD95 and SAP102 at 1W, 3M and 18M. CA1: cornu ammonis 1, CA2: cornu ammonis 2, CA3: cornu ammonis 3, DG: dentate gyrus, gr: granular layer, mo: molecular layer, po: polymorphic cell layer, slm: stratum lacunosum-moleculare, slu: stratum lucidum, so: stratum oriens, sp: stratum pyramidale, sr: stratum radiatum.

B. The summed response (EPSP amplitude) to three patterns (gamma, theta, theta-burst) of 20 action potentials of the 11 x 11 matrix of hippocampus synapses at three ages. Histograms show changes (summed Euclidean distance, ED) between 1W and 3M (purple), and 3M and 18M (yellow).

C. Schematic of the flow of information (arrows) in the trisynaptic hippocampal circuit connecting DG molecular layer (DGmo), CA3 stratum radiatum (CA3sr) and CA1 stratum radiatum (CA1sr), and the lifespan trajectory of synapse subtype density (normalized) in each region. EC, entorhinal cortex.

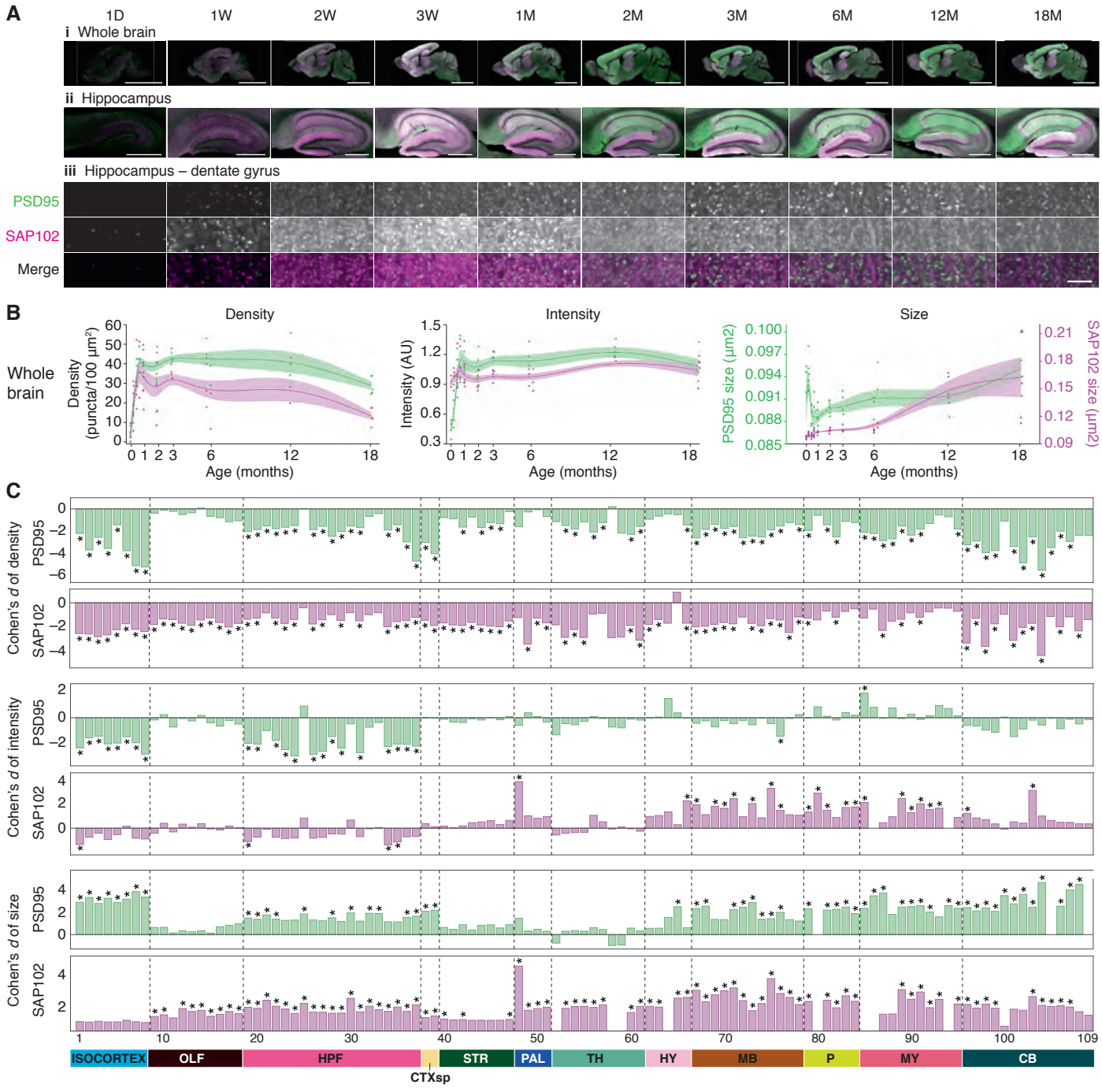
A
1D
1W
2W
3W
1M
2M
3M
6M
12M
18M
i Whole brain
ii Hippocampus
iii Hippocampus – dentate gyrus
PSD95
SAP102
Merge
B
Whole brain
Density
Density (puncta/100 µm²)
Age (months)
Intensity
Intensity (AU)
Size
PSD95 size (µm2)
SAP102 size (µm2)
C
Cohen's d of density
Cohen's d of intensity
Cohen's d of size
PSD95
SAP102
ISOCORTEX
OLF
HPF
CTXsp
STR
PAL
TH
HY
MB
P
MY
CB

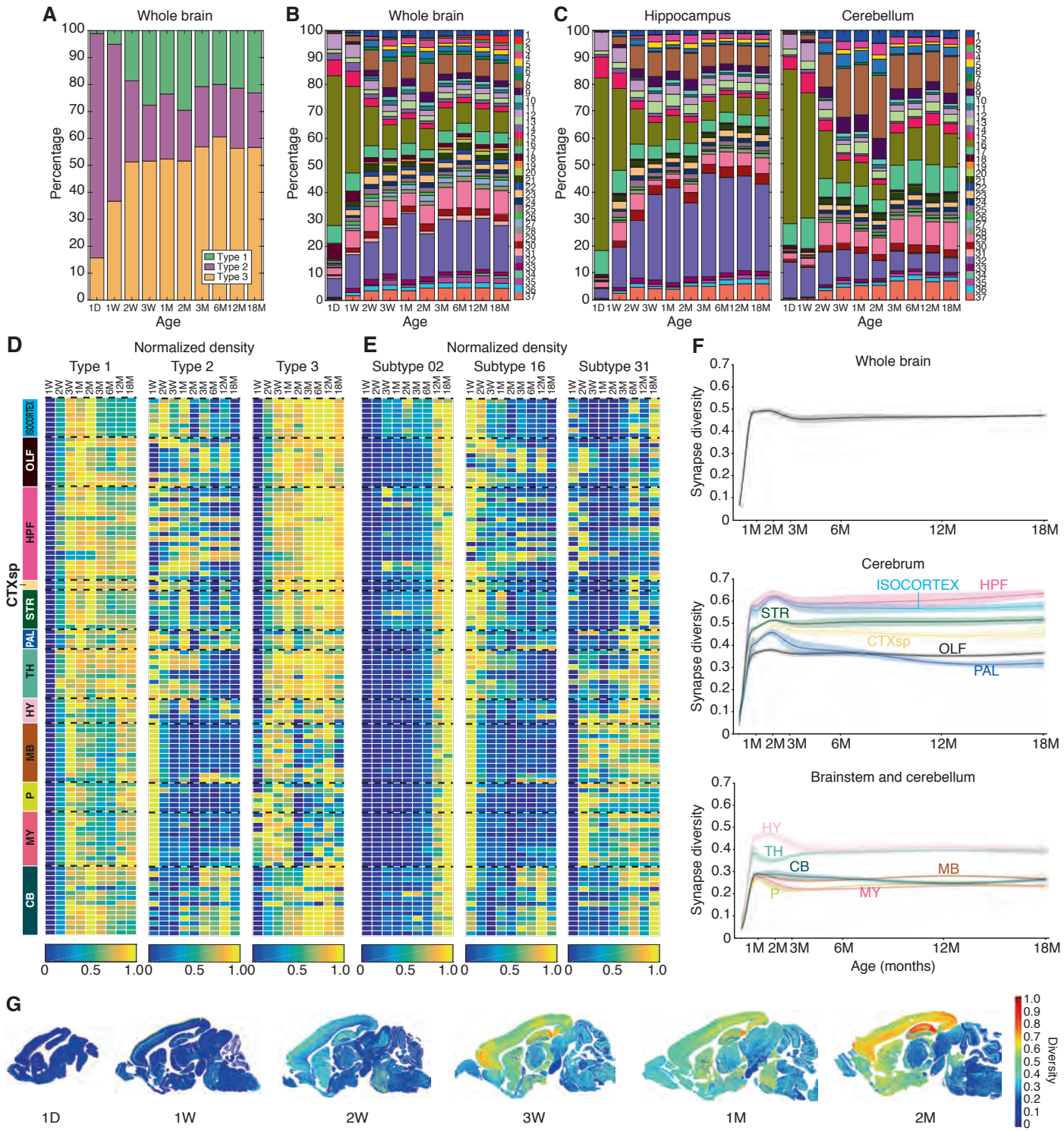
A
Whole brain
Percentage
Age
Type 1
Type 2
Type 3
B
Whole brain
C
Hippocampus
Cerebellum
D
Normalized density
Type 1
Type 2
Type 3
CTXsp
ISOCORTEX
OLF
HPF
STR
PAL
TH
HY
MB
P
MY
CB
E
Normalized density
Subtype 02
Subtype 16
Subtype 31
F
Whole brain
Synapse diversity
Cerebrum
ISOCORTEX
HPF
STR
CTXsp
OLF
PAL
Brainstem and cerebellum
HY
TH
CB
MB
P
MY
Age (months)
G
1D
1W
2W
3W
1M
2M
Diversity

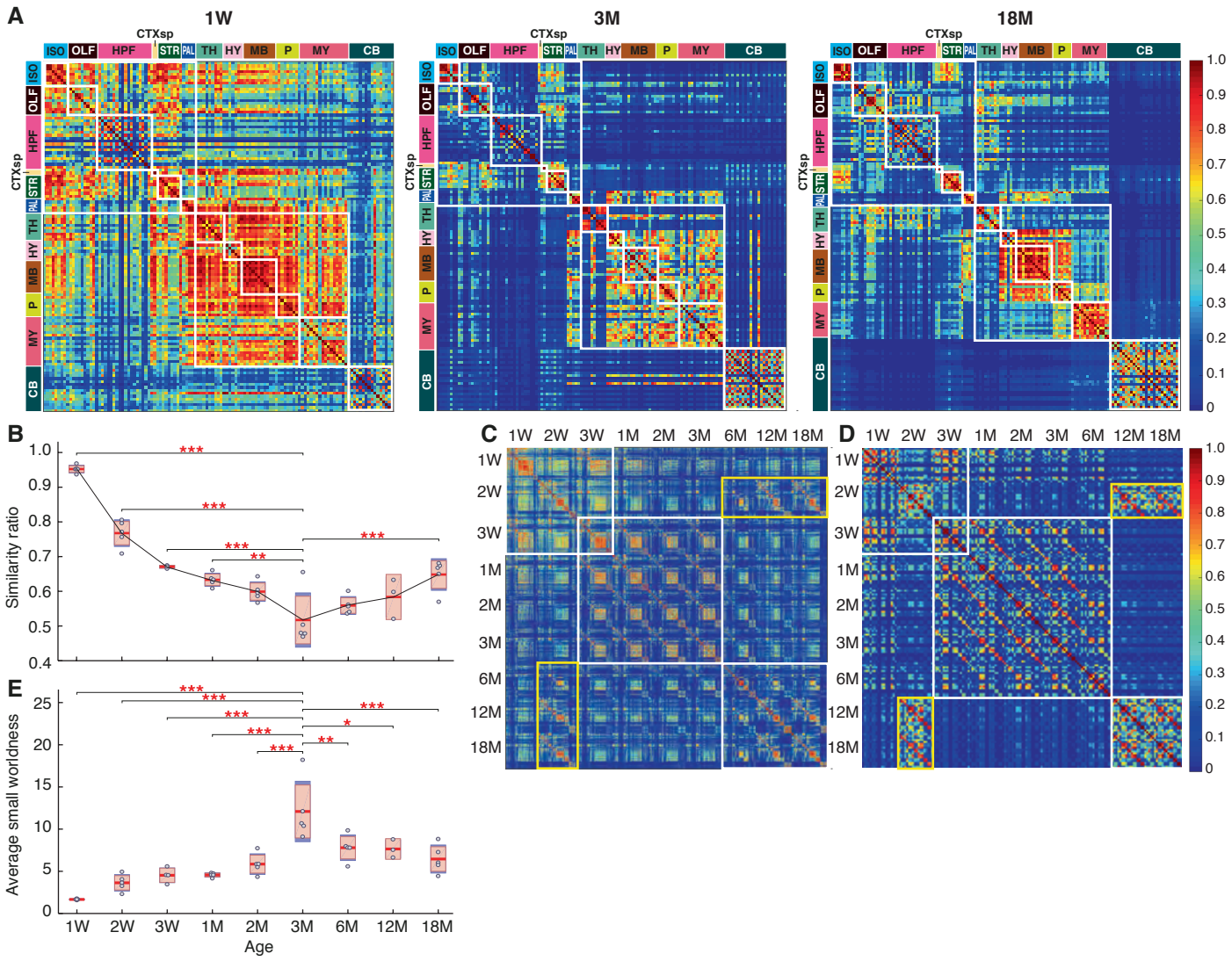
A
1W
3M
18M
CTXsp
ISO
OLF
HPF
STR
PAL
TH
HY
MB
P
MY
CB
1.0
0.9
0.8
0.7
0.6
0.5
0.4
0.3
0.2
0.1
0
B
Similarity ratio
C
D
1W 2W 3W 1M 2M 3M 6M 12M 18M
E
Average small worldness
Age
***
**
*

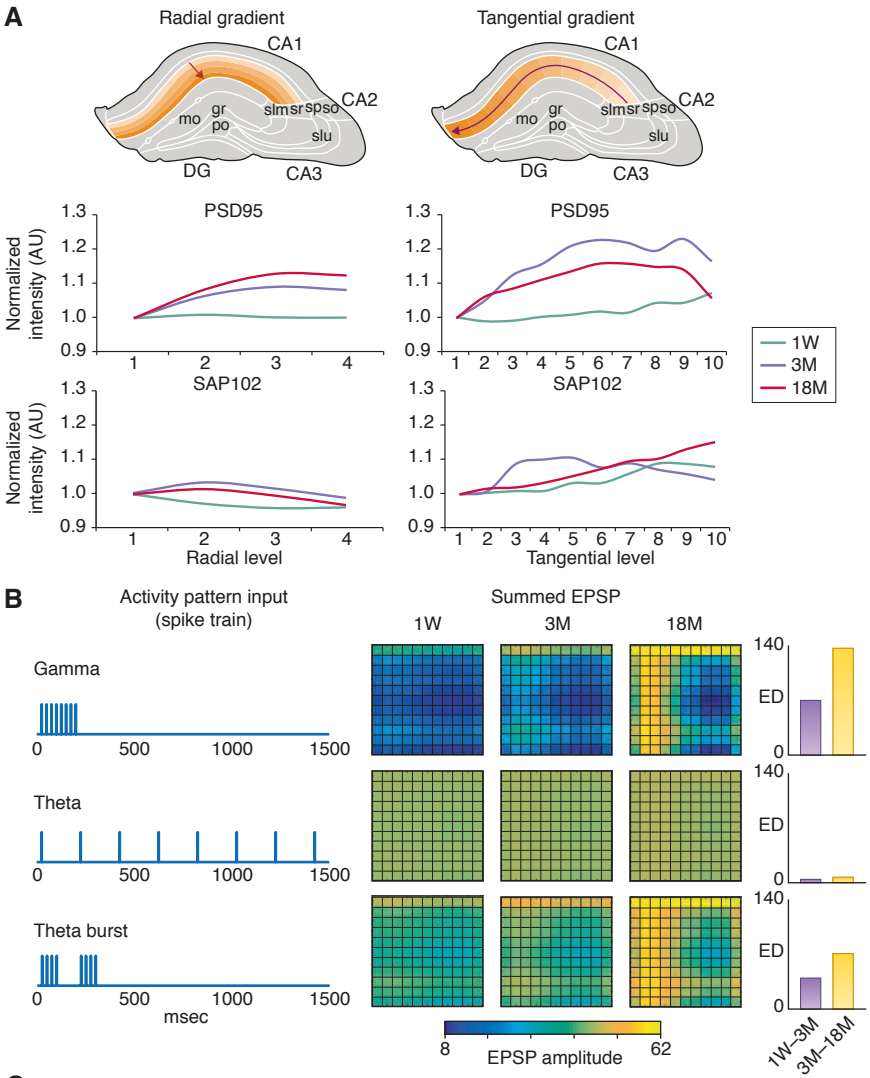
A
Radial gradient
Tangential gradient
CA1
CA2
CA3
DG
mo
gr
po
slm
sr
spo
so
slu
PSD95
SAP102
Normalized intensity (AU)
Radial level
Tangential level
1W
3M
18M
B
Activity pattern input (spike train)
Summed EPSP
Gamma
Theta
Theta burst
msec
ED
EPSP amplitude
1W–3M
3M–18M
C
Trisynaptic corticohippocampal circuit
Dendrite
Axons
EC
DGmo
CA3sr
CA1sr
Subtypes

A brain-wide atlas of synapses across the mouse lifespan

Authors:

Mélissa Cizeron†, Zhen Qiu†, Babis Koniaris, Ragini Gokhale, Noboru H. Komiyama, Erik Fransén & Seth G.N. Grant

† these authors contributed equally

Correspondence to seth.grant@ed.ac.uk

This PDF file includes:

Materials and Methods

Figures S1-S23

Table S1 legend

Supplementary Materials:

Materials and Methods:

Animals

Animal procedures were performed in accordance with UK Home Office regulations and approved by Edinburgh University Director of Biological Services. Generation and characterization of $PSD95^{eGFP/eGFP}$;$SAP102^{mKO2/mKO2}$ knock-in mouse line was described previously(*8*). Para-sagittal brain sections from cohorts of 49 $PSD95^{eGFP/+}$;$SAP102^{mKO2/y}$ male mice were collected at ten postnatal ages: one day (1D, N=5), one week (1W, N=5), two weeks (2W, N=5), three weeks (3W, N=4), one month (1M, N=6), two months (2M, N=6), three months (3M, N=5), six months (6M, N=5), 12 months (12M, N=3) and 18 months (18M, N=5). From 12 months of age, mice were monitored monthly by weight and scoring their body condition as previously described (*38*). No change in mouse weight or body condition was observed in ageing mice.

Tissue collection

Tissue collection was performed at ten ages as described previously(*8*). Briefly, mice were anesthetized by intraperitoneal injection of 20% pentobarbital sodium (Pentoject, Animalcare; 0.03 ml for 1D, 0.05 ml for 1W-1M, and 0.1 ml for 2M-18M animals). Upon complete anesthesia, transcardiac perfusion of phosphate-buffered saline (PBS; Oxoid) was performed and followed by transcardiac perfusion of 4% (v/v in PBS) paraformaldehyde (PFA; Alfa Aesar). PBS and PFA volumes used were: 2 ml (1D), 3 ml (1W), 5 ml (2W), 7ml (3W), 8 ml (1M) and 10 ml (2M-18M). Whole brain was then dissected and post-fixed in 4% PFA for 1h (1D), 1.5h (1W), 2h (2W), 2.5h (3W), 3h (1M) or 3.5h (2M-18M), followed by cryoprotection in 30% sucrose solution (w/v in PBS; VWR Chemicals) for 24h (1D-1W), 48h (2W-3W) or 72h (1M-18M). Brains were then placed in a cryomold, embedded in Optimal Cutting Temperature (OCT, CellPath) and frozen in isopentane cooled with liquid nitrogen. Para-sagittal brain sections were then cut at 18 μm thickness using a Thermo Fisher NX70 cryostat. Cryosections were placed on Superfrost Plus glass slides (Thermo Scientific) and stored at -80°C.

Tissue preparation

Para-sagittal sections from left hemisphere (1.2 mm laterally from the midline in Franklin and Paxinos sagittal atlas, corresponding to sections 12-13/24 from sagittal Allen Brain Reference

Atlas) were washed for 5 min in PBS, incubated for 15 min in 1 mg/ml DAPI (Sigma), washed with PBS, mounted in home-made MOWIOL (Calbiochem) containing 2.5% anti-fading agent DABCO (Sigma-Aldrich), covered with a coverslip (thickness #1.5, VWR International) and imaged the following day.

Slide scanner widefield microscopy

Whole sections were imaged using the Zeiss Axio Scan.Z1 system with a Zeiss Plan-Apochromat 20X lens with a numerical aperture (NA) of 0.8. Samples were illuminated using Colibri.2 at 365 nm for DAPI, 470 nm for EGFP and 555 nm for mKO2. Excitation filters were 365 nm for DAPI, 470/40 nm for EGFP and 546/12 nm for mKO2. Emission filters were 445/50 nm for DAPI, 525/50 nm for eGFP and 607/80 nm for mKO2. Light detection was achieved using a Hamamatsu Orca-flash 4.0 monochrome camera.

Spinning disc confocal microscopy

Fast high-resolution imaging was achieved using the Andor Revolution XDi system, equipped with an Olympus UPlanSAPO 100X oil immersion lens (NA 1.4), a CSU-X1 spinning disc (Yokogawa), an Andor iXon Ultra monochrome back-illuminated EMCCD camera, a 2X post-magnification lens and a Borealis Perfect Illumination Delivery™ system. Images have a pixel dimension of 84 x 84 nm and a depth of 16. A single mosaic grid, with no overlap between adjacent tiles, was set up in the Andor iQ2 software to cover each entire brain section, using an adaptive *z* focus to follow the unevenness of the tissue. eGFP was excited using a 488 nm laser and mKO2 with a 561 nm laser. Emitted light was filtered with a Quad filter (BP 440/40, BP 521/21, BP 607/34 and BP 700/45).

Acquisition parameters in developmental and adult time points

To optimize imaging between time points where synapse intensity was low (development) or high (adulthood), two sets of spinning disc acquisition parameters were used for 1D-3M and 3M-18M time points. Acquisition of the 3M time point was performed with both sets of parameters using adjacent brain sections from the same mice (N=3) and synapse parameters were compared. As no significant difference was found between the two sets of data, no correction was applied and the two sets of time points were merged.

Detection of synaptic puncta

Synaptic puncta were detected using the machine learning-based ensemble detection method(*8*). A training set of 1104 images (10.8 × 10.8 μm) for PSD95 and SAP102 (each for 552 images) was randomly sampled across 12 main brain regions using bootstrapping(*39*) from a data cohort of different age groups. Synaptic puncta were manually annotated by their centroid location in the images by four experts blinded to the tissue sample. A weighting factor (0-1) was then given as the measurement of the annotation quality for each human expert. The ground truth was finally generated by aggregating the weighting factors of the four annotations: puncta annotated with an average weight greater than 0.7 were considered as true puncta.

To avoid any overfitting problems, a K-fold cross-validation strategy was adopted to train the punctum detector using ensemble learning as described previously(*8*): half of the training set was randomly selected to train the detector and the other half to validate and test the performance of the detector. This procedure was repeated 150 times, each using a different random division of the training set for cross validation. An overall 95% detection rate for PSD95 and 92% for SAP102 was achieved on the validation dataset, both of which outperformed conventional puncta/particle detection algorithms(*40*) on fluorescence microscopy images. After training the detector was applied to other images for punctum detection.

Measurement of synaptic parameters

Once detected and localized, all puncta were segmented by thresholding their intensities adaptively: a threshold for each punctum was set as 10% of the height of the intensity profile. Six punctum parameters were then quantified: mean pixel intensity, size, skewness, kurtosis, circularity, and aspect ratio, the latter four of which were used for shape quantification. For details, see previous work(*8*).

Classification of synaptic puncta

Puncta were first classified into three type classes depending on synaptic protein expression: type 1 for PSD95 only, type 2 for SAP102 only, and type 3 for colocalized PSD95 and SAP102(*8*). Using the machine learning methods the three types were further classified into either 37 existing subtypes built from previous work(*8*) or as new subtypes: Bayesian classifiers were first built for each of all subtypes. For each unclassified punctum, the likelihood values (0-1) of all 37 subtypes were calculated based on the punctum parameters and the 37 Bayesian classifiers. The punctum

was finally labelled as the subtype with highest likelihood value, if the value is higher than a given threshold (set at 0.5). Otherwise the punctum is labelled as a new 'other subtypes'. We find that, overall, the 'other subtypes' only accounts for ~0.002% of the whole population of individual synapses quantified from the whole data cohort, and is thus considered not to affect the composition and diversity of synapses across the lifespan.

Measurement of synapse diversity

Synapse diversity, which was measured based on the Shannon entropy, quantified the population differences across 37 subtypes in a given unit brain area: 0 if all puncta belong to a single subtype and 1 if all subtypes occur equally in the population. For details see previous work(*8*).

Segmentation of brain regions and subregions

After high-resolution imaging, a downsized stitched image of the whole section was used for manual delineations of brain subregions in ImageJ, according to the online reference atlas of the Allen Mouse Brain Atlas(*16*). Delineation masks from these delineations were used to generate mean values of synaptic punctum parameters over the corresponding subregion. For region analysis, the corresponding mask was generated by combining all the masks from subregions that belong to this brain region. For 1D mice, region masks were delineated directly as no subregion masks were generated. For estimation of the brain size, the area covered by the masks resulting from all main regions (whole section area) was measured at each time point (Fig. S6).

Bayesian analysis to compare synaptome parameters between 3M and 18M

Bayesian estimation(*41*) in the previously described methods(*8*) was used to test the changes in synaptome parameters between 3M and 18M (Figs. 1C, S13). Posterior probabilities of model parameters were estimated from the data and then used to determine whether age-dependent differences exist. Each parameter (intensity, density, size) and subtype was modelled assuming a t-distribution. For each parameter, each subregion was first modelled and tested separately. The results were finally corrected over all subregions using the Benjamini-Hochberg procedure.

Similarity matrices, hypersimilarity matrix and network analysis

Each row/column in the matrix represents one delineated brain subregion at one age (similarity matrix Figs. 3A and S16) or different ages (hypersimilarity matrix Figs. 3C, D and S17). Elements

in the matrix are the synaptome similarities between two subregions quantified by differences in standardized synaptome parameters, details of which can be found in previous work(*8*).

The similarity ratio S_{ratio} at each of the ages in Fig. 3B is calculated as the between-region similarity divided by the within-region similarity,

$$S_{ratio} = \frac{\sum_{k,l \notin same\ regions} s(k,l) \Big/ M}{\sum_{i,j \in same\ regions} s(i,j) \Big/ N}$$

where *i,j,k,l* represent the indices of subregions, *s*(*x*,*y*) represents the similarity of two subregions *x* and *y*, and *N* or *M* is the number of comparisons between two subregions from same or different overarching region, respectively. Within-region similarity $\sum_{i,j \in same\ regions} s(i,j) \Big/ N$ is defined as the average similarities between any two subregions belonging to the same main overarching brain regions (corresponding to areas marked by the 12 small white boxes distributed diagonally in the similarity matrix in Figs. 3A and S16). The between-region similarity $\sum_{k,l \notin same\ regions} s(k,l) \Big/ M$ is the average similarities between any two subregions coming from different overarching brain regions (the areas that are outside the 12 white boxes lying on the diagonal in Figs. 3A and S16).

The lifespan trajectories of the similarity ratio in each of 12 brain regions were used to correlate with the density percentage of 37 subtypes in the same regions. The correlation was quantified by Pearson coefficients and significance level (*P* values) given by the Mantel test.

The network analysis (Fig. 3E) was based on the similarity matrices of individual brain sections quantified in a similar way to those in Figs. 3A and S16. Nodes in the network are representations of the delineated subregion. The small worldness is the topology quantification of the network where the whole set of nodes are divided into small and clustered groups: nodes within the same groups are highly connected/similar, whereas those between groups are disconnected/dissimilar(*42*). For a given network the small worldness $\sigma(D)$ is a function of network density *D* and is calculated as the ratio of the clustering coefficient (CC) and average path length normalized by the random networks with equivalent density and degree distribution,

$$\sigma(D) = [C_{net}(D) / C_{rand}(D)] / [l_{net}(D) / l_{rand}(D)],$$

where C_{net} , C_{rand} represent the CCs of the synaptome and random network, respectively, and l_{net} , l_{rand} are the path length of the synaptome and random network, respectively. Small worldness is usually plotted as a curve against the network density(*8*). To facilitate comparison of small worldness between different age groups, we converted the small-worldness curve of each brain section into a single value (average small worldness) by averaging the curve between 0% and 30% network densities. The average small-worldness value is presented for each age group in scatter plots (Fig. 3E).

Statistical tests on similarity matrices and hypersimilarity matrix

Permutation testing was used to ask if the similarity matrices (Figs. 3A, S16) were different from random patterns. Each matrix (S_{simi}) was randomly shuffled in space, time, and space-time 200,000 times, each of which resulted in a shuffled matrix and similarity ratio S_{ratio}(rand). A probability distribution was then generated to compare with the ratio of the original similarity matrix (S_{simi}). 132 permutation tests (each brain section was tested in space, time, and space-time) with $P < 0.05$ and Cohen's $d > 2$ rejected the null hypothesis that the similarity matrices are random patterns.

To test whether the synaptome of 18M or 3M is more similar to that of 2W, data from two submatrices (2W-3M, 2W-18M, Fig. S19) were first extracted from the hypersimilarity matrix (Figs. 3C, S18) and reordered according to subregions. Bayesian analysis was applied to test if the mean difference of the two submatrices was significantly larger than zero. The *P* value was based on the maximal size for the highest density interval and the region of practical equivalence centered around zero(*8*).

Hippocampal gradient analysis

To analyze the lifespan trajectories of intraregional synapse diversity, we focused on hippocampal CA1 stratum radiatum (CA1sr) gradients. For mice aged 1W-18M, the CA1sr subregion was subdivided in two directions: four sublayers of equal thickness were delineated in the radial direction, starting from deep (close to CA1 stratum pyramidale) to superficial CA1sr (close to CA1 stratum lacunosum-moleculare, Fig. S21A); and 10 subfields of equal width were delineated in the tangential direction, from proximal (close to the CA2 field) to distal (close to the subiculum, Fig. S21B). Average punctum parameters were measured in these different sublayers/subfields. Pearson coefficients were calculated between parameter values in a given sublayer/subfield and its sublayer/subfield level (i.e. 1 to 4 and 1 to 10 for radial and tangential gradients, respectively).

The slope value was calculated as the slope of the linear regression curve between parameter values in a given sublayer/subfield and its sublayer/subfield level.

Computational modelling of synaptic responses

Computational modeling of synaptic responses was based on our previously described model(*8*) representing physiology at 3M. To model synaptic physiology corresponding to 1W and 18M, differences in synaptome gradients between 1W and 3M and between 3M and 18M were estimated from PSD95 and SAP102 size data obtained in this study. For each protein a size gradient was estimated in the tangential direction from the CA1sr and in the radial direction from the layers stratum oriens, pyramidale, radiatum and lacunosum moleculare of CA1. Differences in gradients were used to scale the amplitude of short-term depression and facilitation (the PSD95 and SAP102 tangential gradient decrement factor, respectively), as well as the time constant of short-term depression and facilitation (the PSD95 and SAP102 radial gradient decrement factor, respectively). Scalings of younger and older ages were relative to the 3M age (which is identical to our previous work(*8*)). Moreover, differences in responses to patterned stimulation were quantified as the Euclidean distance between a synaptic response (summed EPSP amplitude) at the two respective ages, summed over all synapses. Our model is constrained to consider only age-dependent changes in synapse protein composition and does not consider potential changes in dendritic morphology or other neuronal properties.

Lifespan Synaptome Explorer and Homology Viewer

To visualize the generated datasets interactively, we developed the tools Synaptome Explorer v2 and Synaptome Homology Viewer. Synaptome Explorer v2 is an improved version of existing software(*8*) that is used for in-depth exploration of the synaptome of a single brain section. It enables interactive visualization of the brain region in full resolution, as captured by the microscope, and uses overlays to display the synaptic puncta and all their parameters, providing users with extensive parameter range filters to display subsets of puncta accordingly. The granularity of the data visualization is at the level of individual puncta, as users can click on a single punctum and see its parameters. An additional feature is region-based and tile-based filtered punctum statistics, where users can set up parameter range filters, select a combination of regions or subregions and interactively calculate statistics, such as mean intensity, mean size and density, visualized over the corresponding regions or tiles, respectively. Synaptome Explorer v2 requires the Windows 10 operating system with at least 4GB of RAM, an Intel Core i3 or

equivalent processor, and graphic card supporting OpenGL 4.5 (see *43*) as the minimum requirement.

Synaptome Homology Viewer is a tool that enables interactive visualization of similarity matrices whose values correspond to brain regions/subregions, puts the data in a spatial context and allows simultaneous visualization of different brain section data that are delineated similarly. Users can hover over a brain region or a similarity matrix entry and immediately see how that region is similar to all other regions using a heatmap. Likewise, when using multiple brain regions, users can visualize how a hovered-over region in a brain section is similar to all other regions in all other brain sections. Thus, the tool makes the results of similarity matrices visually accessible owing to the direct mapping of the data on the brain section(s).

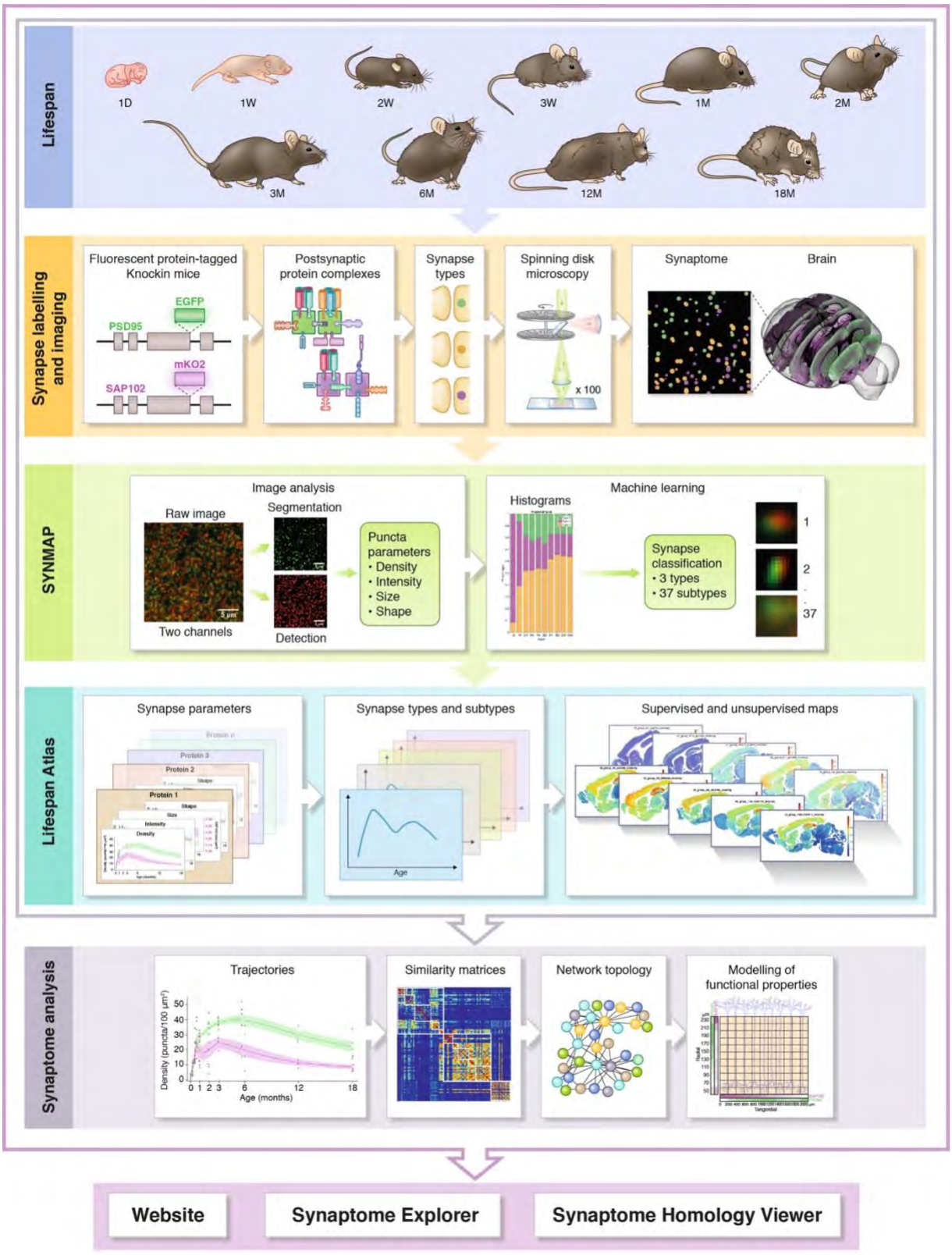
Lifespan
1D
1W
2W
3W
1M
2M
3M
6M
12M
18M
Synapse labelling and imaging
Fluorescent protein-tagged Knockin mice
EGFP
PSD95
mKO2
SAP102
Postsynaptic protein complexes
Synapse types
Spinning disk microscopy
x 100
Synaptome
Brain
SYNMAP
Image analysis
Raw image
Segmentation
Two channels
Detection
Puncta parameters
• Density
• Intensity
• Size
• Shape
Machine learning
Histograms
Synapse classification
• 3 types
• 37 subtypes
1
2
37
Lifespan Atlas
Synapse parameters
Protein 3
Protein 2
Protein 1
Shape
Size
Intensity
Density
Synapse types and subtypes
Age
Supervised and unsupervised maps
Synaptome analysis
Trajectories
Density (puncta/100 µm²)
Age (months)
Similarity matrices
Network topology
Modelling of functional properties
Website
Synaptome Explorer
Synaptome Homology Viewer

Fig. S1: The Mouse Lifespan Synaptome Architecture project

Lifespan, indicates the ten ages analyzed from birth to 18M. Synapse labelling and imaging, shows genetic modification of PSD95 with eGFP and SAP102 with mKO2, which labels the proteins and their respective multiprotein complexes, which are distributed into synapse types/subtypes that can be visualized in brain sections using confocal spinning disc microscopy. SYNMAP, image analysis pipeline that detects, segments, classifies and quantifies synapse puncta, which are categorized into types and subtypes by machine learning. Lifespan Atlas, describes the trajectories of synapse parameters, types and subtypes and houses supervised and unsupervised maps. Synaptome analysis, graphs and heatmaps of trajectories, similarity and hypersimilarity matrices of brain regions, synaptome network topology and modelling of physiological properties. The outputs are disseminated on the Mouse Synaptome Atlas website, using Synaptome Explorer and Synaptome Homology Viewer tools.

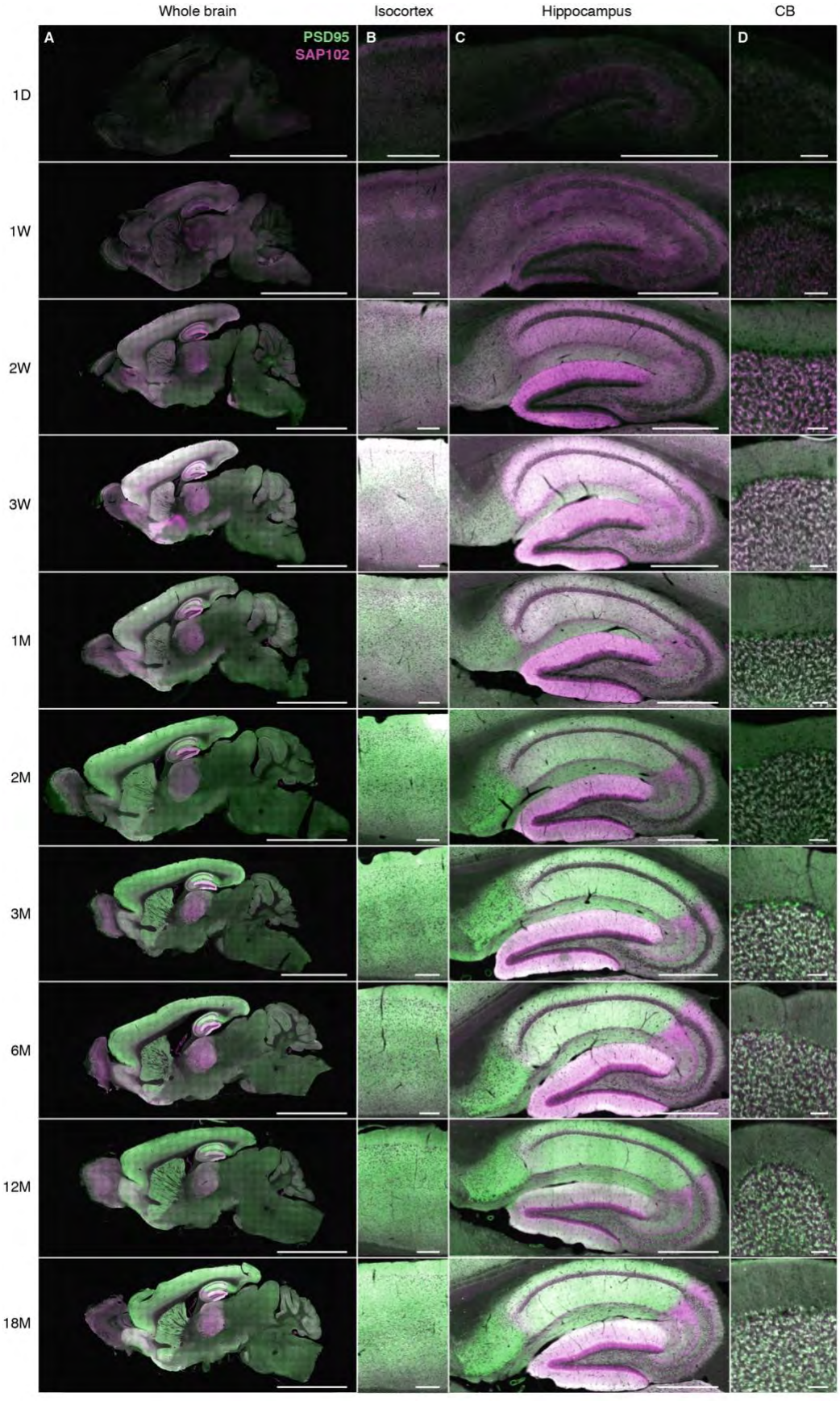
Whole brain
Isocortex
Hippocampus
CB
A
PSD95
SAP102
B
C
D
1D
1W
2W
3W
1M
2M
3M
6M
12M
18M

Fig. S2: Lifespan expression of PSD95-eGFP and SAP102-mKO2 in the mouse brain

Low-magnification images (20X) showing expression of PSD95-eGFP (green) and SAP102-mKO2 (magenta) in the whole brain (A), isocortex (B), hippocampus (C) and cerebellum (CB) (D) at 1D, 1W, 2W, 3W, 1M, 2M, 3M, 6M, 12M and 18M. Scale bars: 4 mm (A); 200 µm (B); 500 µm (C); 50 µm (D).

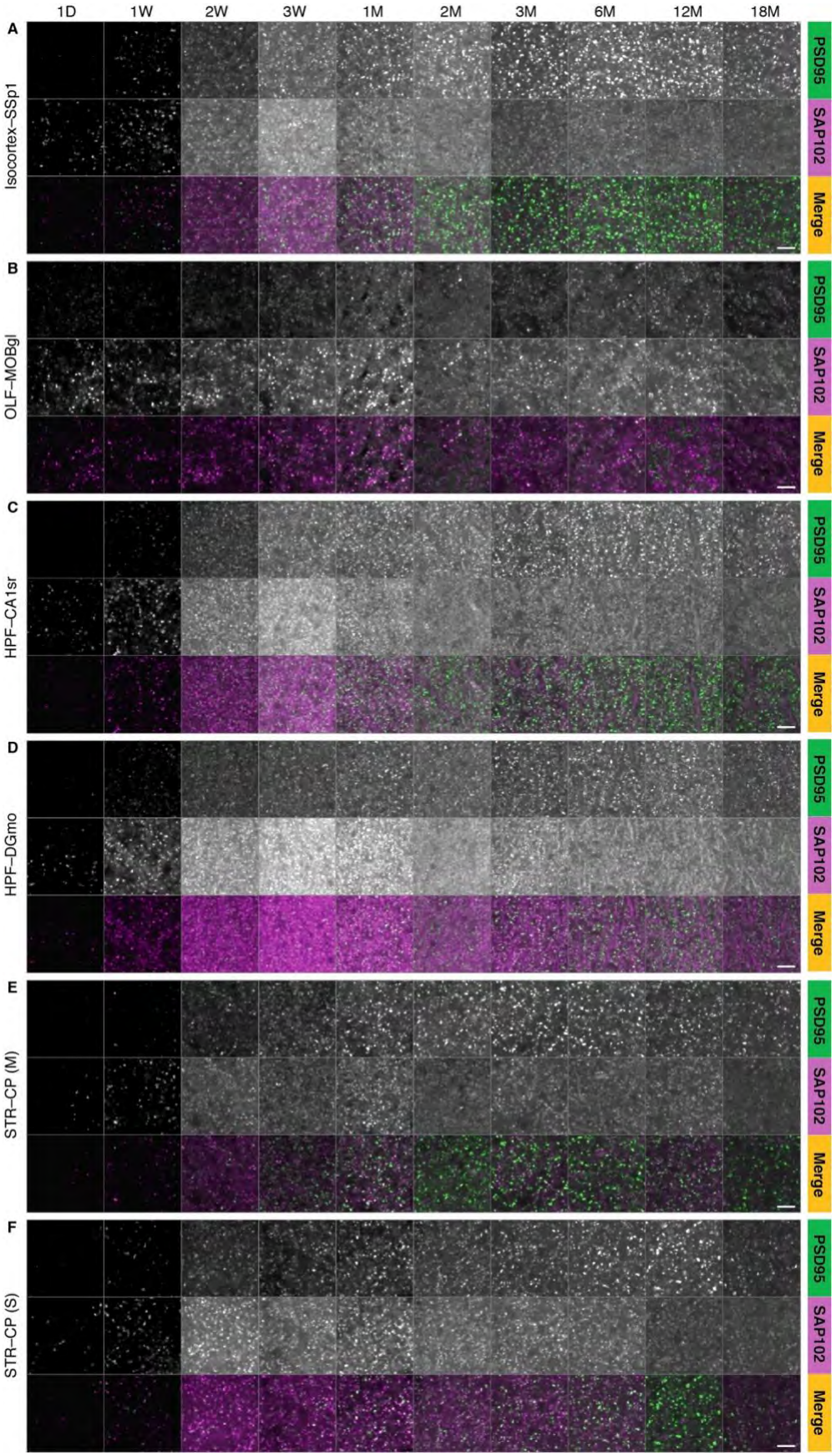
1D
1W
2W
3W
1M
2M
3M
6M
12M
18M
A
Isocortex–SSp1
B
OLF–MOBgl
C
HPF–CA1sr
D
HPF–DGmo
E
STR–CP (M)
F
STR–CP (S)
PSD95
SAP102
Merge

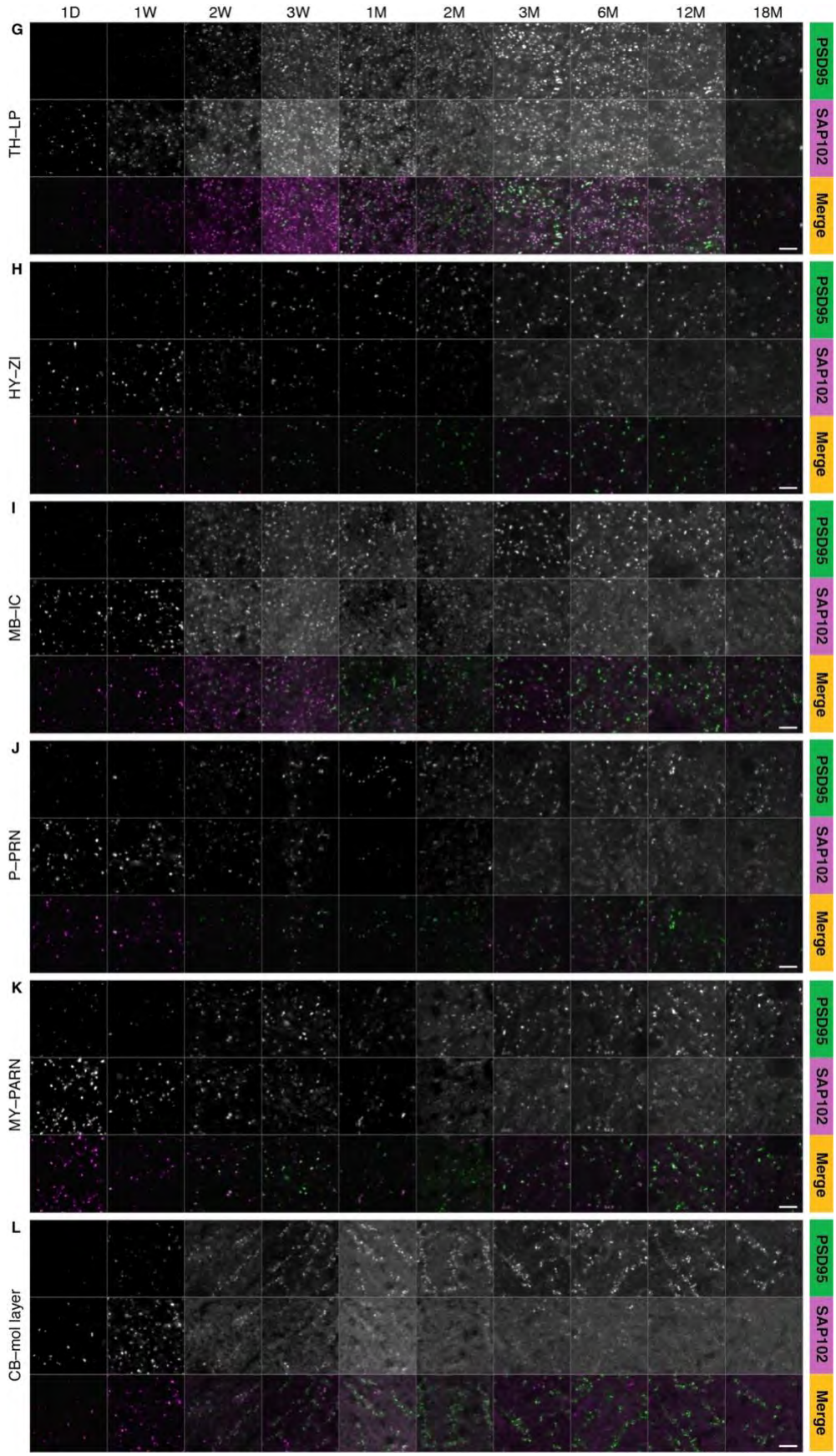
1D
1W
2W
3W
1M
2M
3M
6M
12M
18M
G
TH–LP
H
HY–ZI
I
MB–IC
J
P–PRN
K
MY–PARN
L
CB–mol layer
PSD95
SAP102
Merge

Fig. S3: High-resolution images of PSD95-eGFP and SAP102-mKO2 expression across the mouse lifespan

High-resolution images (100X objective) showing expression of PSD95-eGFP (green, top panels), SAP102-mKO2 (magenta, middle panels) and merge (bottom panels) at the indicated time points in the following brain regions: isocortex, primary somatosensory area (SSp1) (A); olfactory areas (OLF), glomerular layer of the main olfactory bulb (MOBgl) (B); hippocampal formation (HPF), stratum radiatum of CA1 field (CA1sr) (C) and dentate gyrus molecular layer (DGmo) (D); striatum (STR), caudate putamen (CP): matrix compartment (E) and striosomes (F); thalamus (TH), lateral posterior nucleus (LP) (G); hypothalamus (HY), zona incerta (ZI) (H); midbrain (MB), inferior colliculus (IC) (I); pons (P), pontine reticular nucleus (PRN) (J); medulla (MY), parvicellular reticular nucleus (PARN) (K); cerebellum (CB), molecular (mol) layer (L). Scale bars: 3.5 µm.

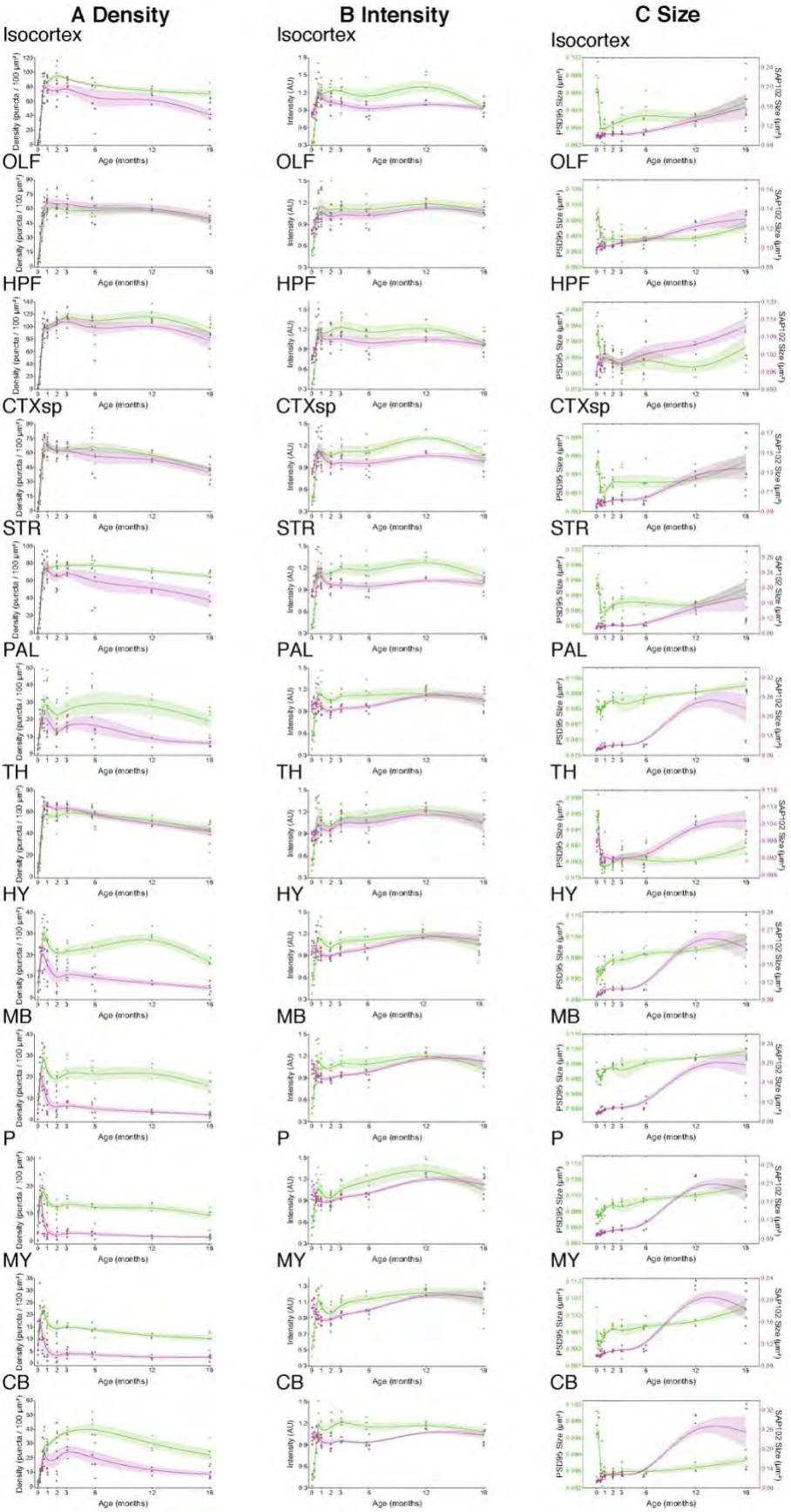
A Density
B Intensity
C Size
Isocortex
OLF
HPF
CTXsp
STR
PAL
TH
HY
MB
P
MY
CB
Density (puncta / 100 µm²)
Intensity (AU)
PSD95 Size (µm²)
SAP102 Size (µm²)
Age (months)

Fig. S4: Lifespan trajectories of PSD95 and SAP102 synapse parameters in brain regions

Lifespan trajectories of PSD95 (green) and SAP102 (magenta) synapse density (A), intensity (normalized to mean intensity) (B) and size (C) from 1D to 18M in 12 main brain regions. Scatter points indicate the value of the parameter averaged over space for individual mice, lines are the β-spline curves of mean values across mice (1D, N=5; 1W, N=5; 2W, N=5; 3W, N=4; 1M, N=6; 2M, N=6; 3M, N=5; 6M, N=5; 12M, N=3; 18M, N=5) and grayed areas represent the standard error of the mean. Twelve brain regions shown: isocortex, olfactory areas (OLF), hippocampal formation (HPF), cortical subplate (CTXsp), striatum (STR), pallidum (PAL), thalamus (TH), hypothalamus (HY), midbrain (MB), pons (P), medulla (MY) and cerebellum (CB).

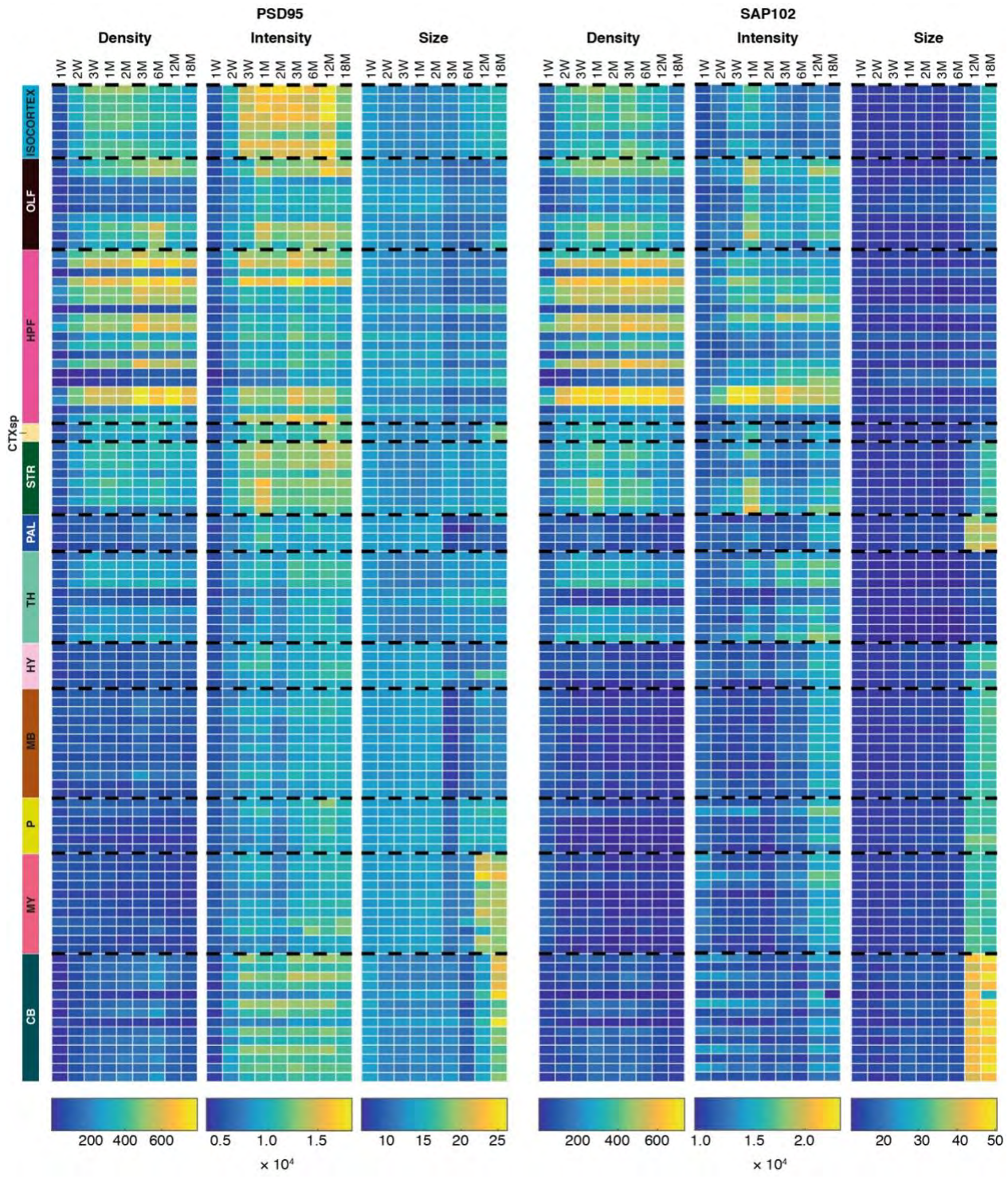
PSD95
SAP102
Density
Intensity
Size
1W
2W
3W
1M
2M
3M
6M
12M
18M
ISOCORTEX
OLF
HPF
CTXsp
STR
PAL
TH
HY
MB
P
MY
CB
200 400 600
0.5 1.0 1.5
× 10⁴
10 15 20 25
200 400 600
1.0 1.5 2.0
× 10⁴
20 30 40 50

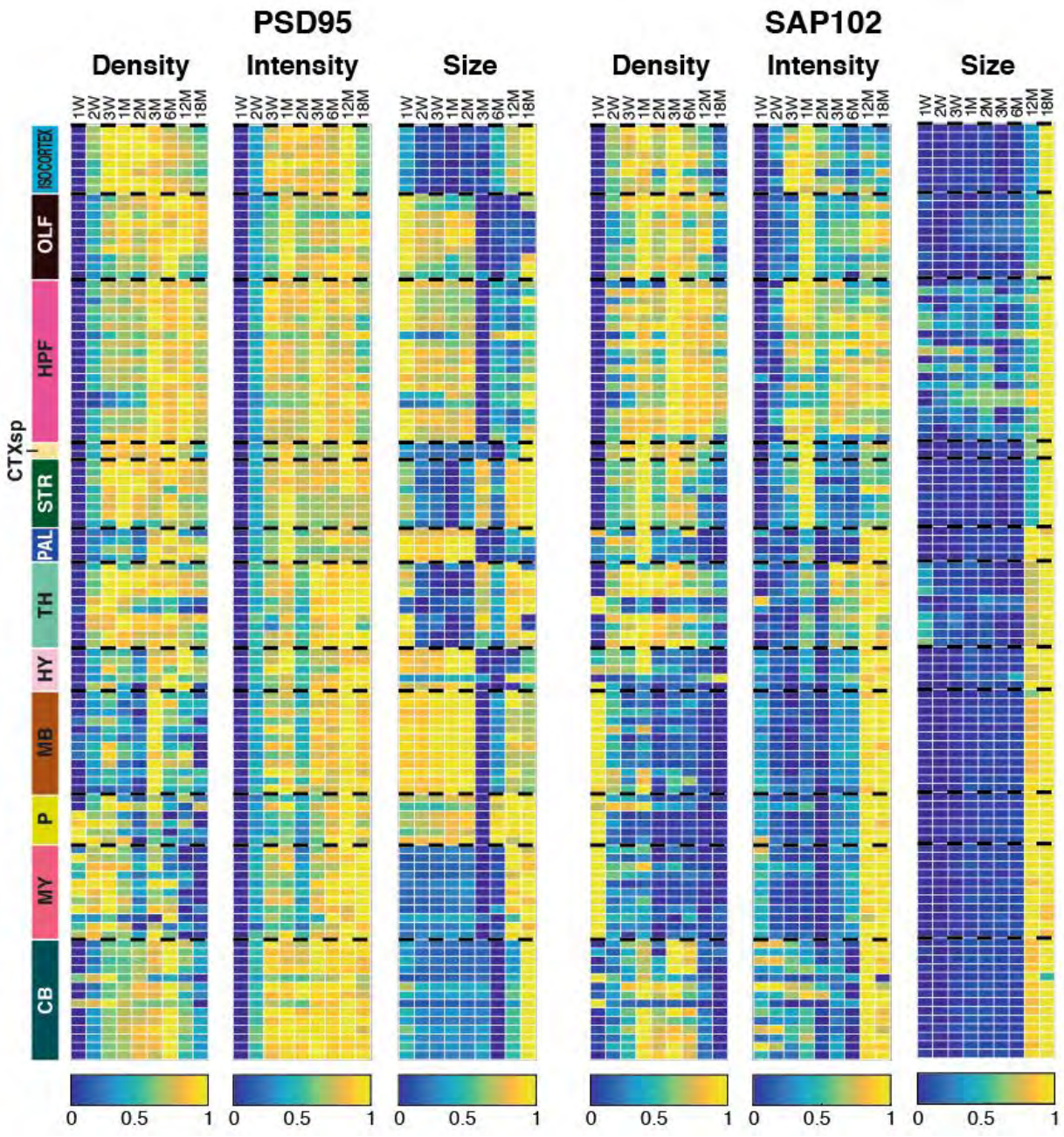

Fig. S5: Heatmaps of lifespan trajectories of PSD95 and SAP102 synapse parameters in brain subregions

Top six panels show lifespan trajectories of raw (mean) values of density, intensity and size of PSD95 and SAP102 puncta in 109 brain subregions (see Table S1 for subregion names). Scale: puncta number per 21.5 × 21.5μm unit area for density, 16-bit grayscale values for intensity, pixel

number for size (1 pixel = 84 nm). Bottom six panels show lifespan trajectories of normalized values (normalization between 0-1 across lifespan each subregion) of density, intensity and size of PSD95 and SAP102 puncta in brain subregions. Heatmaps of raw values are useful to compare different brain subregions whereas normalized heatmaps highlight differences across the lifespan within individual subregions. Twelve brain regions shown: isocortex, olfactory areas (OLF), hippocampal formation (HPF), cortical subplate (CTXsp), striatum (STR), pallidum (PAL), thalamus (TH), hypothalamus (HY), midbrain (MB), pons (P), medulla (MY) and cerebellum (CB). Subregion key, Table S1.

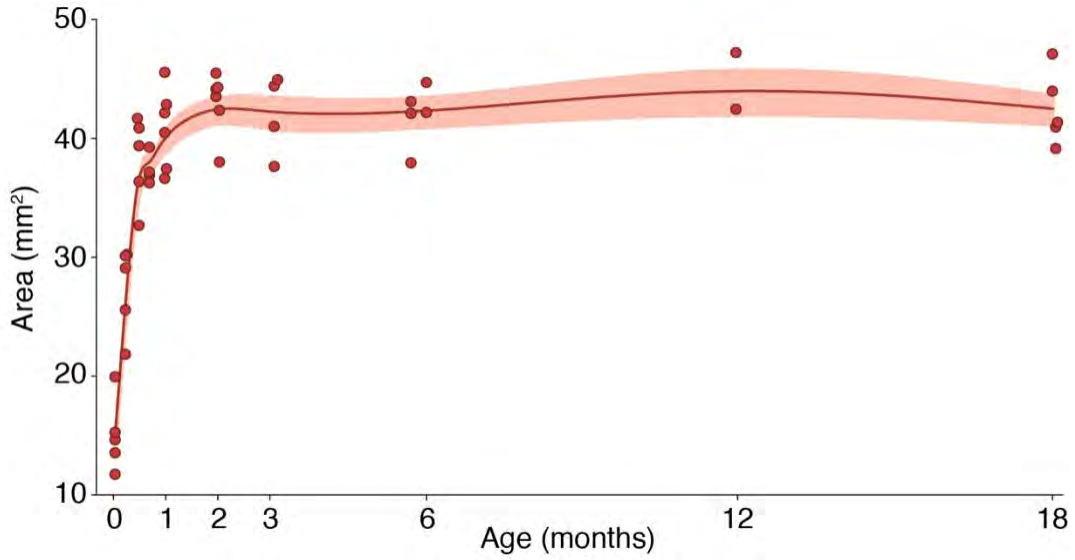

Figure S6. Trajectory of brain size across the lifespan

Area of the whole brain section was measured at each time point (1D, N=5; 1W, N=5; 2W, N=5; 3W, N=4; 1M, N=6; 2M, N=6; 3M, N=4; 6M, N=5; 12M, N=2; 18M, N=5). Scatter points indicate the area for individual mice, lines are the β-spline curves of mean values across mice and grayed areas represent the standard error of the mean. Brain size does not significantly vary between 3M (41.98 ± 1.69 mm_2) and 18M (42.50 ± 1.39 mm_2) (Cohen's *d* = 0.29; t-test *P* = 0.82).

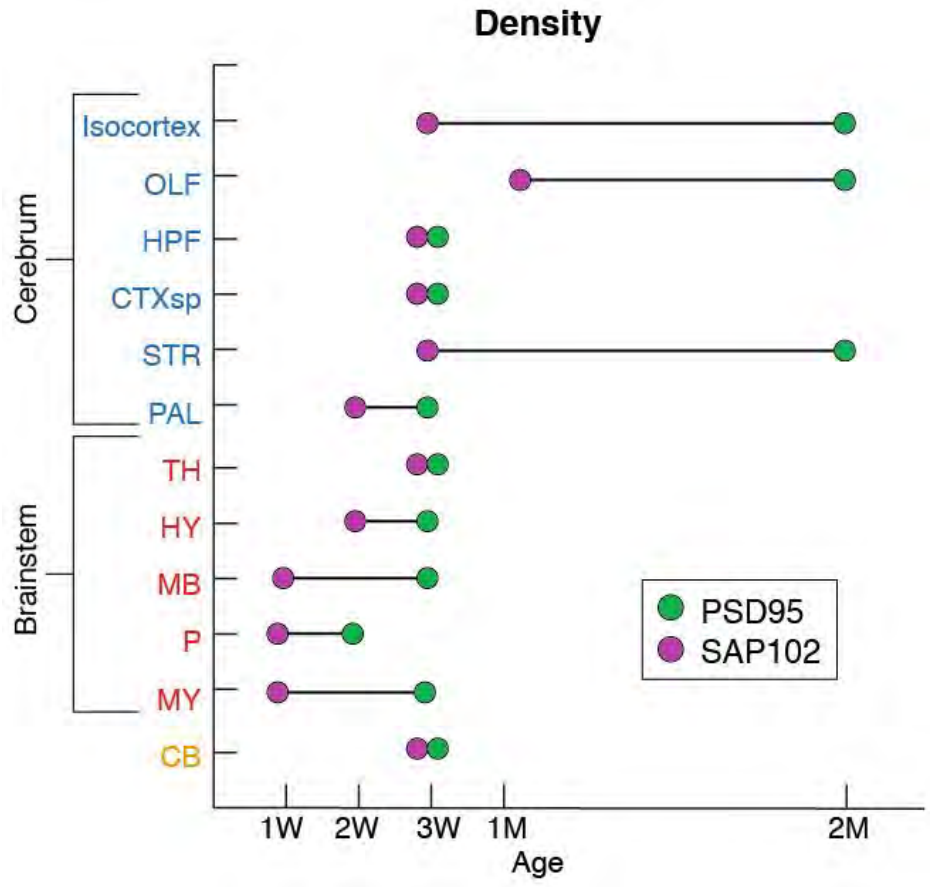

Fig. S7: Age of the first peak value for the density parameter

PSD95-eGFP (green) and SAP102-mKO2 (magenta). Regions: isocortex, olfactory areas (OLF), hippocampal formation (HPF), cortical subplate (CTXsp), striatum (STR), pallidum (PAL), thalamus (TH), hypothalamus (HY), midbrain (MB), pons (P), medulla (MY), cerebellum (CB).

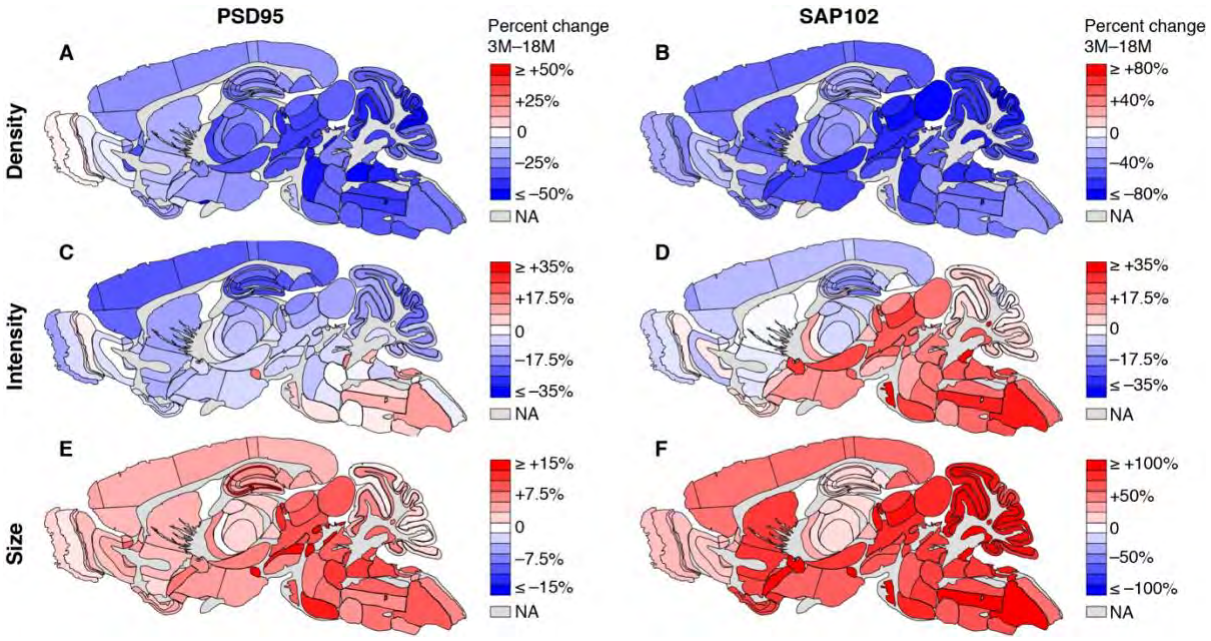

Fig. S8: Spatial maps of synapse changes between 3M and 18M

Percentage change between 3M and 18M is color coded in each subregion for PSD95 density (A), SAP102 density (B), PSD95 intensity (C), SAP102 intensity (D), PSD95 size (E) and SAP102 size (F). Increase is indicated in red and decrease in blue; NA, not assessed.

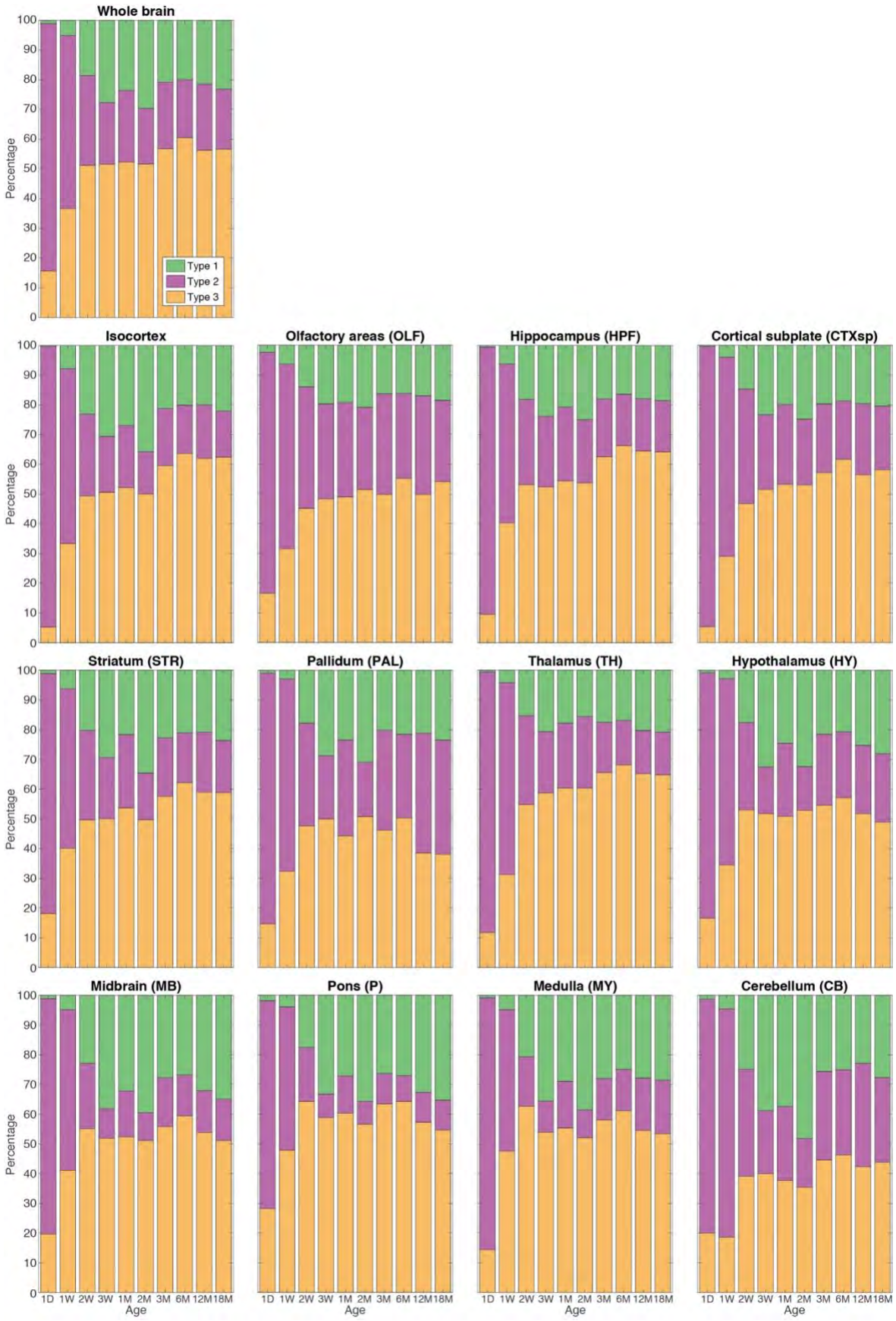
Whole brain
Isocortex
Olfactory areas (OLF)
Hippocampus (HPF)
Cortical subplate (CTXsp)
Striatum (STR)
Pallidum (PAL)
Thalamus (TH)
Hypothalamus (HY)
Midbrain (MB)
Pons (P)
Medulla (MY)
Cerebellum (CB)
Type 1
Type 2
Type 3
Percentage
Age
1D 1W 2W 3W 1M 2M 3M 6M 12M 18M

Fig. S9: Relative abundance of synapse types in whole brain and brain regions

Stacked bar plots of the percentage of type 1 (PSD95 only), type 2 (SAP102 only) and type 3 (PSD95+SAP102) synapses in the whole brain and 12 main regions across the lifespan.

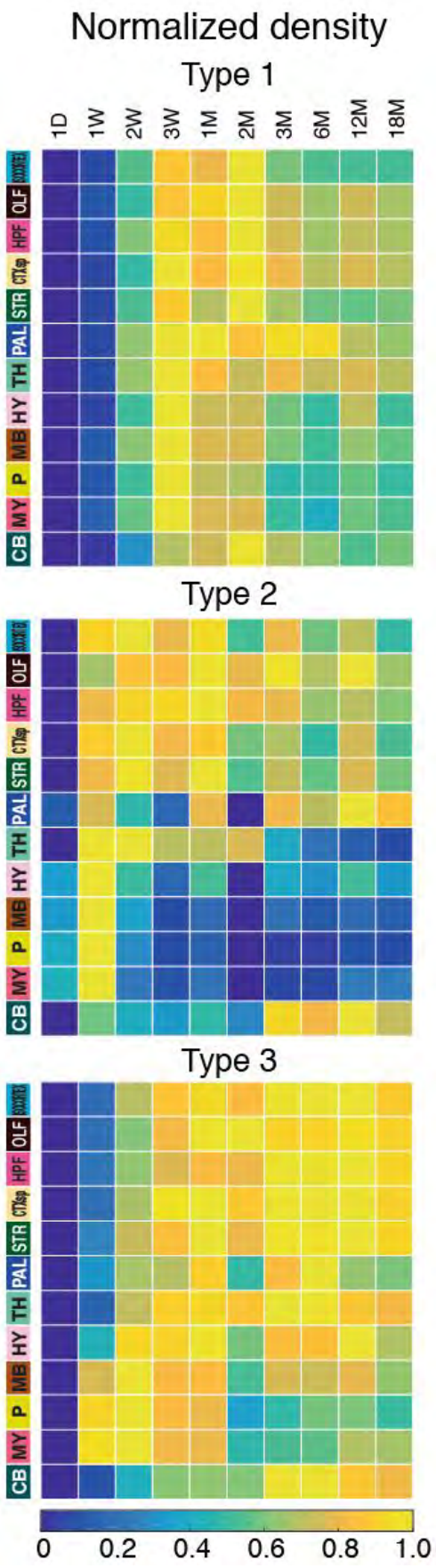
Normalized density
Type 1
1D
1W
2W
3W
1M
2M
3M
6M
12M
18M
OLF
HPF
STR
PAL
TH
HY
MB
P
MY
CB
Type 2
Type 3
0
0.2
0.4
0.6
0.8
1.0

Fig. S10: Lifespan trajectories of synapse type density for each of 12 main brain regions

Lifespan trajectories of synapse type density for each of 12 main brain regions (rows). Density in each region was normalized (0-1) to its maximal density across the lifespan (columns). Twelve brain regions shown: isocortex, olfactory areas (OLF), hippocampal formation (HPF), cortical subplate (CTXsp), striatum (STR), pallidum (PAL), thalamus (TH), hypothalamus (HY), midbrain (MB), pons (P), medulla (MY) and cerebellum (CB).

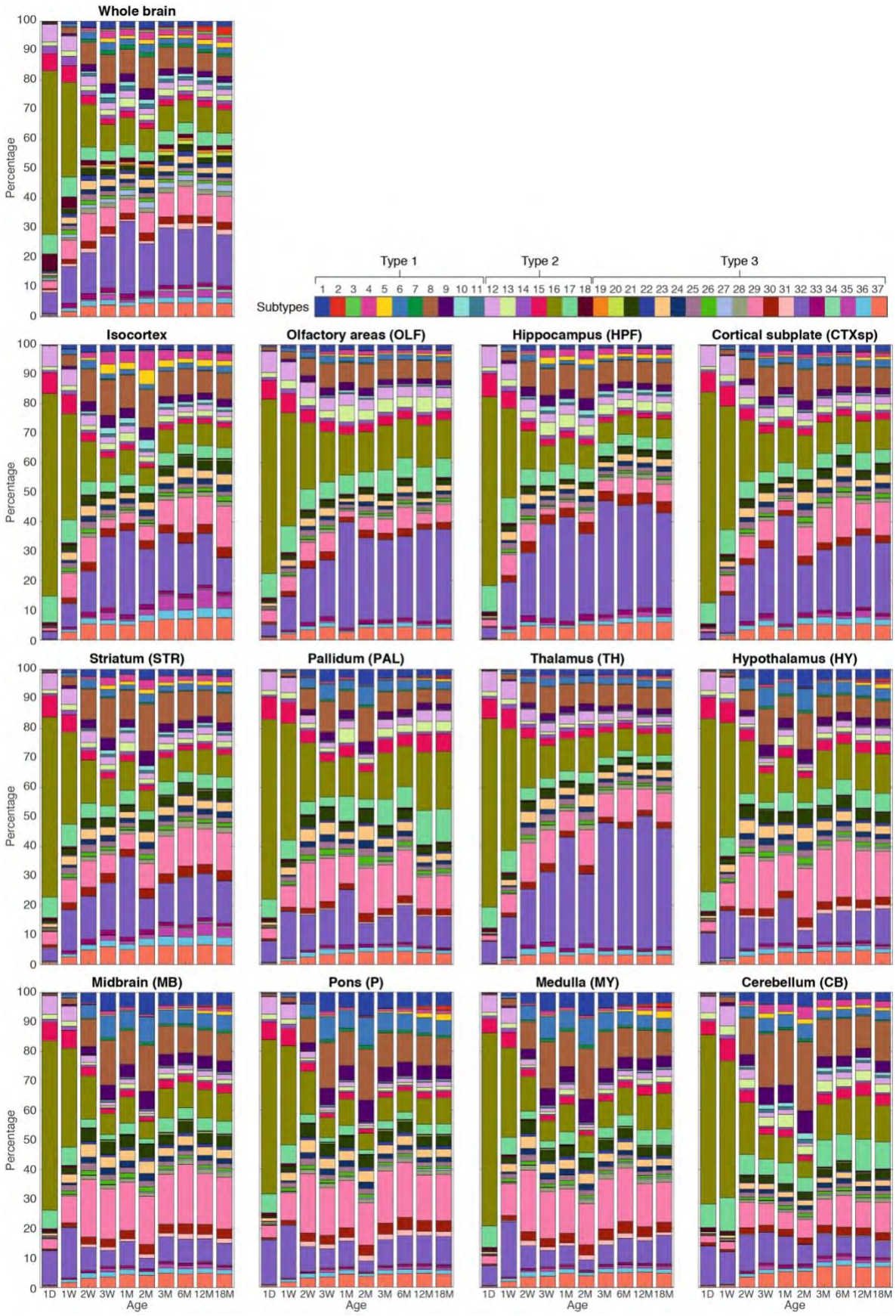
Whole brain
Type 1
Type 2
Type 3
1 2 3 4 5 6 7 8 9 10 11 12 13 14 15 16 17 18 19 20 21 22 23 24 25 26 27 28 29 30 31 32 33 34 35 36 37
Subtypes
Isocortex
Olfactory areas (OLF)
Hippocampus (HPF)
Cortical subplate (CTXsp)
Striatum (STR)
Pallidum (PAL)
Thalamus (TH)
Hypothalamus (HY)
Midbrain (MB)
Pons (P)
Medulla (MY)
Cerebellum (CB)
Percentage
0 10 20 30 40 50 60 70 80 90 100
1D 1W 2W 3W 1M 2M 3M 6M 12M 18M
Age

Fig. S11: Relative abundance of synapse subtypes in whole brain and brain regions

Stacked bar plots of the percentage of 37 synapse subtypes in the whole brain and 12 main regions across the lifespan. Key: color codes for synapse types and subtypes.

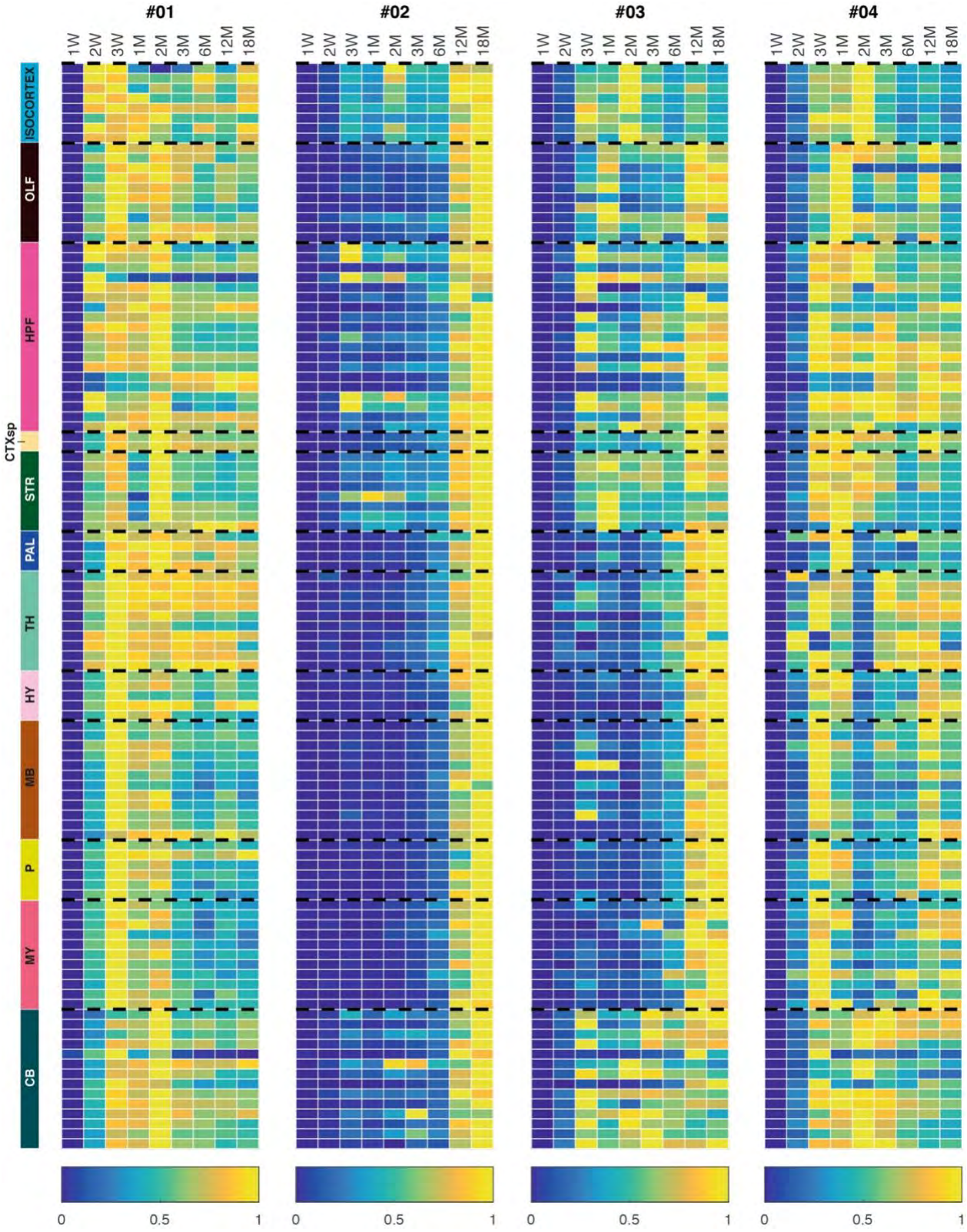
#01
#02
#03
#04
1W
2W
3W
1M
2M
3M
6M
12M
18M
ISOCORTEX
OLF
HPF
CTXsp
STR
PAL
TH
HY
MB
P
MY
CB
0
0.5
1

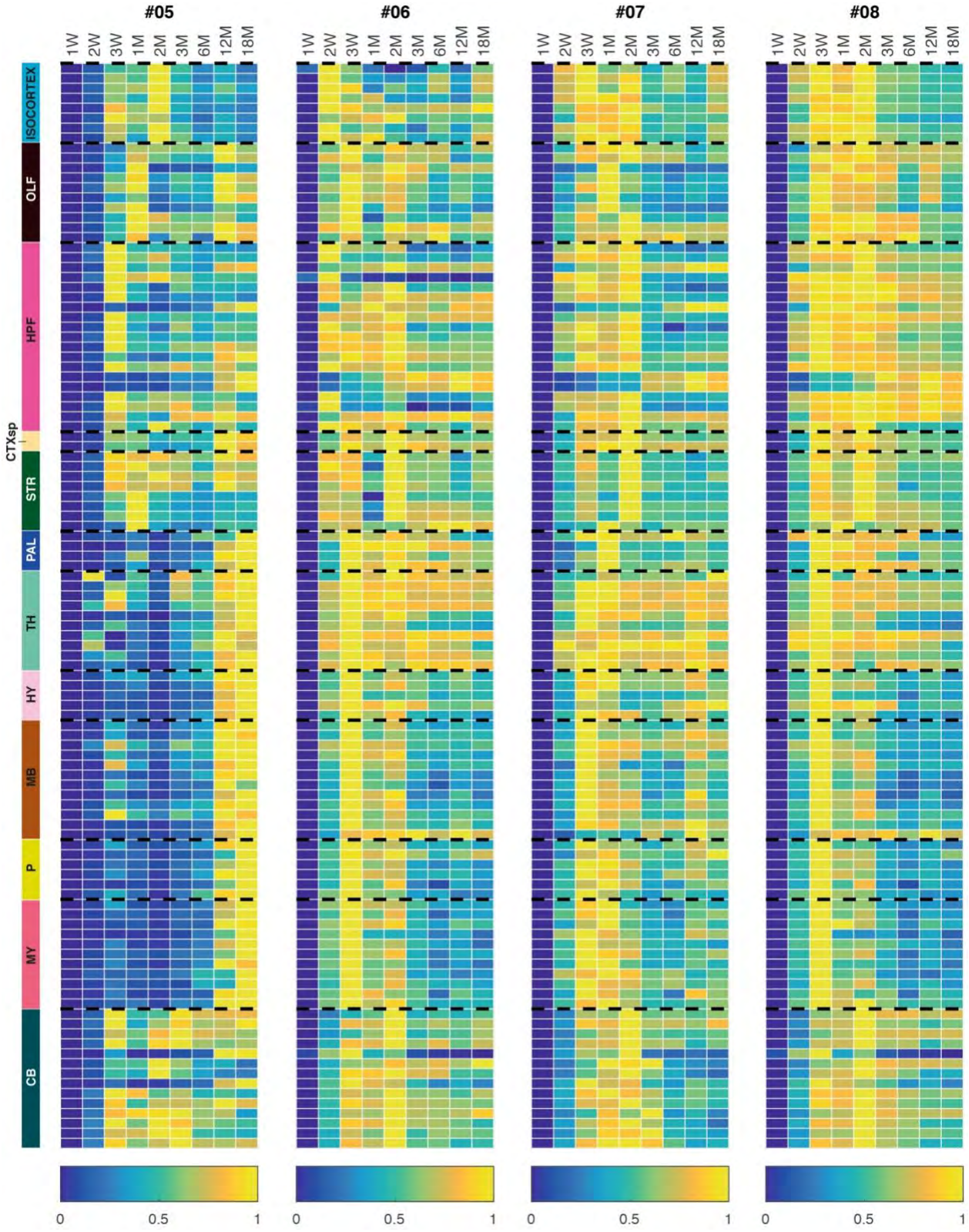
#05
#06
#07
#08
1W
2W
3W
1M
2M
3M
6M
12M
18M
ISOCORTEX
OLF
HPF
CTXsp
STR
PAL
TH
HY
MB
P
MY
CB
0
0.5
1

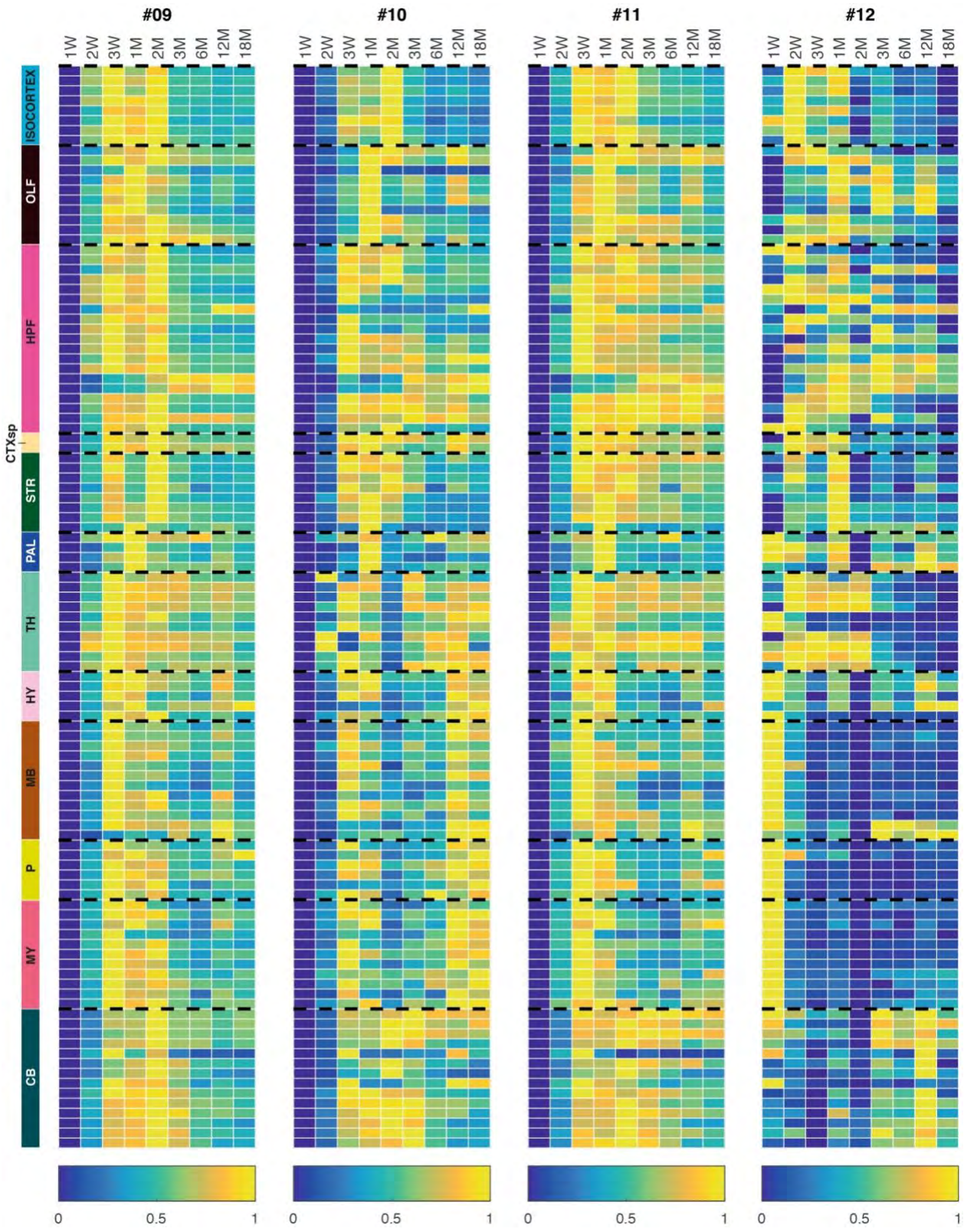
#09
#10
#11
#12
1W
2W
3W
1M
2M
3M
6M
12M
18M
ISOCORTEX
OLF
HPF
CTXsp
STR
PAL
TH
HY
MB
P
MY
CB
0
0.5
1

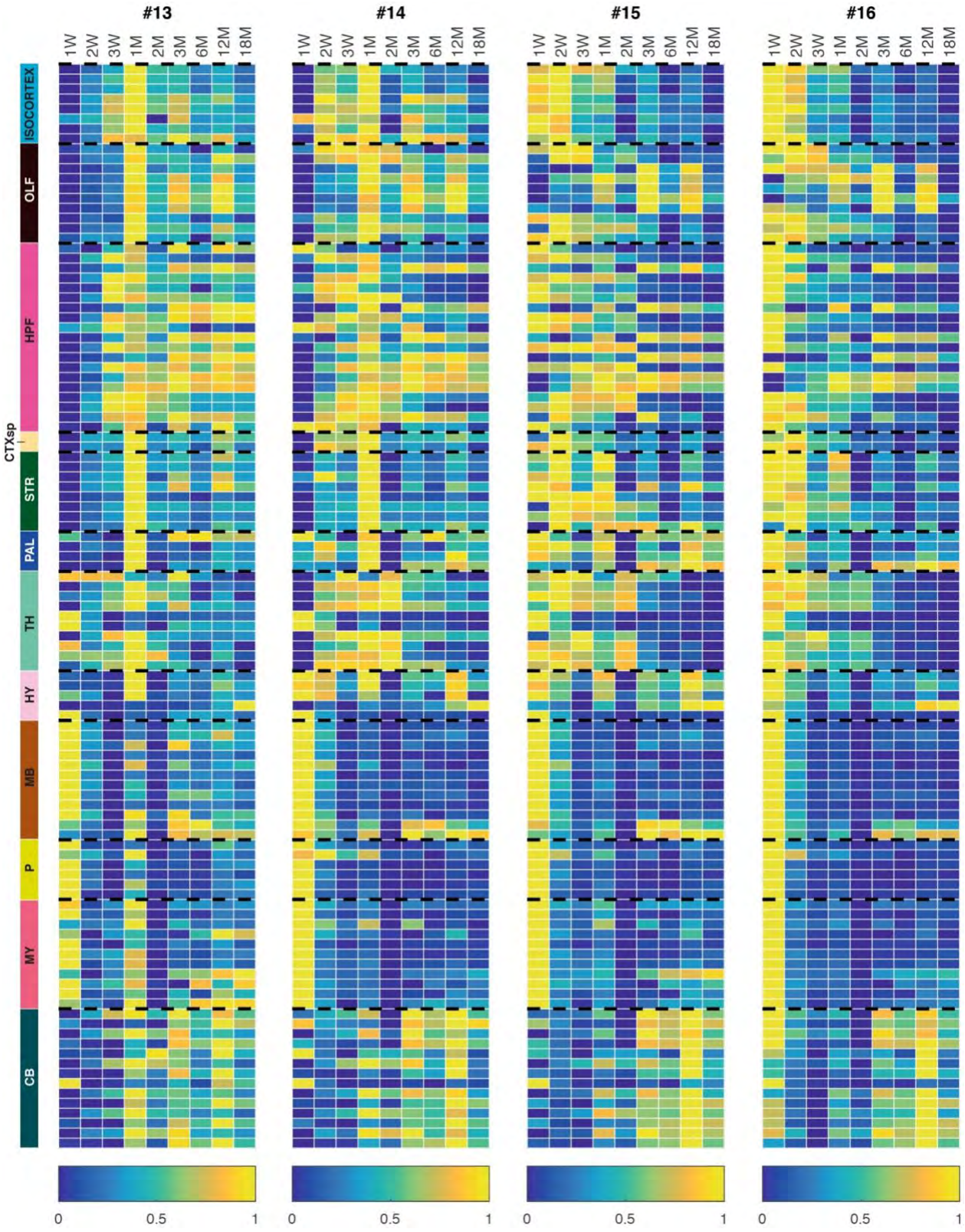
#13
#14
#15
#16
1W
2W
3W
1M
2M
3M
6M
12M
18M
ISOCORTEX
OLF
HPF
CTXsp
STR
PAL
TH
HY
MB
P
MY
CB
0
0.5
1

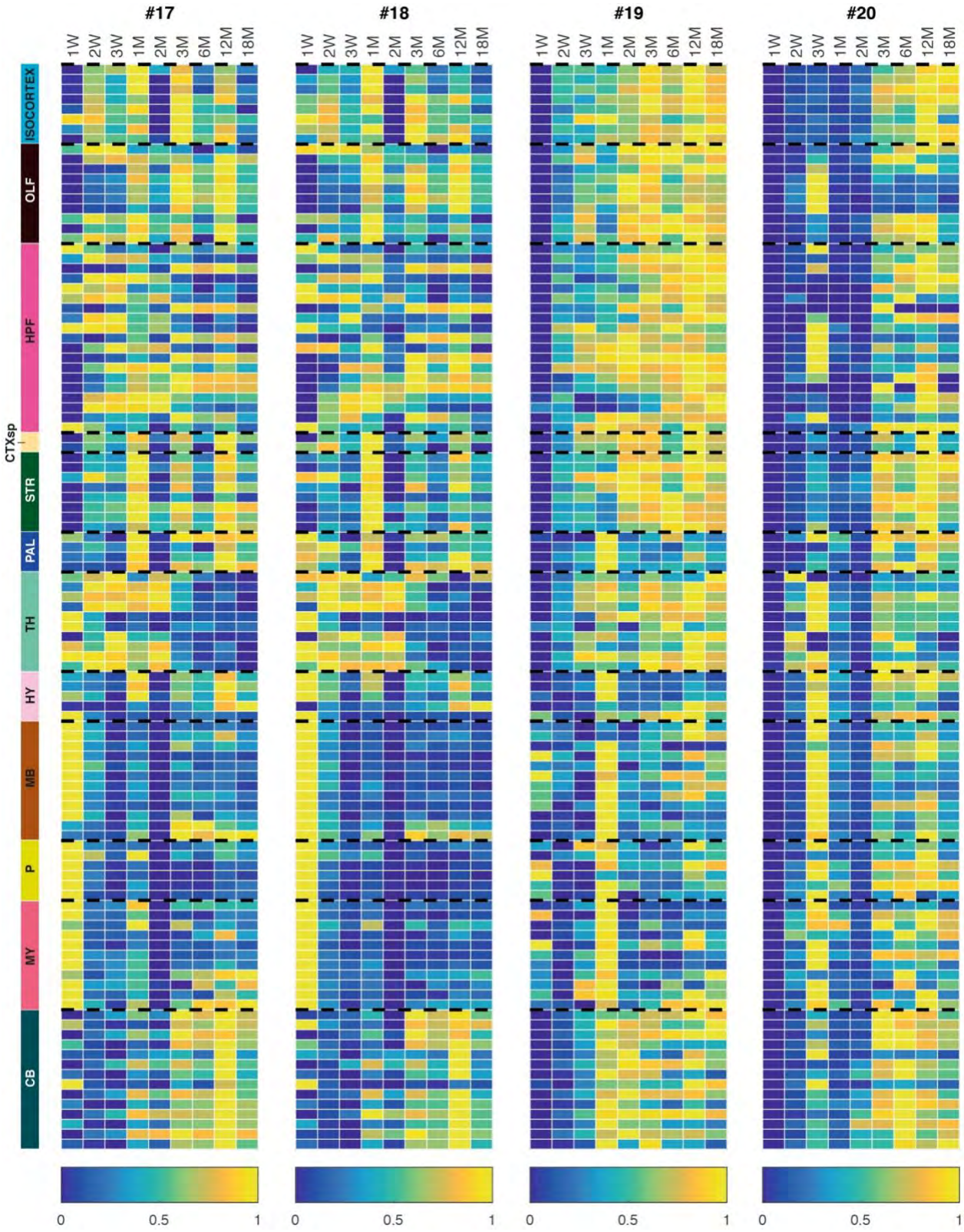
#17
#18
#19
#20
1W
2W
3W
1M
2M
3M
6M
12M
18M
ISOCORTEX
OLF
HPF
CTXsp
STR
PAL
TH
HY
MB
P
MY
CB
0
0.5
1

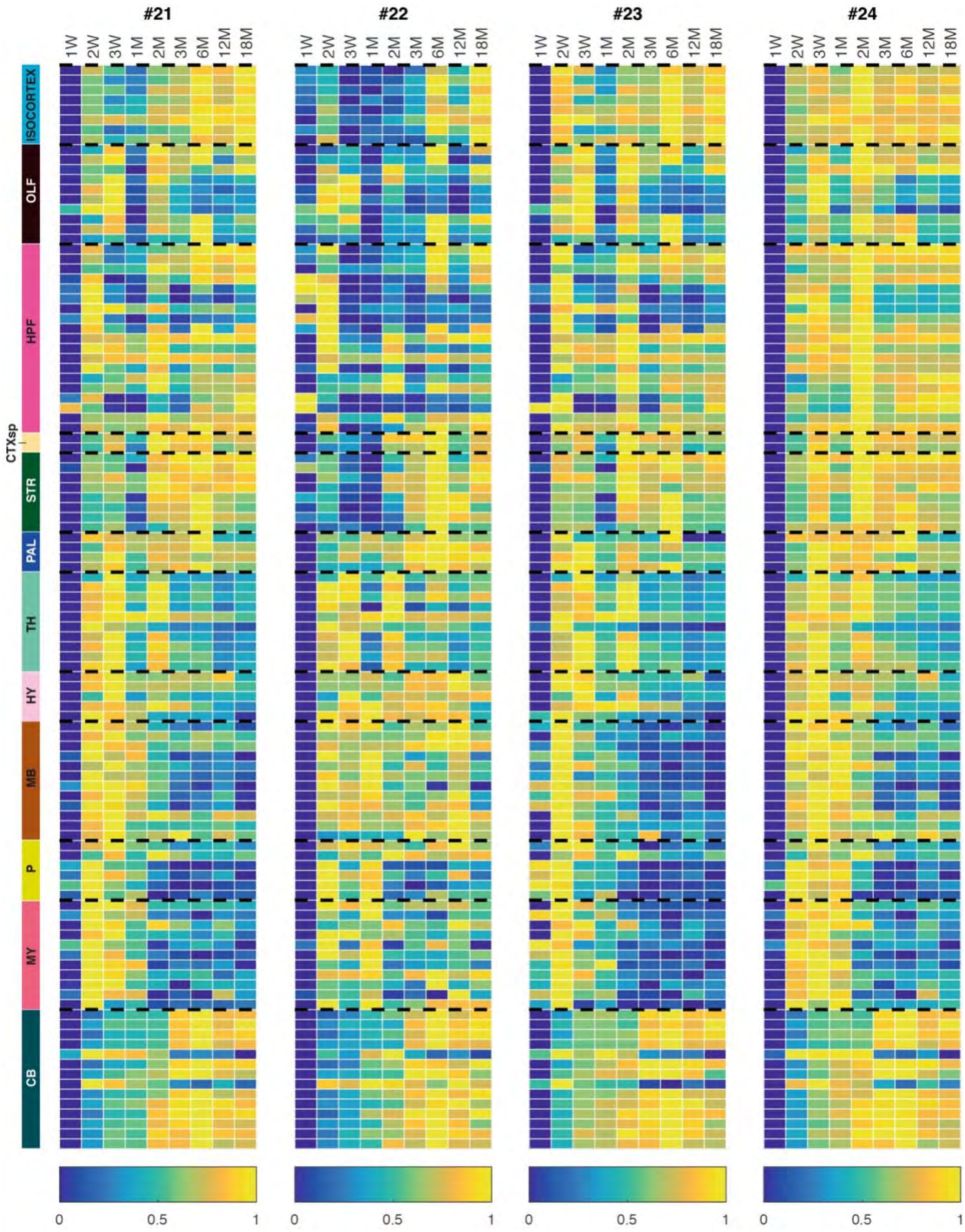
#21
#22
#23
#24
1W
2W
3W
1M
2M
3M
6M
12M
18M
ISOCORTEX
OLF
HPF
CTXsp
STR
PAL
TH
HY
MB
P
MY
CB
0
0.5
1

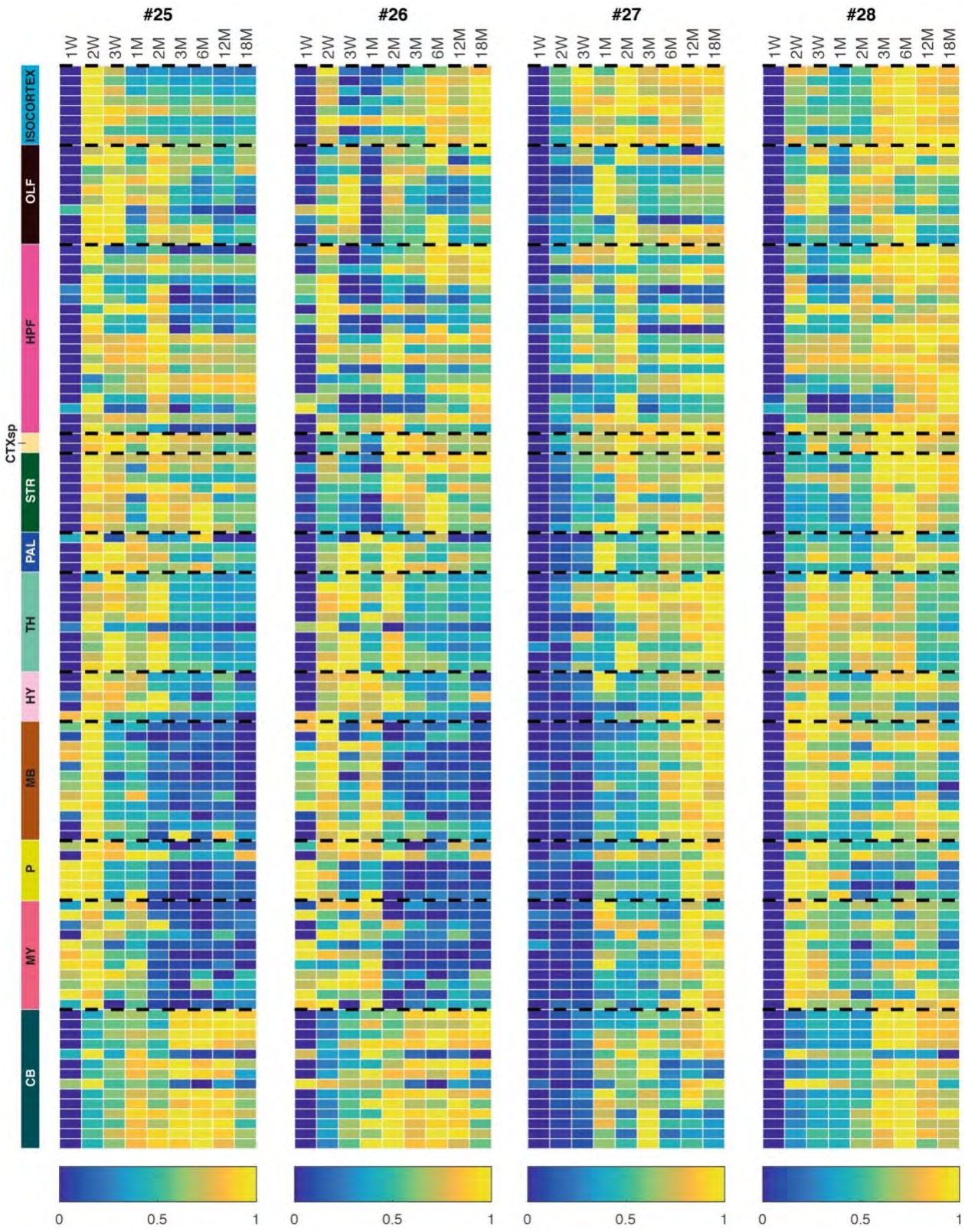
#25
#26
#27
#28
1W
2W
3W
1M
2M
3M
6M
12M
18M
ISOCORTEX
OLF
HPF
CTXsp
STR
PAL
TH
HY
MB
P
MY
CB
0
0.5
1

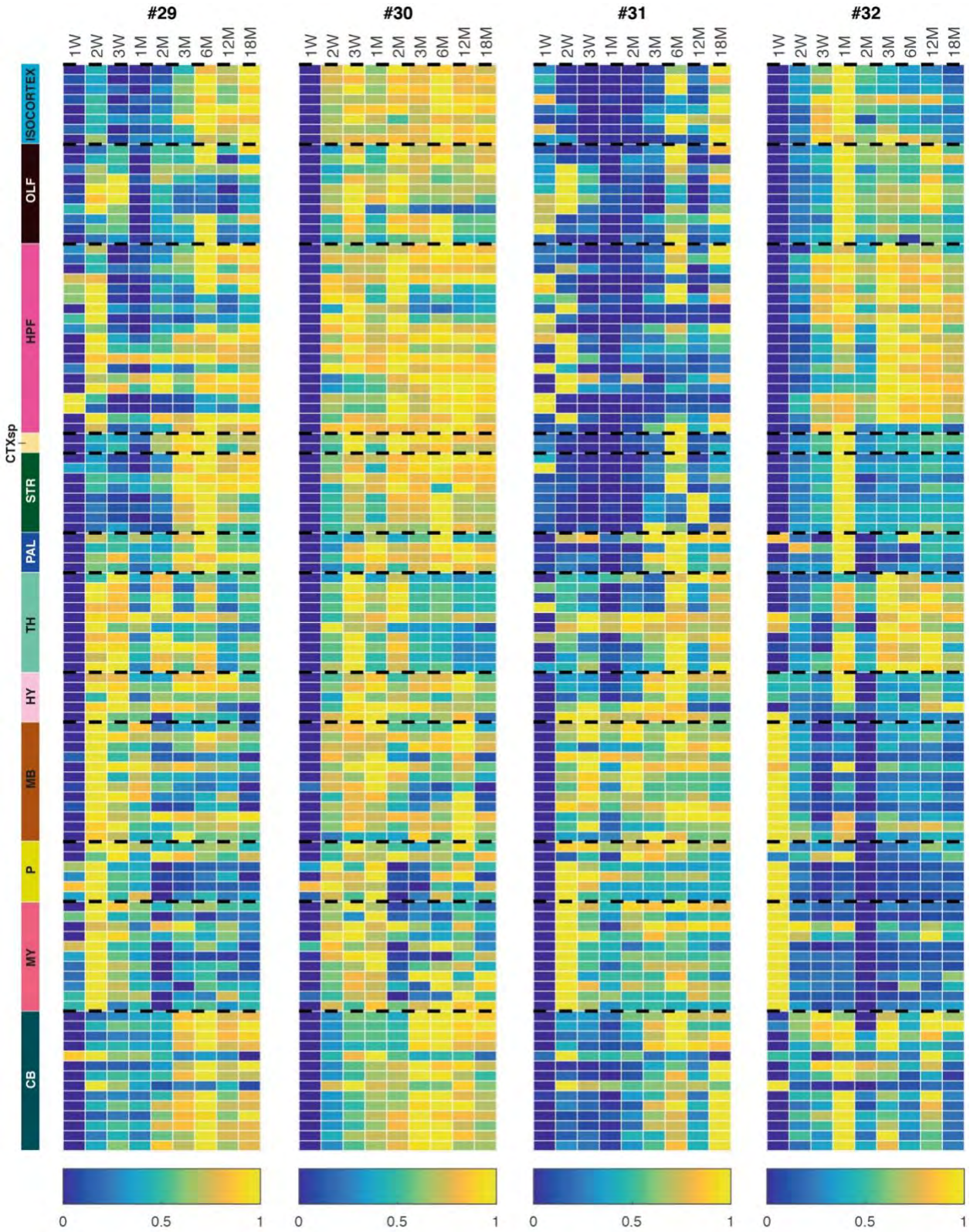
#29
#30
#31
#32
1W
2W
3W
1M
2M
3M
6M
12M
18M
ISOCORTEX
OLF
HPF
CTXsp
STR
PAL
TH
HY
MB
P
MY
CB
0
0.5
1

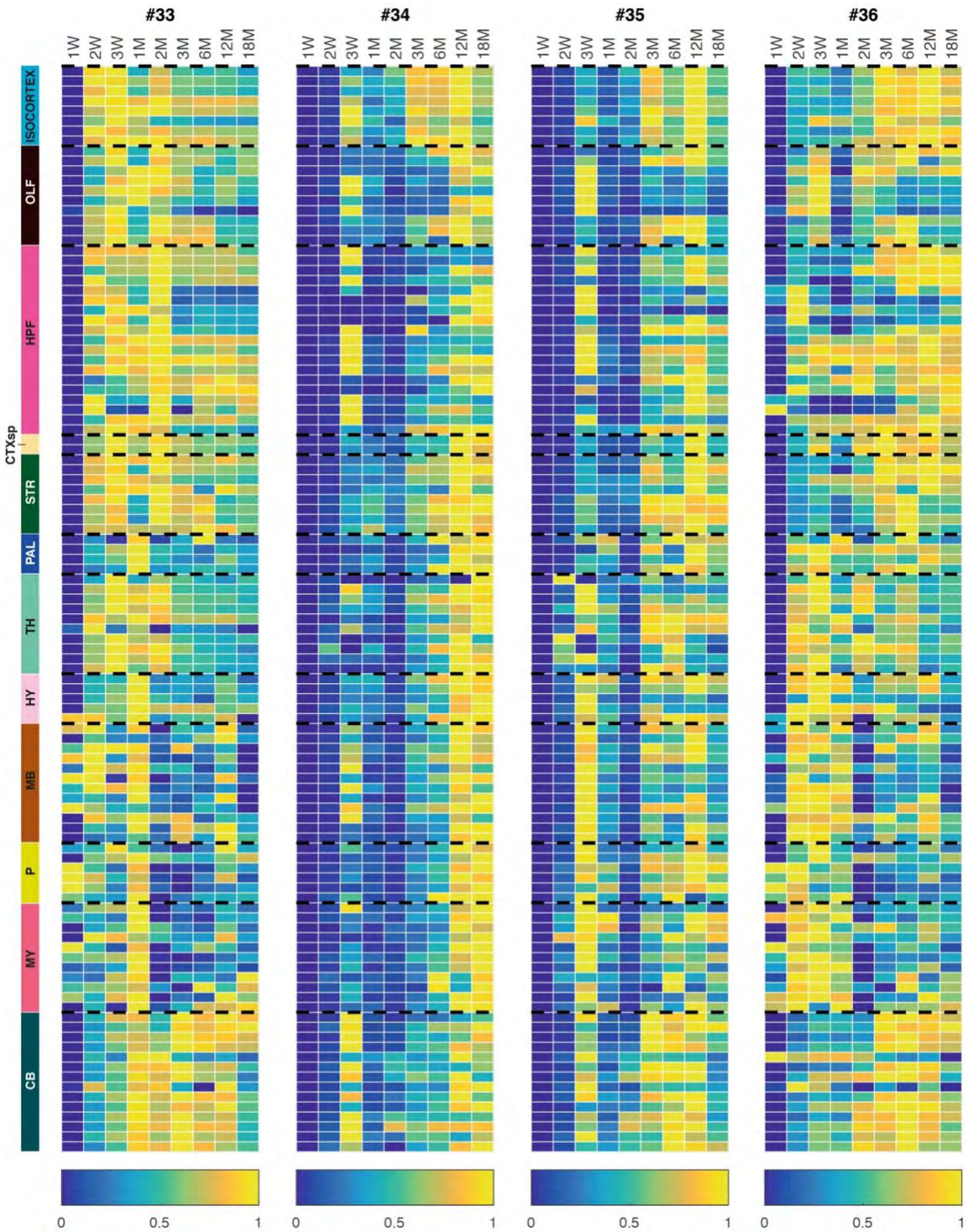
#33
#34
#35
#36
1W
2W
3W
1M
2M
3M
6M
12M
18M
ISOCORTEX
OLF
HPF
CTXsp
STR
PAL
TH
HY
MB
P
MY
CB
0
0.5
1

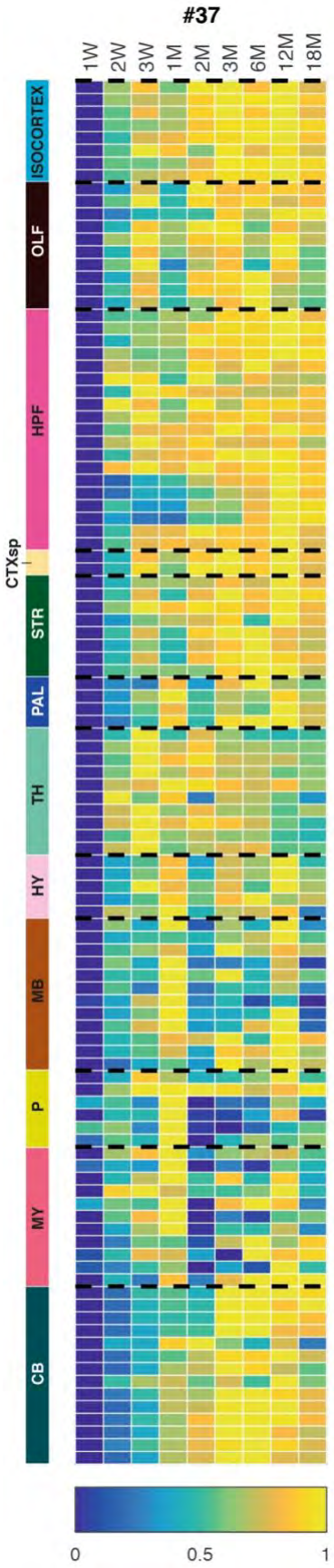
#37
1W
2W
3W
1M
2M
3M
6M
12M
18M
ISOCORTEX
OLF
HPF
CTXsp
STR
PAL
TH
HY
MB
P
MY
CB
0
0.5
1

Fig. S12: Heatmaps of lifespan trajectories of 37 synapse subtypes

Lifespan trajectories of (normalized) density in each of 109 subregions (rows, see Table S1) for each of 37 synapse subtypes. Density in each subregion was normalized (0-1) to its maximal and minimal densities across the lifespan (rows). Twelve brain regions shown: isocortex, olfactory areas (OLF), hippocampal formation (HPF), cortical subplate (CTXsp), striatum (STR), pallidum (PAL), thalamus (TH), hypothalamus (HY), midbrain (MB), pons (P), medulla (MY) and cerebellum (CB). Subregion key, Table S1.

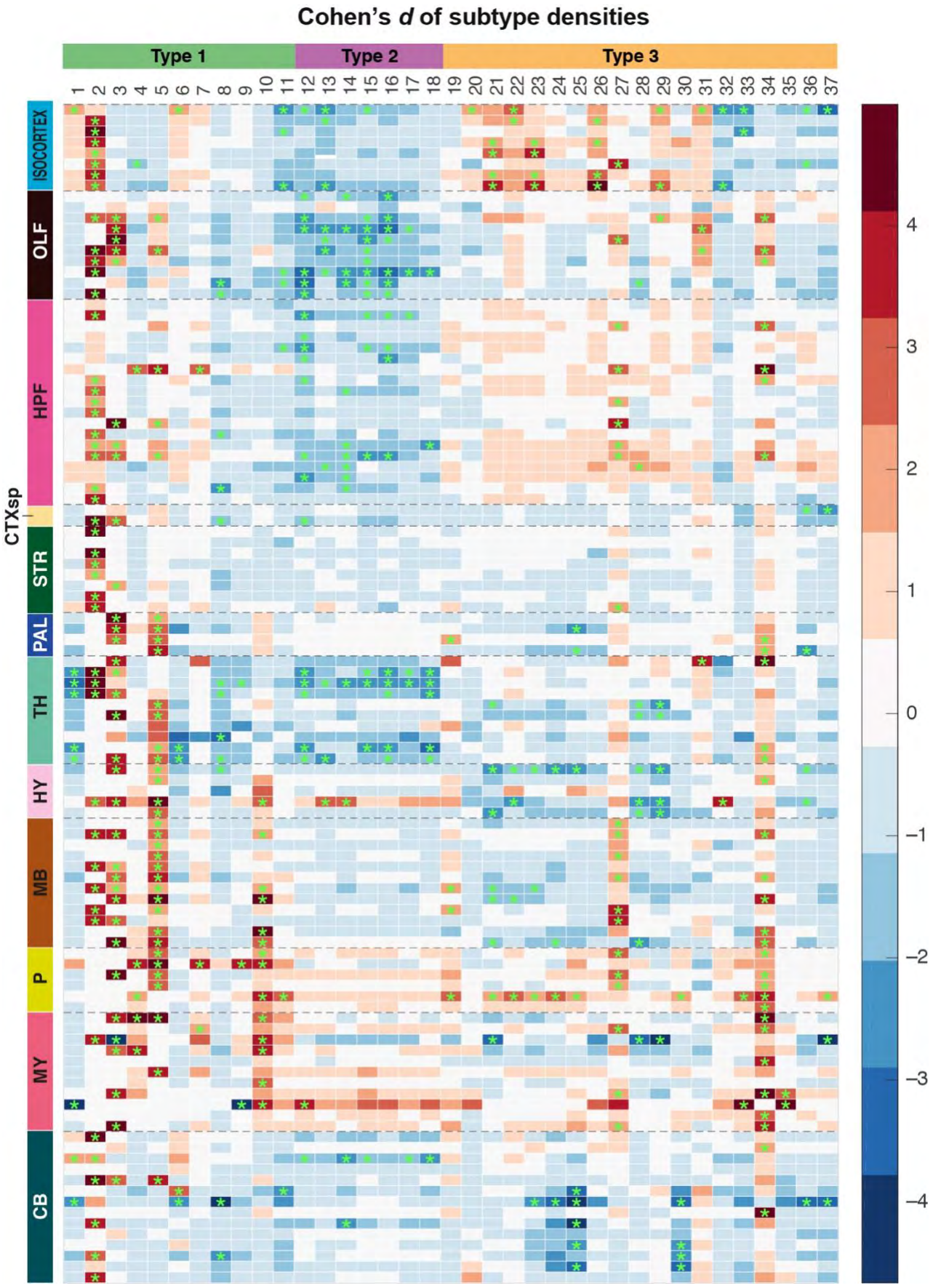
Cohen's d of subtype densities
Type 1
Type 2
Type 3
1 2 3 4 5 6 7 8 9 10 11 12 13 14 15 16 17 18 19 20 21 22 23 24 25 26 27 28 29 30 31 32 33 34 35 36 37
ISOCORTEX
OLF
HPF
CTXsp
STR
PAL
TH
HY
MB
P
MY
CB
4
3
2
1
0
−1
−2
−3
−4

Fig. S13: Changes in synapse subtypes in brain subregions between 3M and 18M

Heatmap showing the change (Cohen's *d*, scale bar indicates increase in red and decrease in blue) in the density of 37 synapse subtypes in brain subregions between 3M and 18M. *$P < 0.05$ adjusted by the Benjamini-Hochberg multiple comparison correction after the Bayesian-based significance test method. Twelve brain regions shown: isocortex, olfactory areas (OLF), hippocampal formation (HPF), cortical subplate (CTXsp), striatum (STR), pallidum (PAL), thalamus (TH), hypothalamus (HY), midbrain (MB), pons (P), medulla (MY) and cerebellum (CB). Subregion key, Table S1.

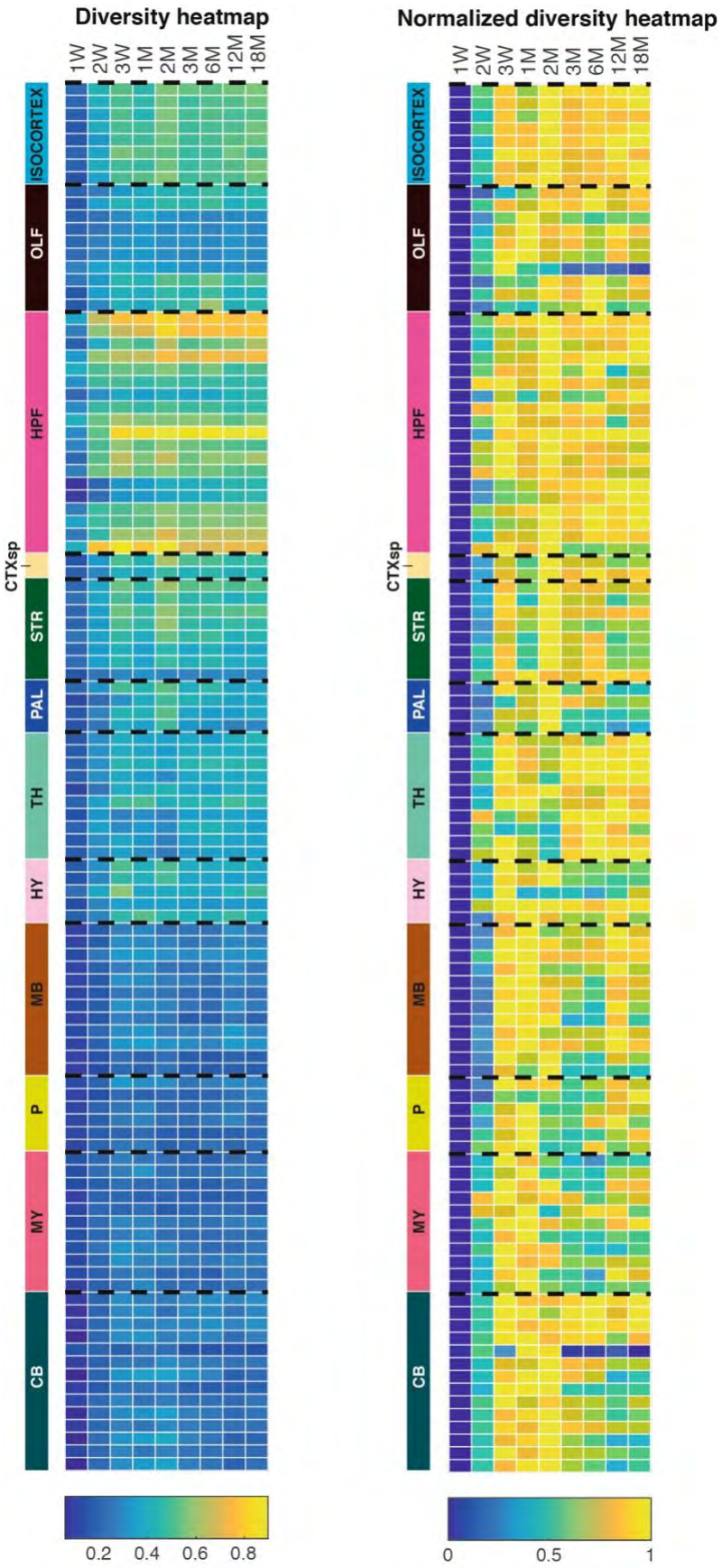
Diversity heatmap
Normalized diversity heatmap
1W
2W
3W
1M
2M
3M
6M
12M
18M
ISOCORTEX
OLF
HPF
CTXsp
STR
PAL
TH
HY
MB
P
MY
CB
0.2
0.4
0.6
0.8
0
0.5
1

Fig. S14: Lifespan trajectories of synapse diversity in brain subregions

(Left) Lifespan trajectories of raw (mean) values of synapse diversity in brain subregions (see Table S1 for subregion names). Scale, Shannon entropy (0-1). (Right) Lifespan trajectories of subregion-normalized values of synapse diversity in brain subregions. Scale, normalized Shannon entropy (0-1). Diversity in each subregion was normalized to its maximal and minimal diversity across the lifespan (rows).

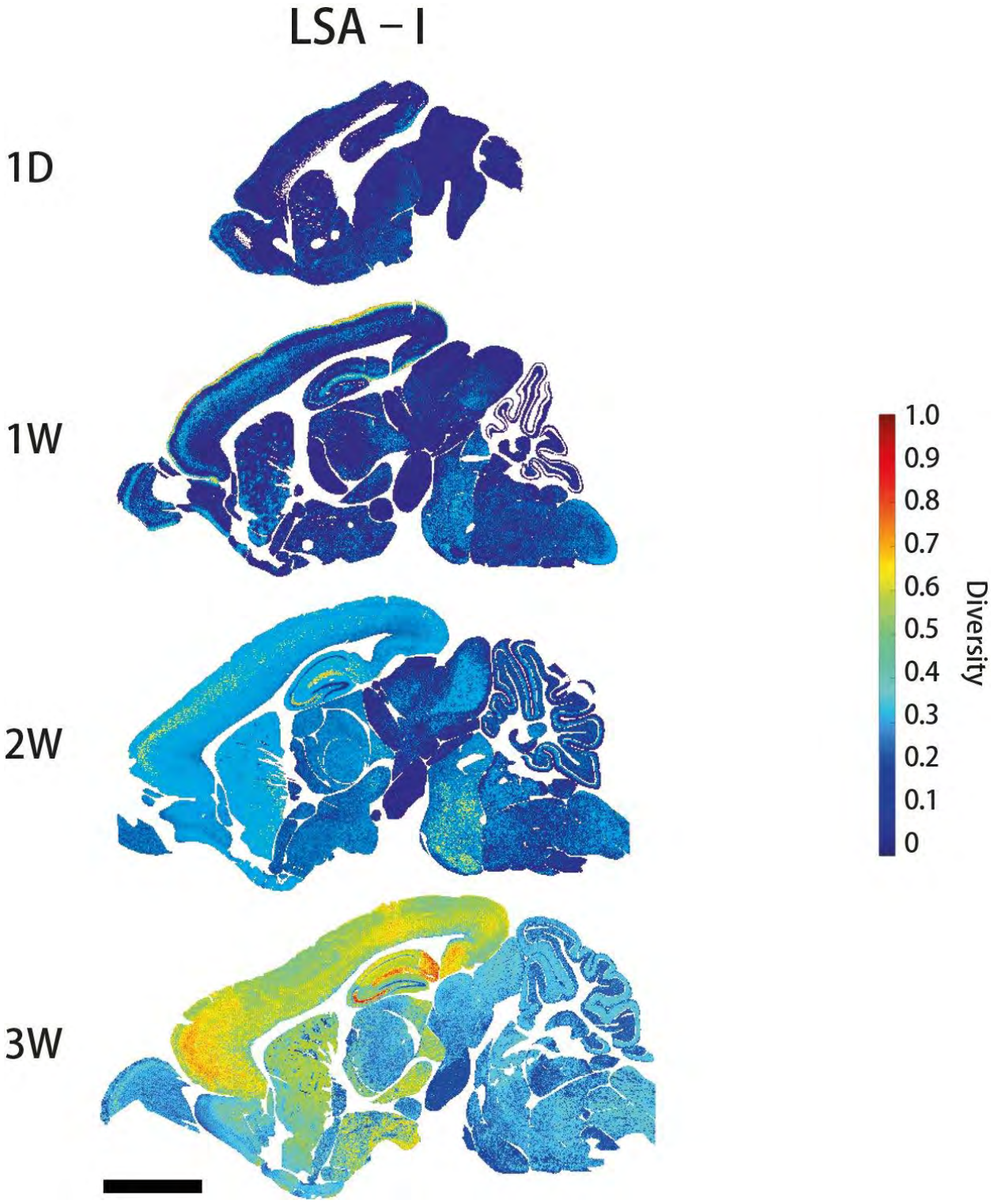
LSA – I
1D
1W
2W
3W
1.0
0.9
0.8
0.7
0.6
0.5
0.4
0.3
0.2
0.1
0
Diversity

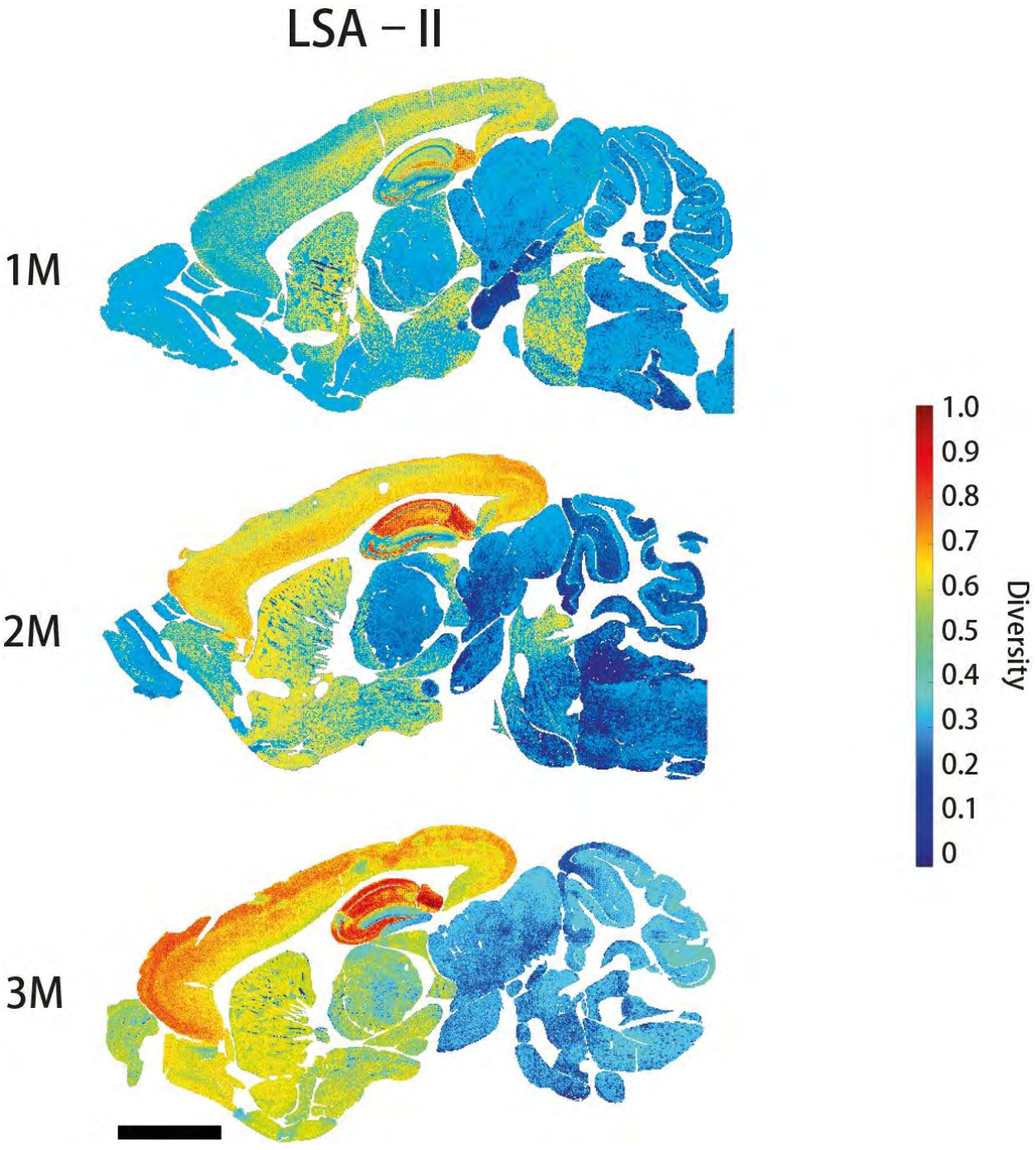
LSA – II
1M
2M
3M
1.0
0.9
0.8
0.7
0.6
0.5
0.4
0.3
0.2
0.1
0
Diversity

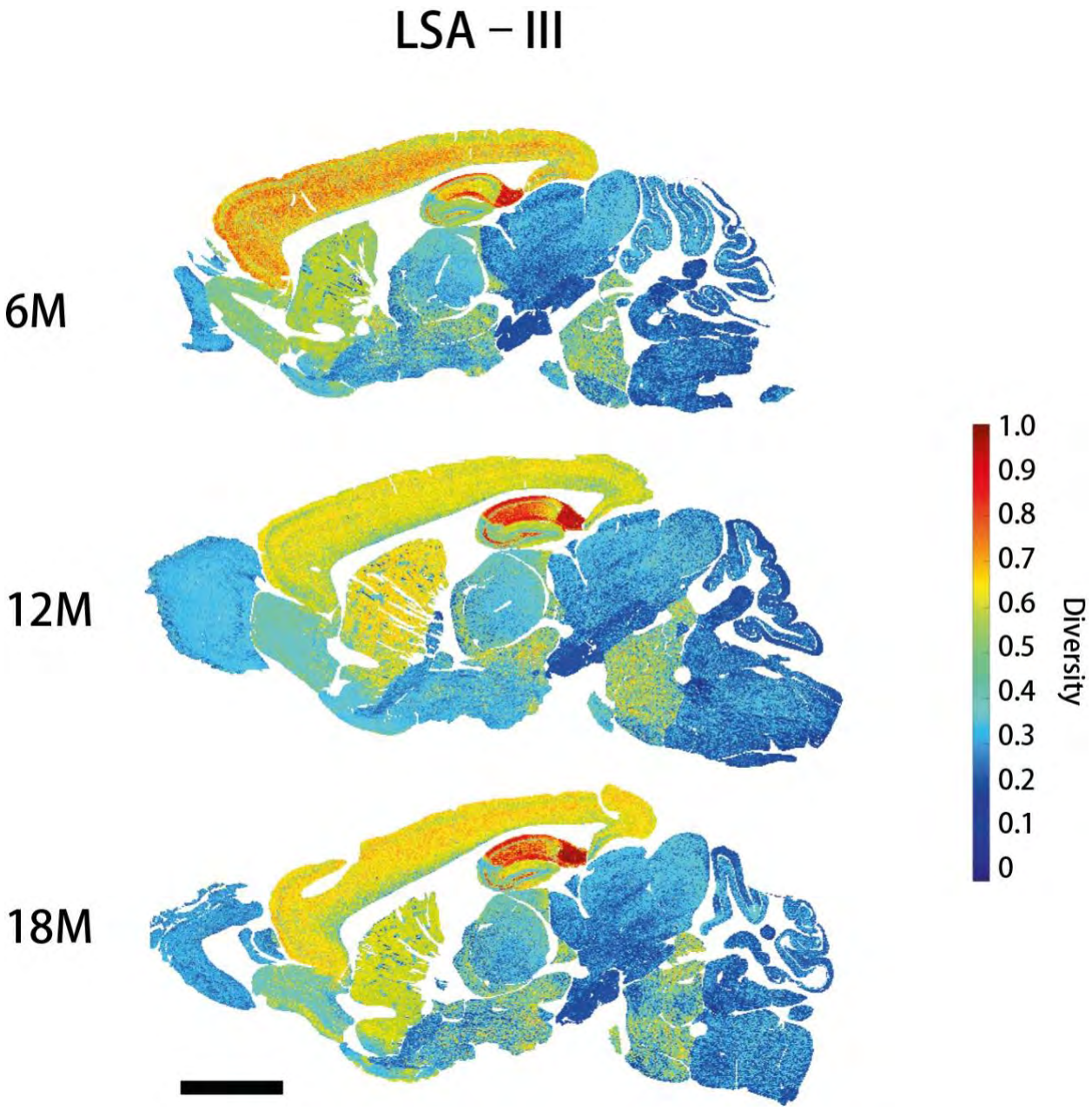

Fig. S15: Unsupervised synaptome maps from birth to 18 months

Unsupervised synaptome maps showing the spatial patterning of synapse diversity (Shannon entropy) per area (pixel size 21.5 µm x 21.5 µm) in representative para-sagittal sections. Scale bar, 2mm.

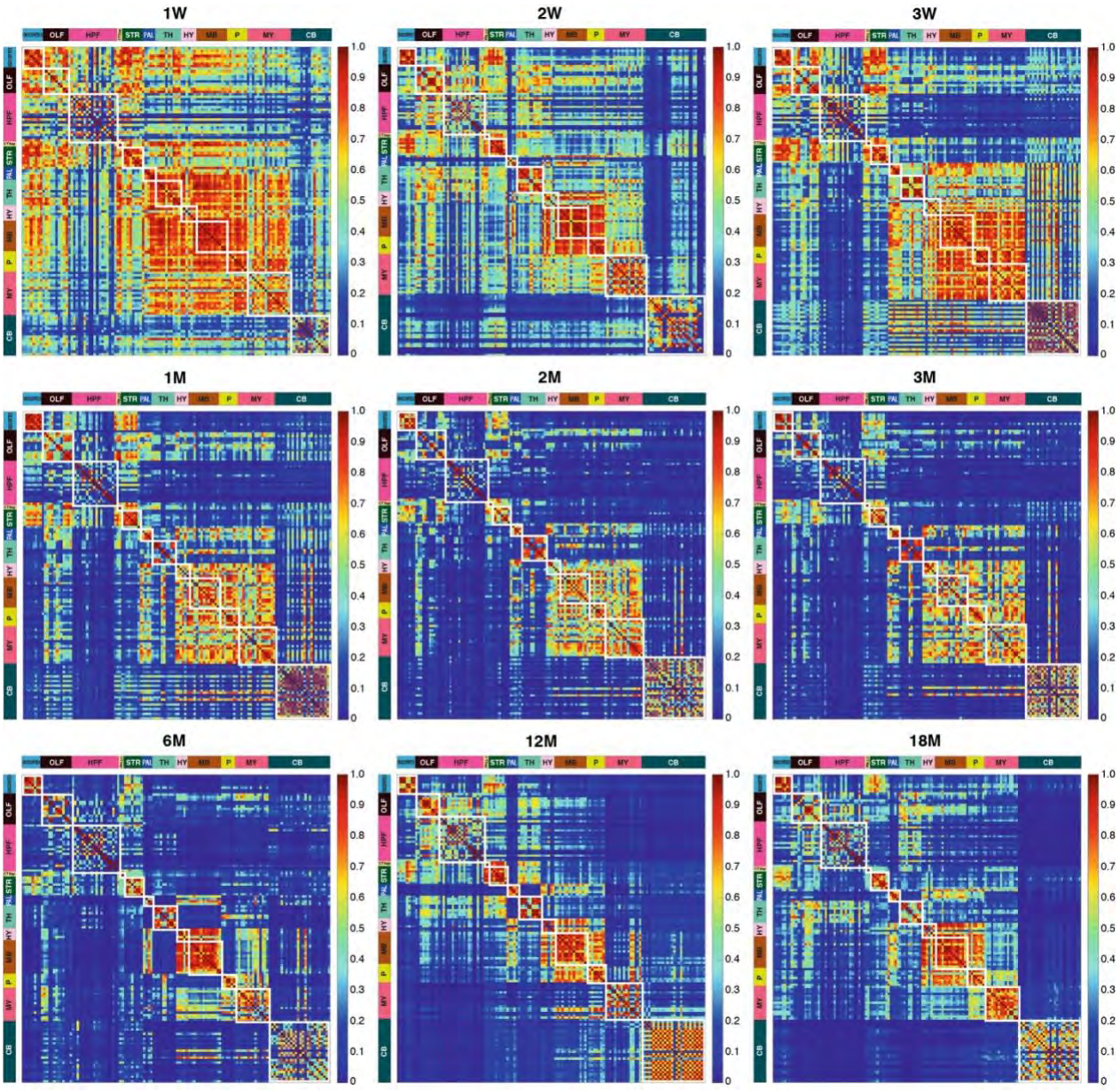
1W
2W
3W
1M
2M
3M
6M
12M
18M
OLF
HPF
STR
PAL
TH
HY
MB
P
MY
CB
1.0
0.9
0.8
0.7
0.6
0.5
0.4
0.3
0.2
0.1
0

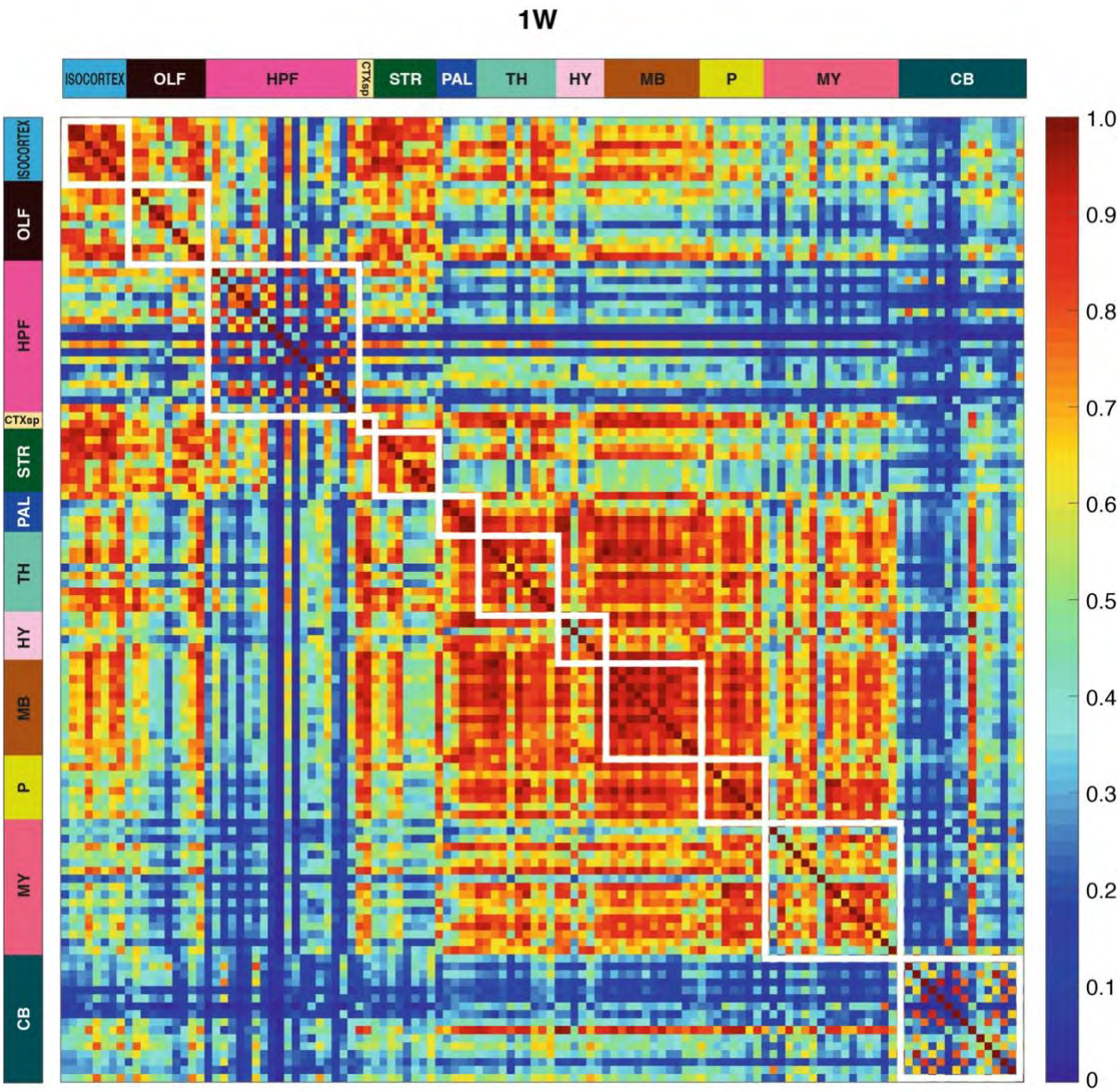
1W
ISOCORTEX
OLF
HPF
CTXsp
STR
PAL
TH
HY
MB
P
MY
CB
1.0
0.9
0.8
0.7
0.6
0.5
0.4
0.3
0.2
0.1
0

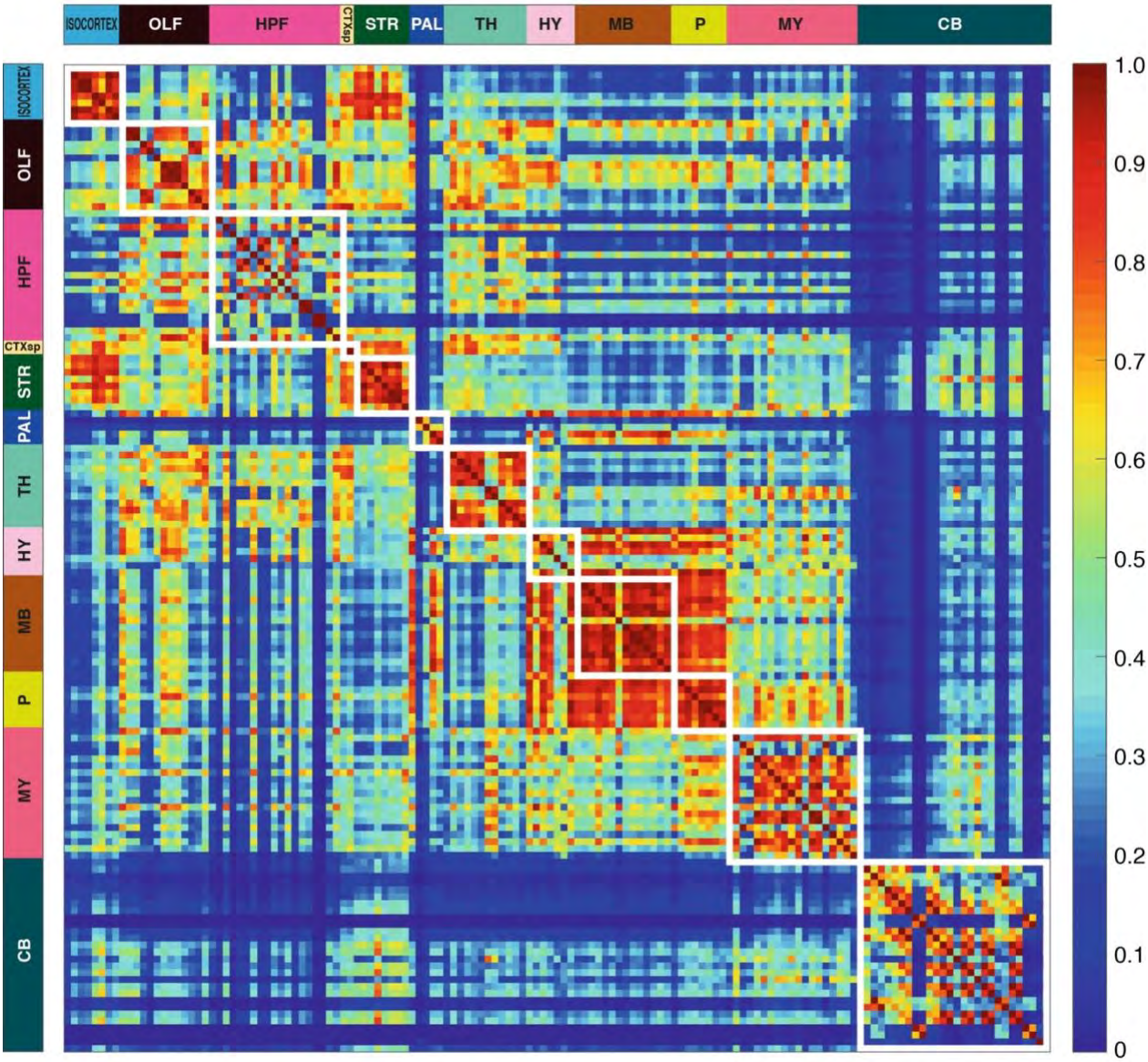
2W
ISOCORTEX
OLF
HPF
CTXsp
STR
PAL
TH
HY
MB
P
MY
CB
1.0
0.9
0.8
0.7
0.6
0.5
0.4
0.3
0.2
0.1
0

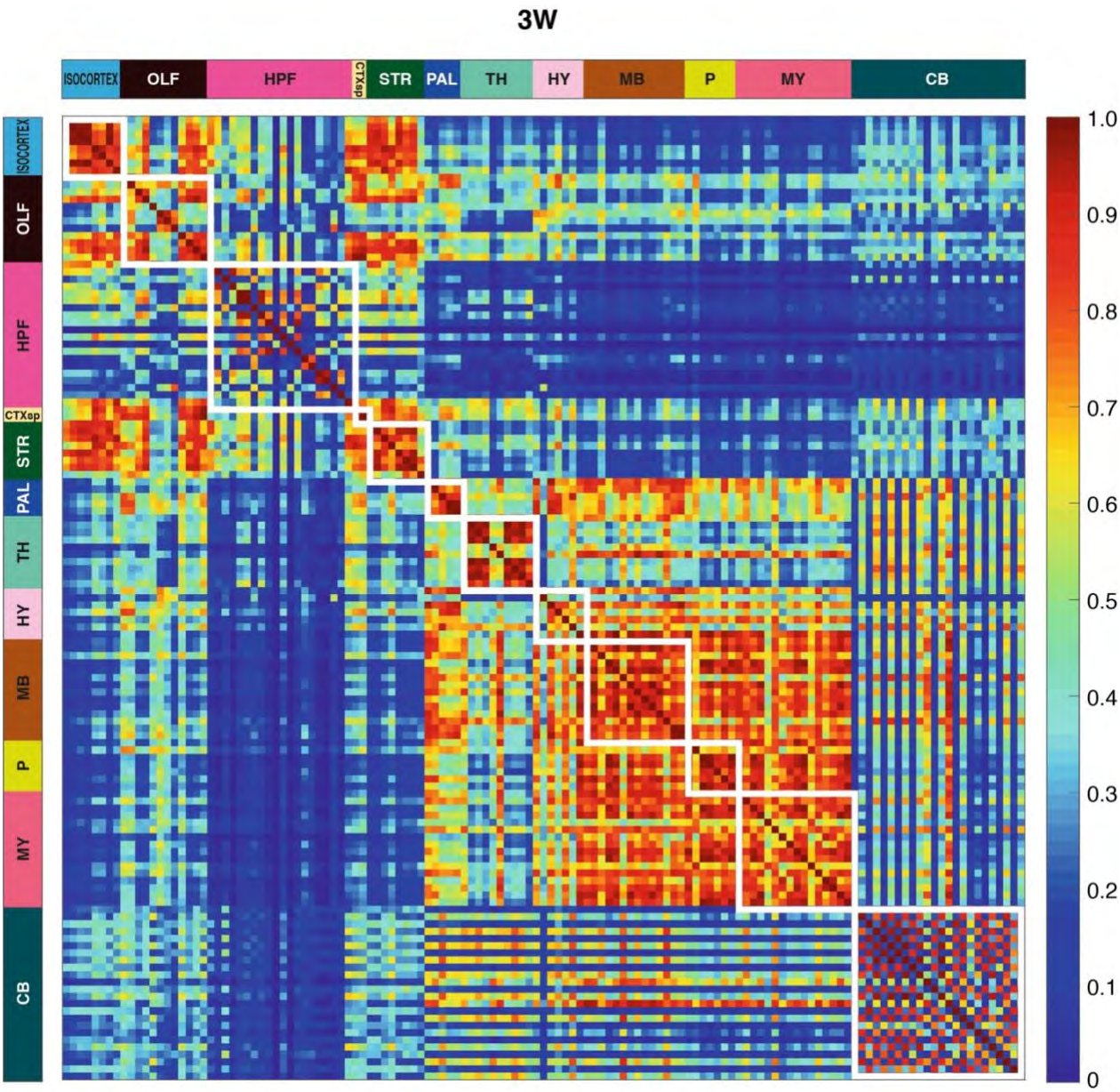
3W
ISOCORTEX
OLF
HPF
CTXsp
STR
PAL
TH
HY
MB
P
MY
CB
1.0
0.9
0.8
0.7
0.6
0.5
0.4
0.3
0.2
0.1
0

1M

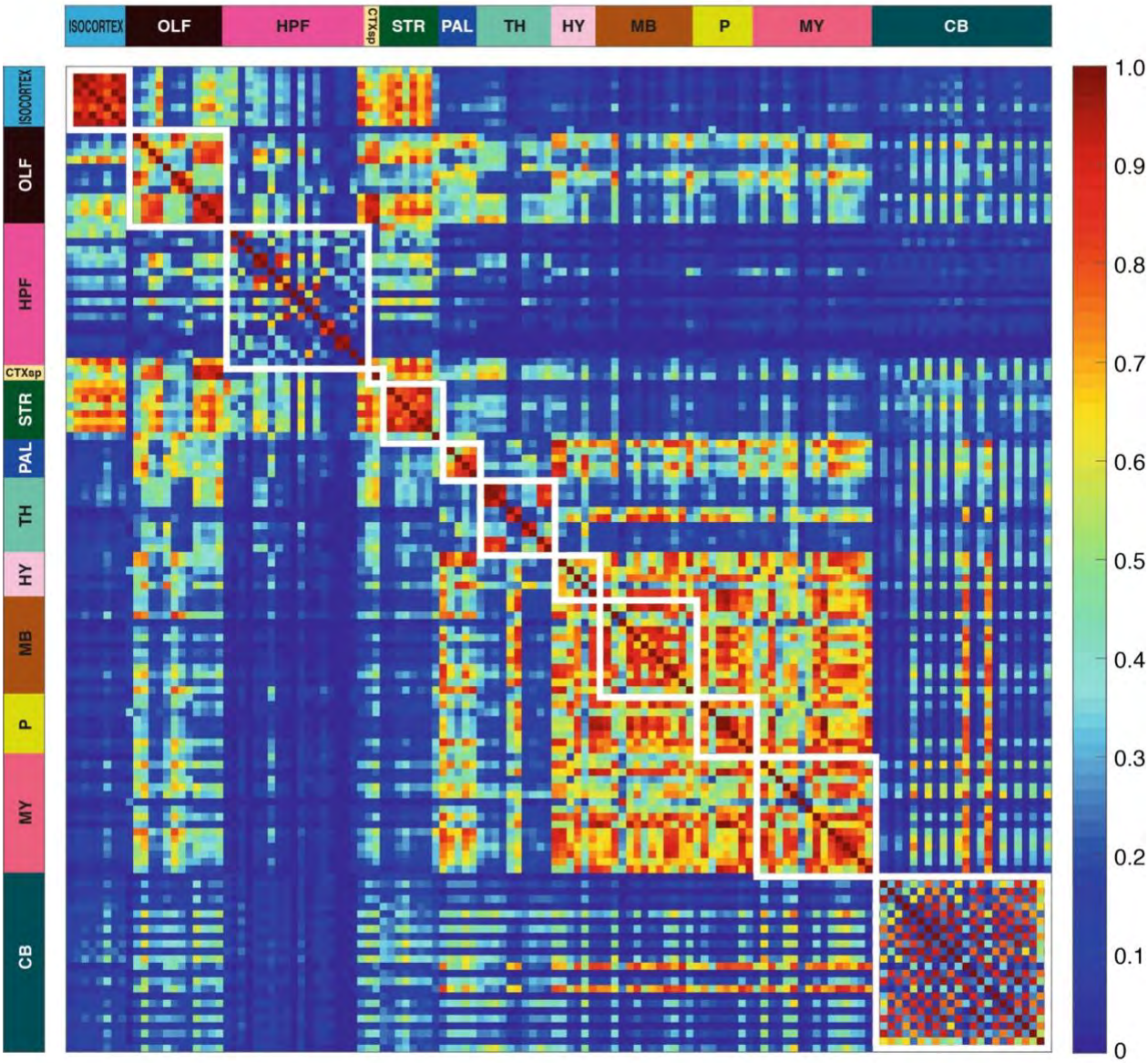
ISOCORTEX
OLF
HPF
CTXsp
STR
PAL
TH
HY
MB
P
MY
CB
1.0
0.9
0.8
0.7
0.6
0.5
0.4
0.3
0.2
0.1
0

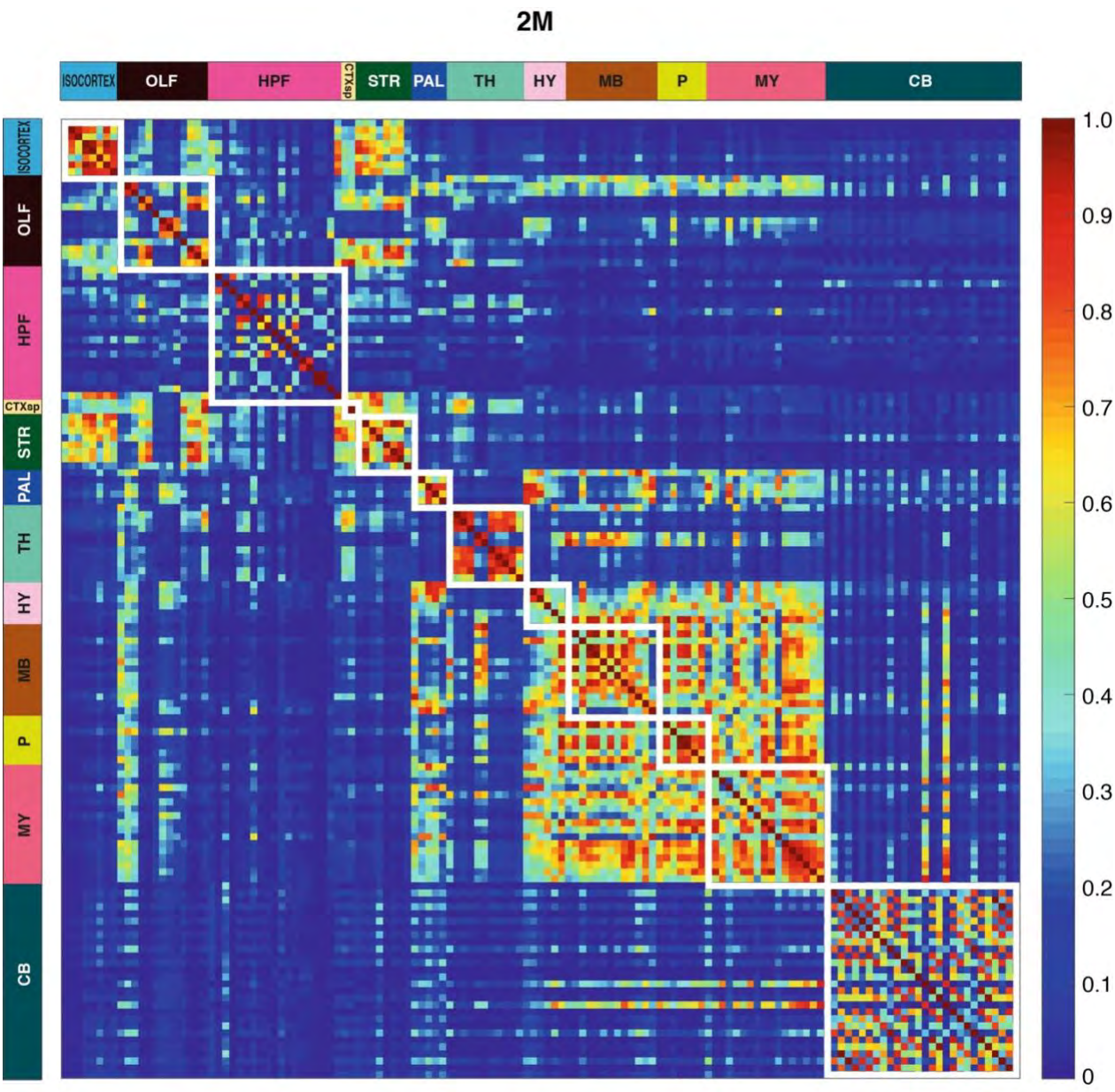
2M
ISOCORTEX
OLF
HPF
CTXsp
STR
PAL
TH
HY
MB
P
MY
CB
1.0
0.9
0.8
0.7
0.6
0.5
0.4
0.3
0.2
0.1
0

3M

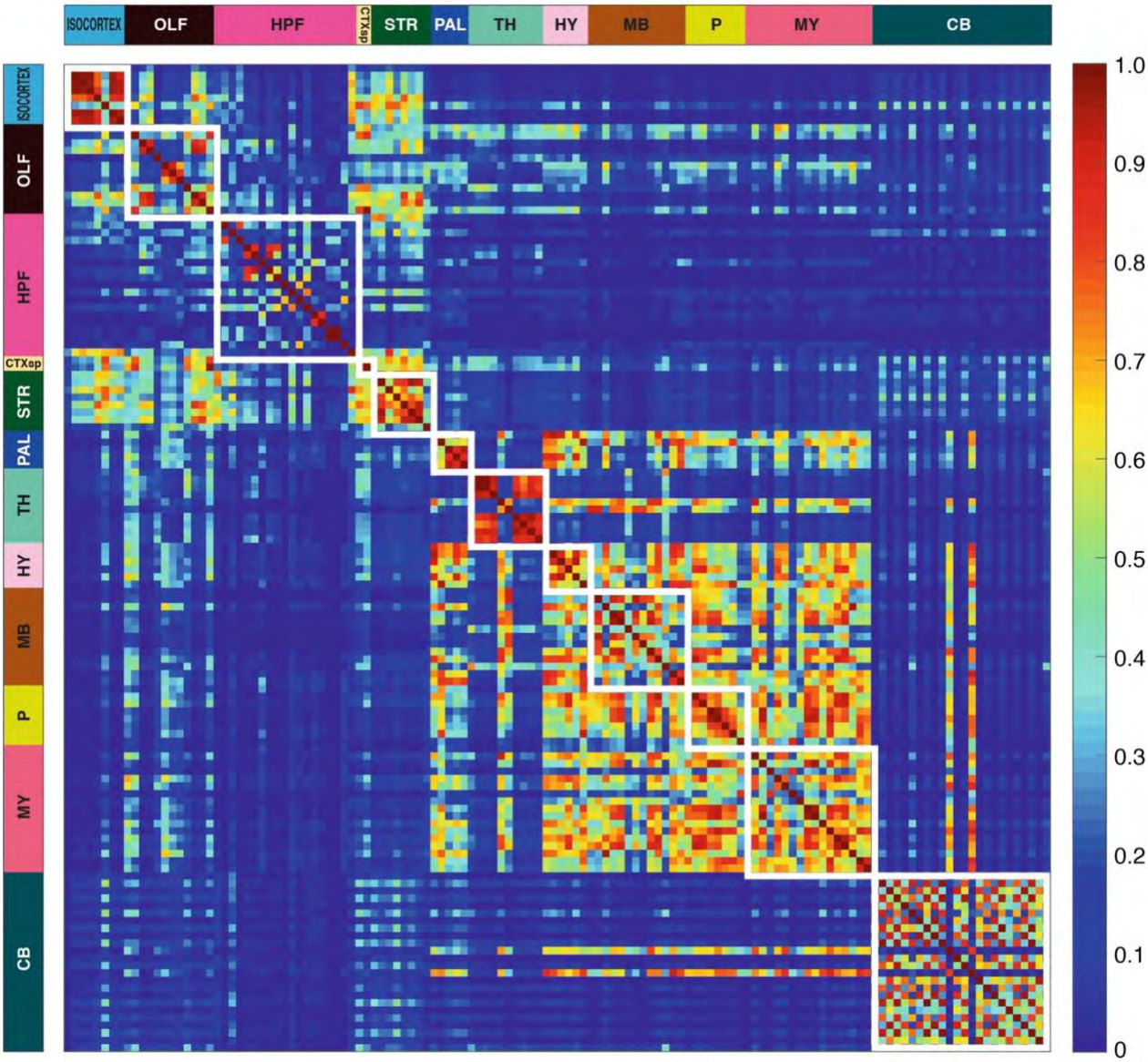
ISOCORTEX
OLF
HPF
CTXsp
STR
PAL
TH
HY
MB
P
MY
CB
1.0
0.9
0.8
0.7
0.6
0.5
0.4
0.3
0.2
0.1
0

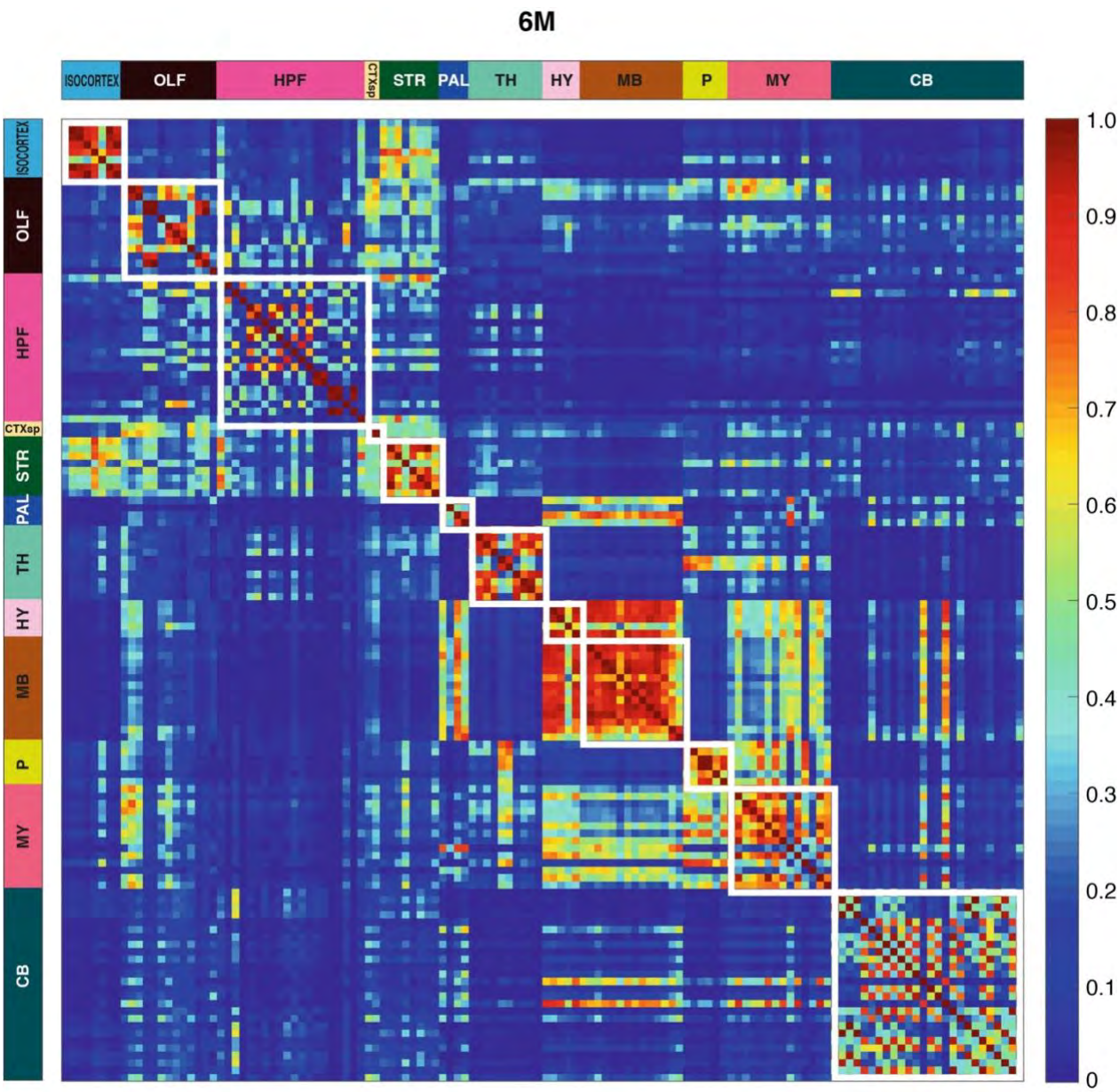
6M
ISOCORTEX
OLF
HPF
CTXsp
STR
PAL
TH
HY
MB
P
MY
CB
1.0
0.9
0.8
0.7
0.6
0.5
0.4
0.3
0.2
0.1
0

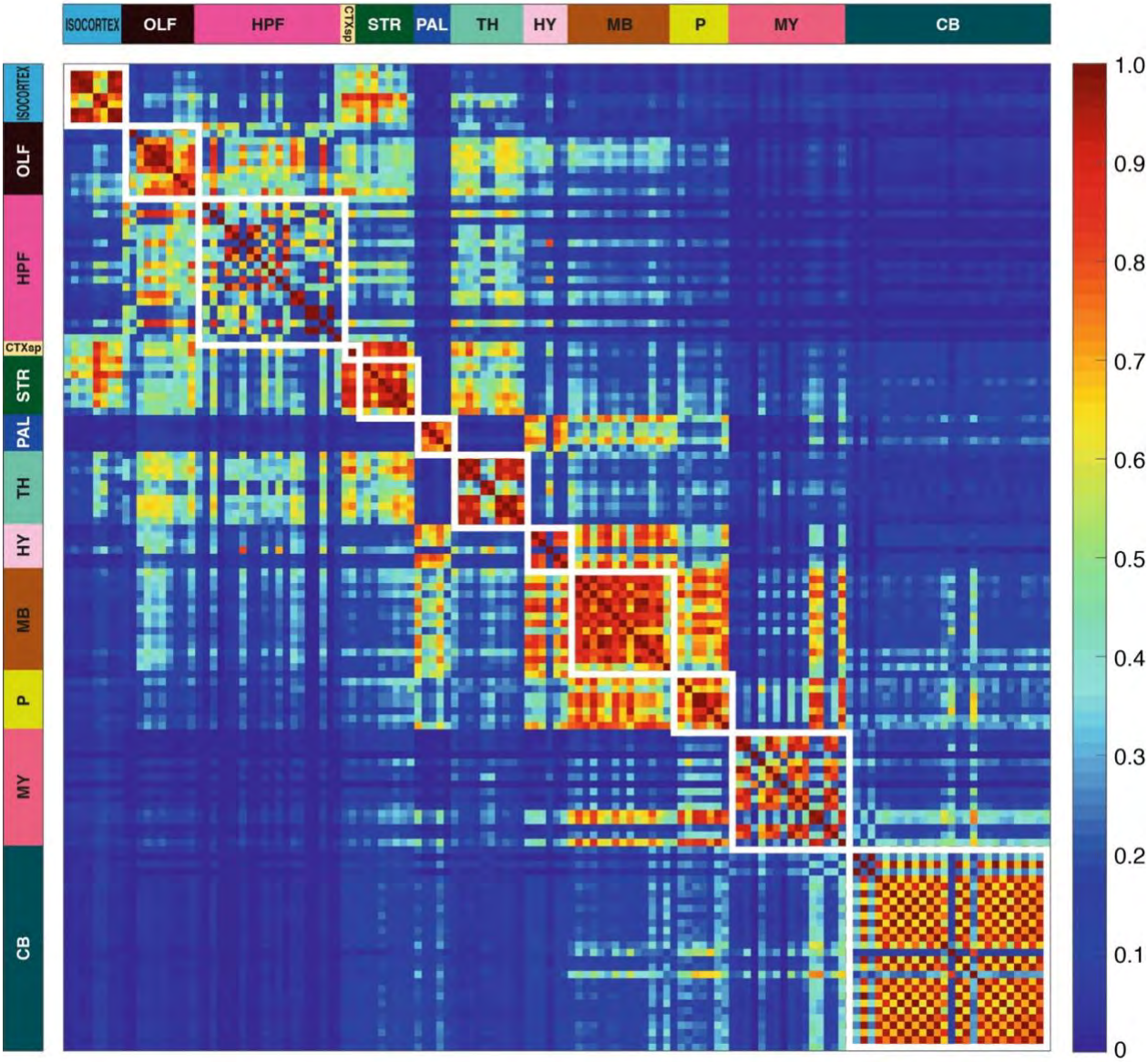
12M
ISOCORTEX
OLF
HPF
CTXsp
STR
PAL
TH
HY
MB
P
MY
CB
1.0
0.9
0.8
0.7
0.6
0.5
0.4
0.3
0.2
0.1
0

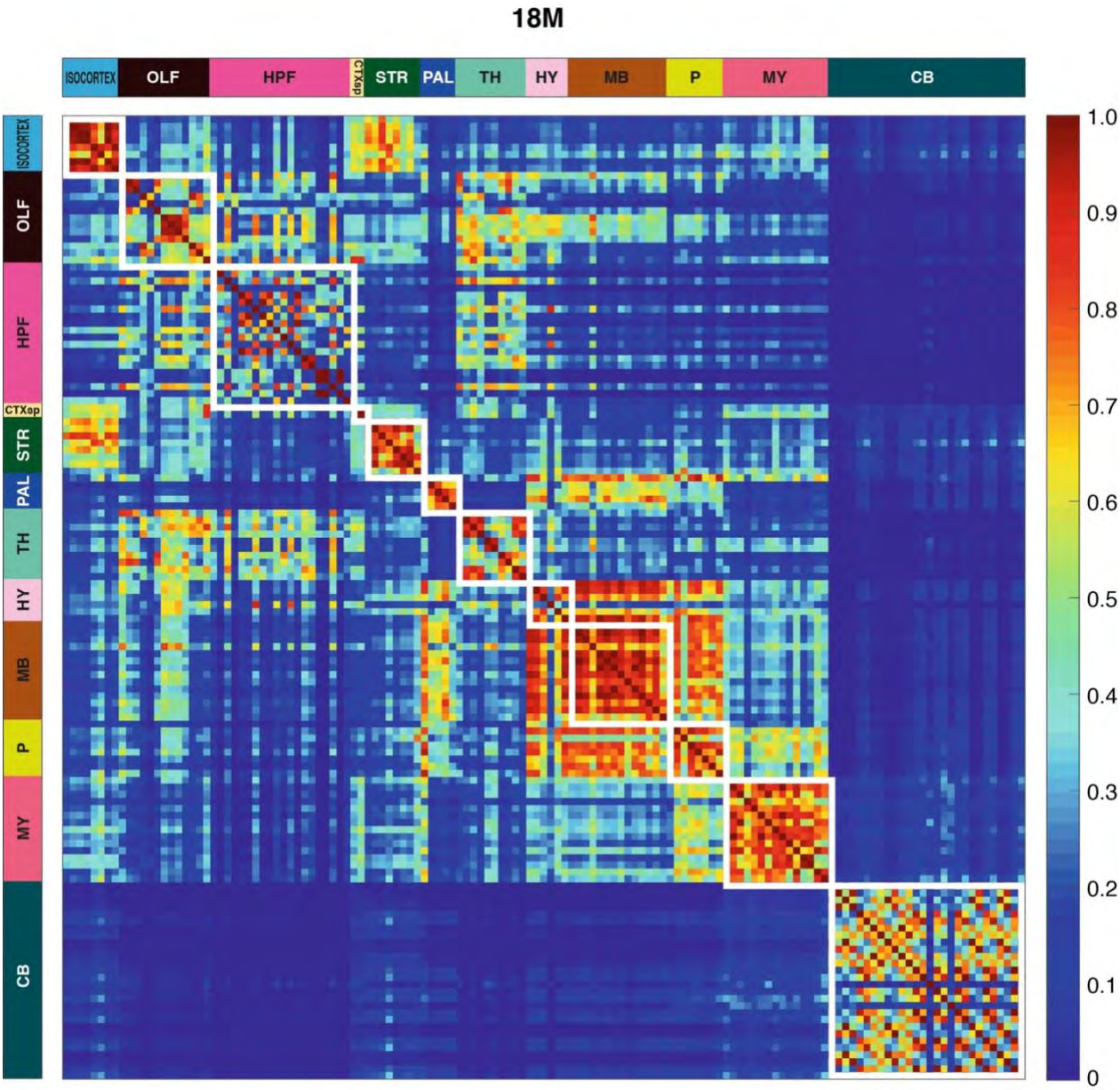

Fig. S16: Brain subregion similarity matrices

Matrix of similarities between pairs of subregions (rows and columns) from 1W to 18M (the first figure shows the nine similarity matrices together, then an enlargement of each is shown). White boxes indicate the subregions that belong to the same main brain region (see color code, left and top). Color scale bar indicates the similarity level ranging from 0 (blue) to 1 (red). The similarity is calculated based on the differences in synaptome parameters between two subregions, details of which can be found in previous work(*8*) (see Table S1 for subregion names).

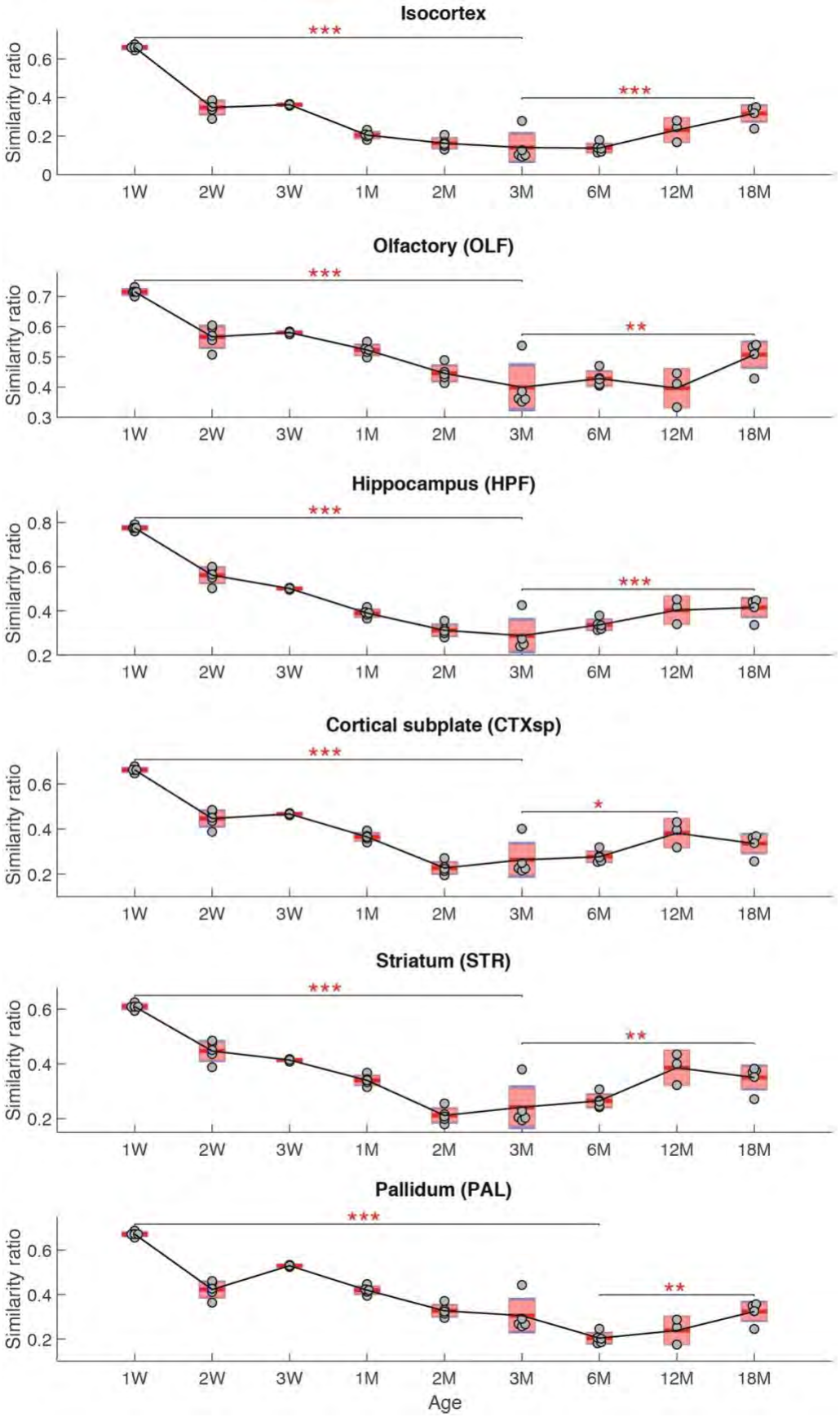
Isocortex
Olfactory (OLF)
Hippocampus (HPF)
Cortical subplate (CTXsp)
Striatum (STR)
Pallidum (PAL)
Similarity ratio
1W
2W
3W
1M
2M
3M
6M
12M
18M
Age
***
**
*

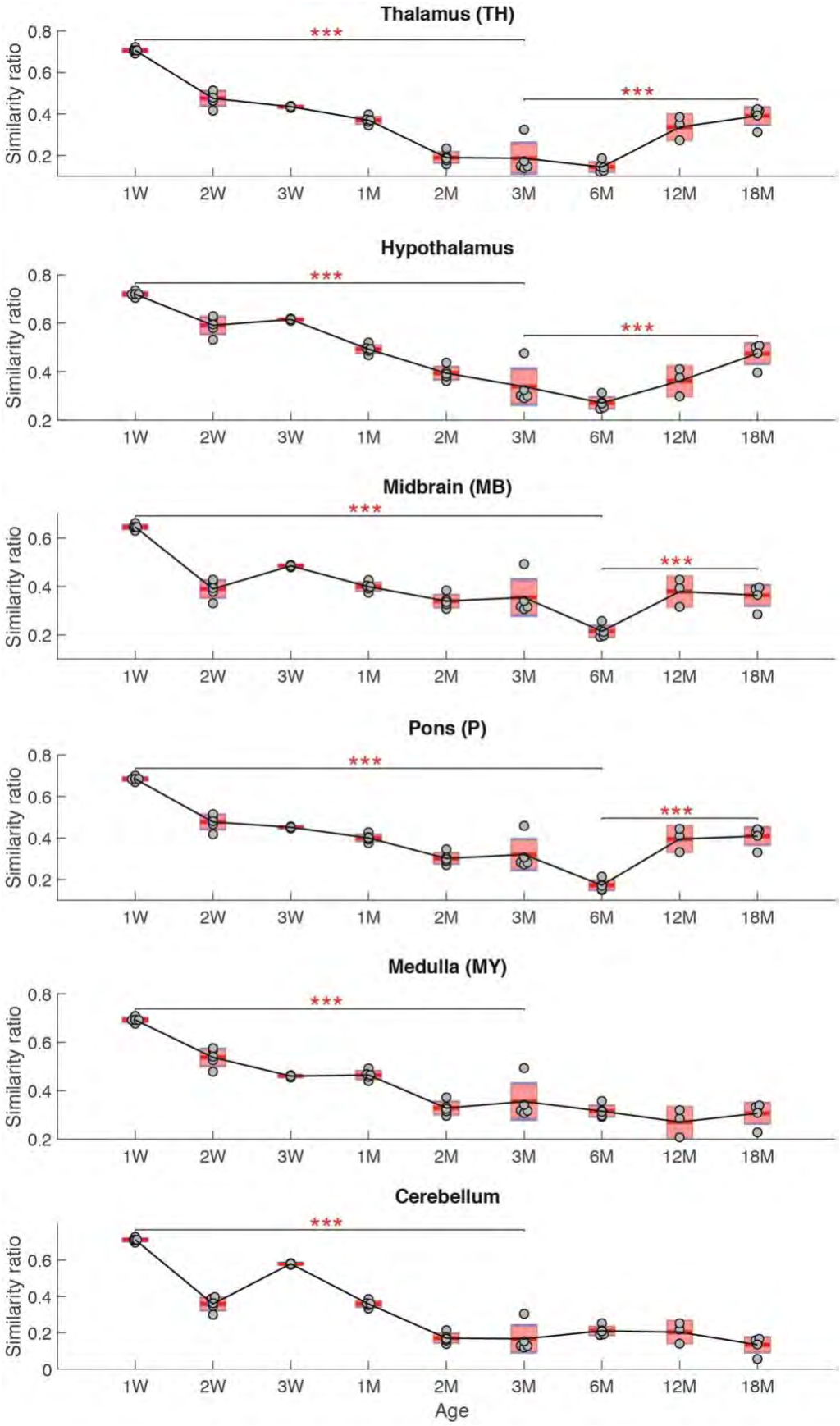
Thalamus (TH)
Hypothalamus
Midbrain (MB)
Pons (P)
Medulla (MY)
Cerebellum
Similarity ratio
0.8
0.6
0.4
0.2
0
***
1W
2W
3W
1M
2M
3M
6M
12M
18M
Age

Fig. S17: Lifespan trajectories of similarity ratio for 12 overarching regions

Between birth and 3M/6M, each brain region shows a significant reduction in similarity with the rest of the brain. From 3M/6M to 18M a significant increase in similarity is found in all areas except medulla and cerebellum. *$P < 0.05$, **$P < 0.01$, ***$P < 0.001$; two-way ANOVA with the post-hoc multiple comparison test.

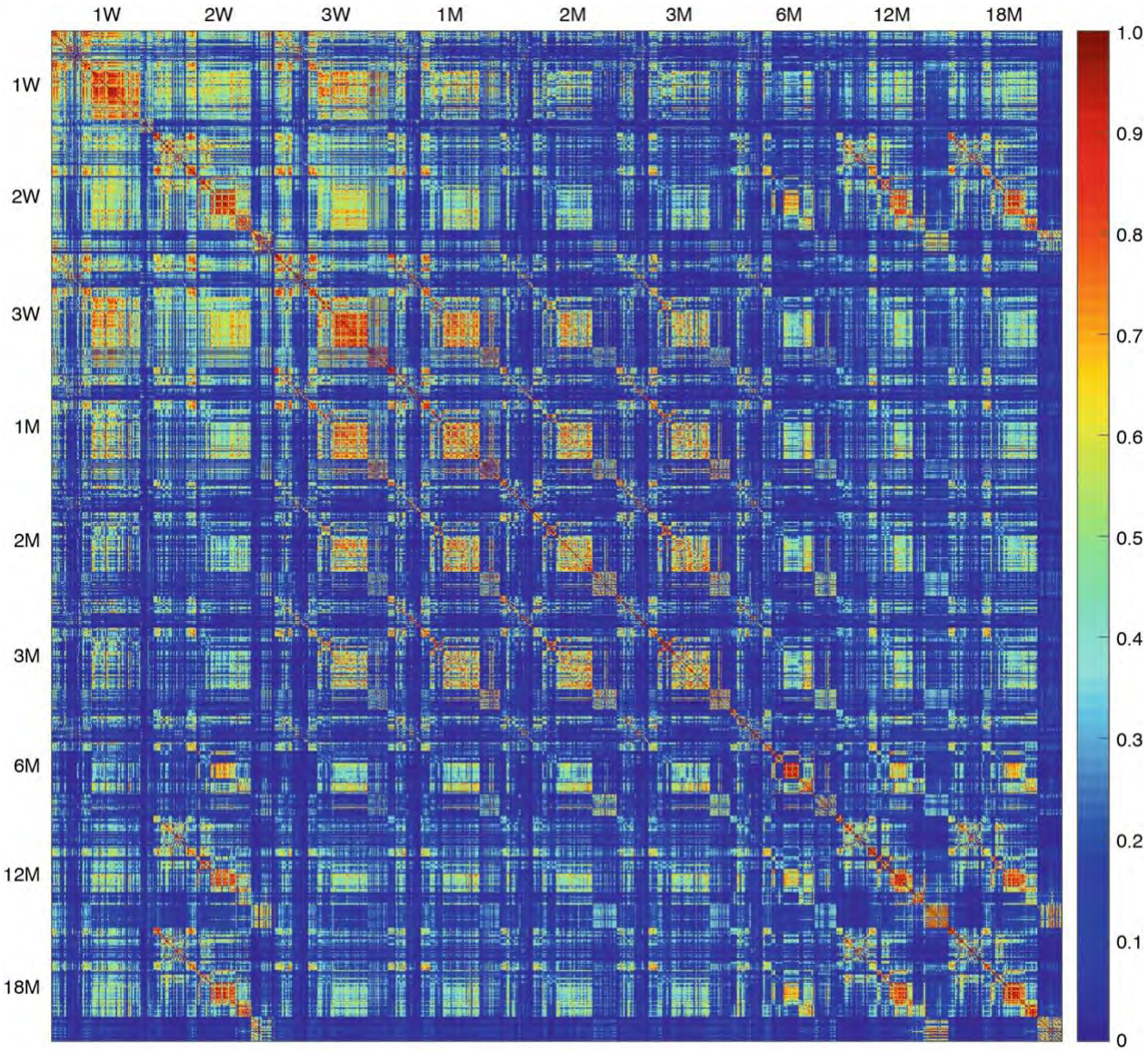
1W
2W
3W
1M
2M
3M
6M
12M
18M
1.0
0.9
0.8
0.7
0.6
0.5
0.4
0.3
0.2
0.1
0

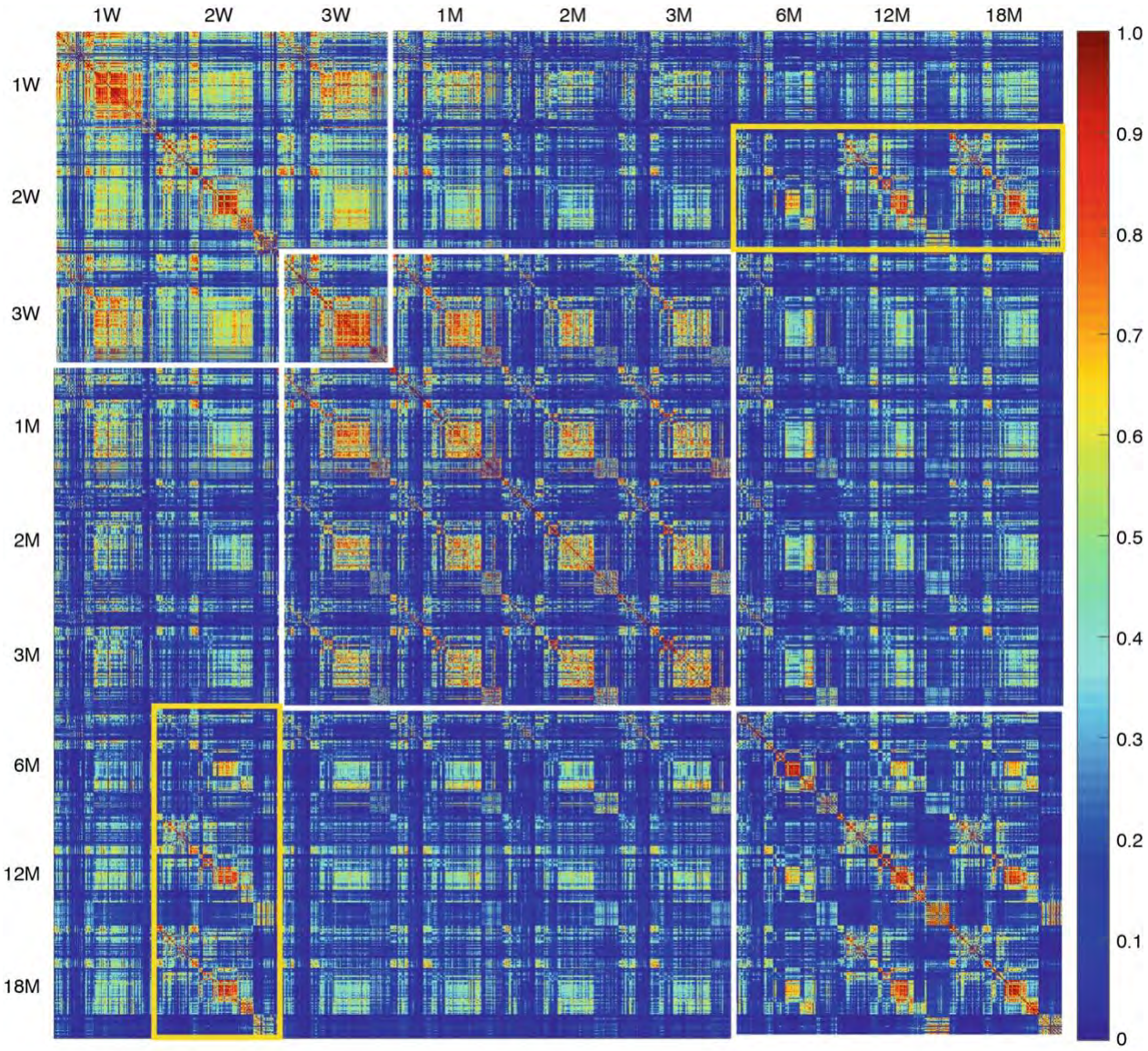

Fig. S18: Hypersimilarity matrix comparing all brain subregions across all ages

Enlargement of hypersimilarity matrix in Fig. 3D without superimposed boxes (top) and with boxes (bottom); white boxes indicate the main three clusters, which correspond to LSA-I, -II and -III. Yellow boxes show increased similarity of the old brain (LSA-III) with young brain (2W), in contrast to that of adult brain (LSA-II) with young brain (2W). Color scale bar indicates the similarity level ranging from 0 (blue) to 1 (red).

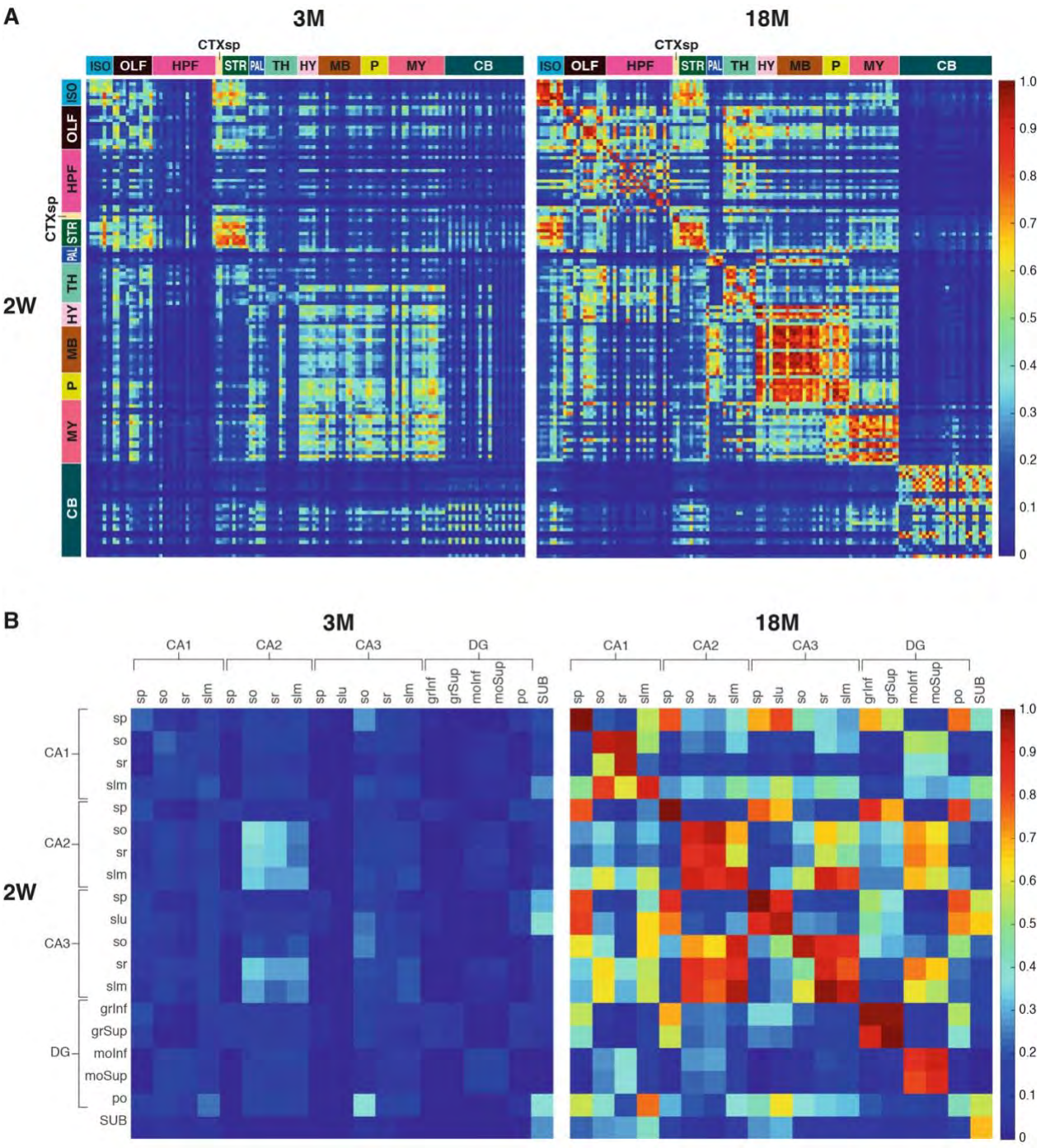

Fig. S19: Similarity matrices comparing 3M and 18M brain with 2W brain

(A) Matrix of similarities of brain subregions (rows and columns) between 2W and 3M (left matrix), and 2W and 18M (right matrix). They are both sub-matrices extracted from the whole-section hypersimilarity matrix Fig. S18. Color scale bar indicates the similarity level ranging from 0 (blue) to 1 (red). See Table S1 for subregion names.

(B) Matrix of similarities between hippocampal subregions (rows and columns) between 2W and 3M (left matrix), and 2W and 18M (right matrix). They are both sub-matrices subtracted from the hippcampal hypersimilarity matrices Fig. 3D. Color scale bar indicates the similarity level ranging from 0 (blue) to 1 (red). CA1: cornu ammonis 1, CA2: cornu ammonis 2, CA3: cornu ammonis 3, DG: dentate gyrus, grInf: granular layer inferior blade, grSup: granular layer superior blade, moInf: molecular layer inferior blade, moSup: molecular layer superior blade, po: polymorphic cell layer, slm: stratum lacunosum-moleculare, slu: stratum lucidum, so: stratum oriens, sp: stratum pyramidale, sr: stratum radiatum, SUB: subiculum.

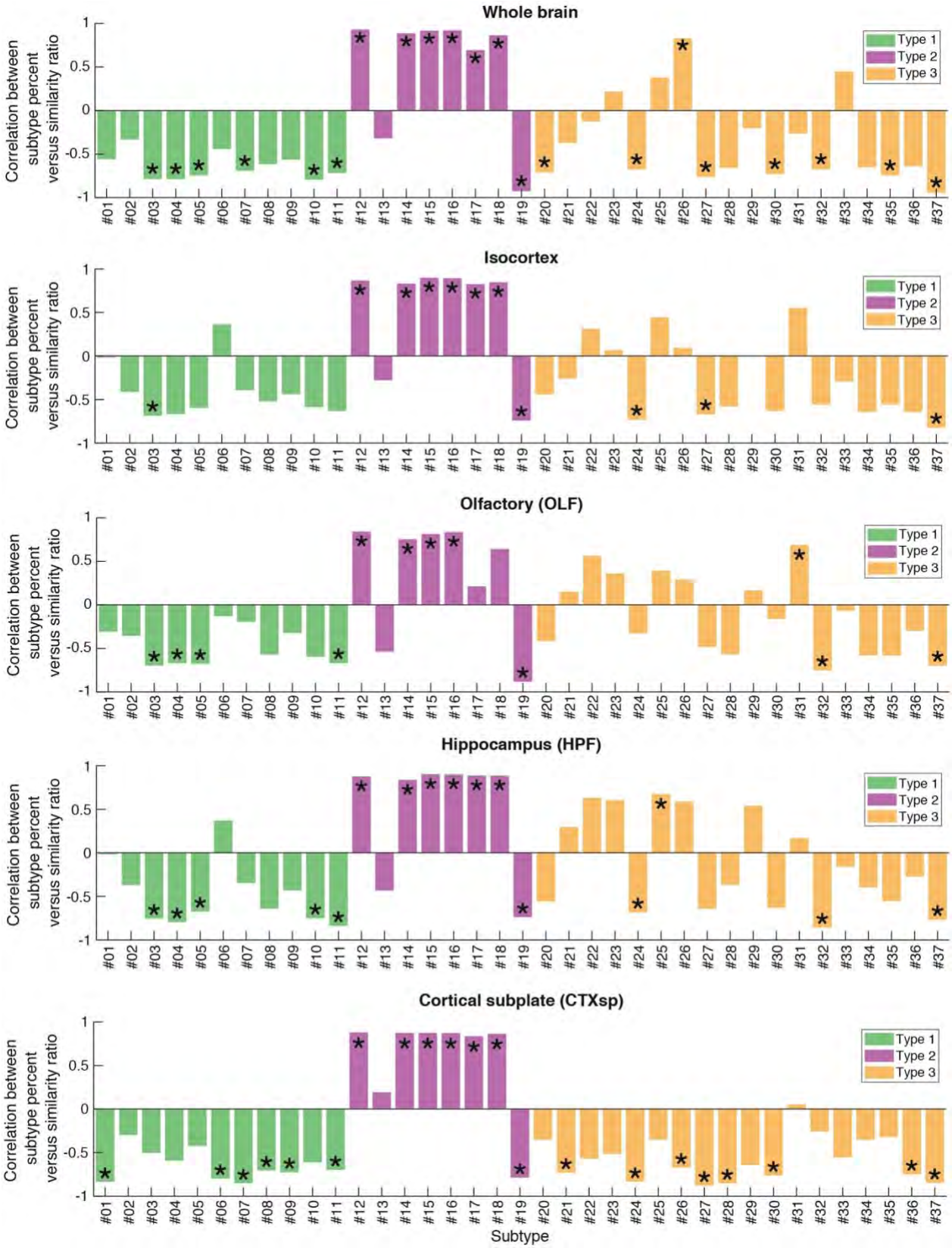
Whole brain
Isocortex
Olfactory (OLF)
Hippocampus (HPF)
Cortical subplate (CTXsp)
Correlation between subtype percent versus similarity ratio
Type 1
Type 2
Type 3
Subtype

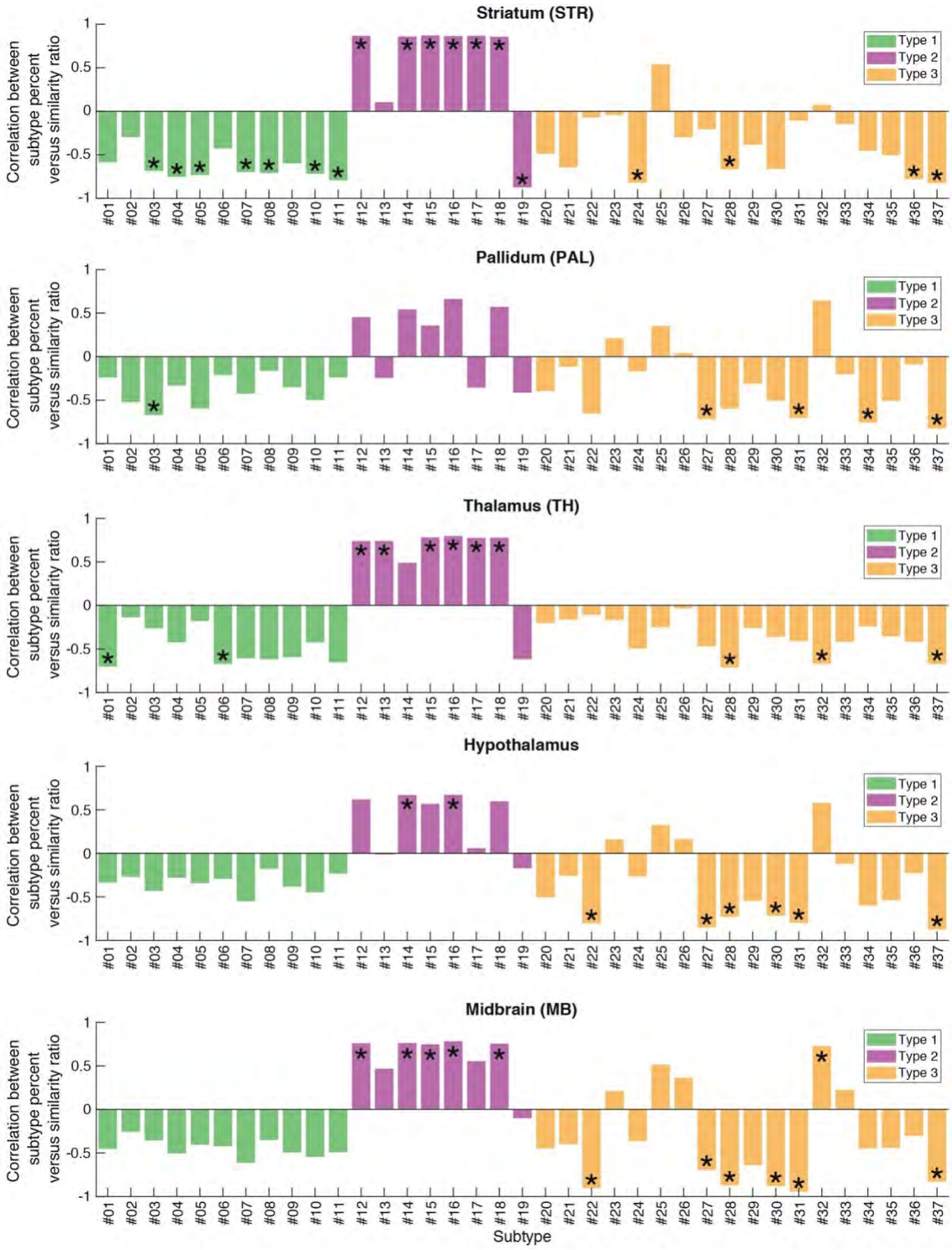
Striatum (STR)
Pallidum (PAL)
Thalamus (TH)
Hypothalamus
Midbrain (MB)
Correlation between subtype percent versus similarity ratio
Type 1
Type 2
Type 3
Subtype

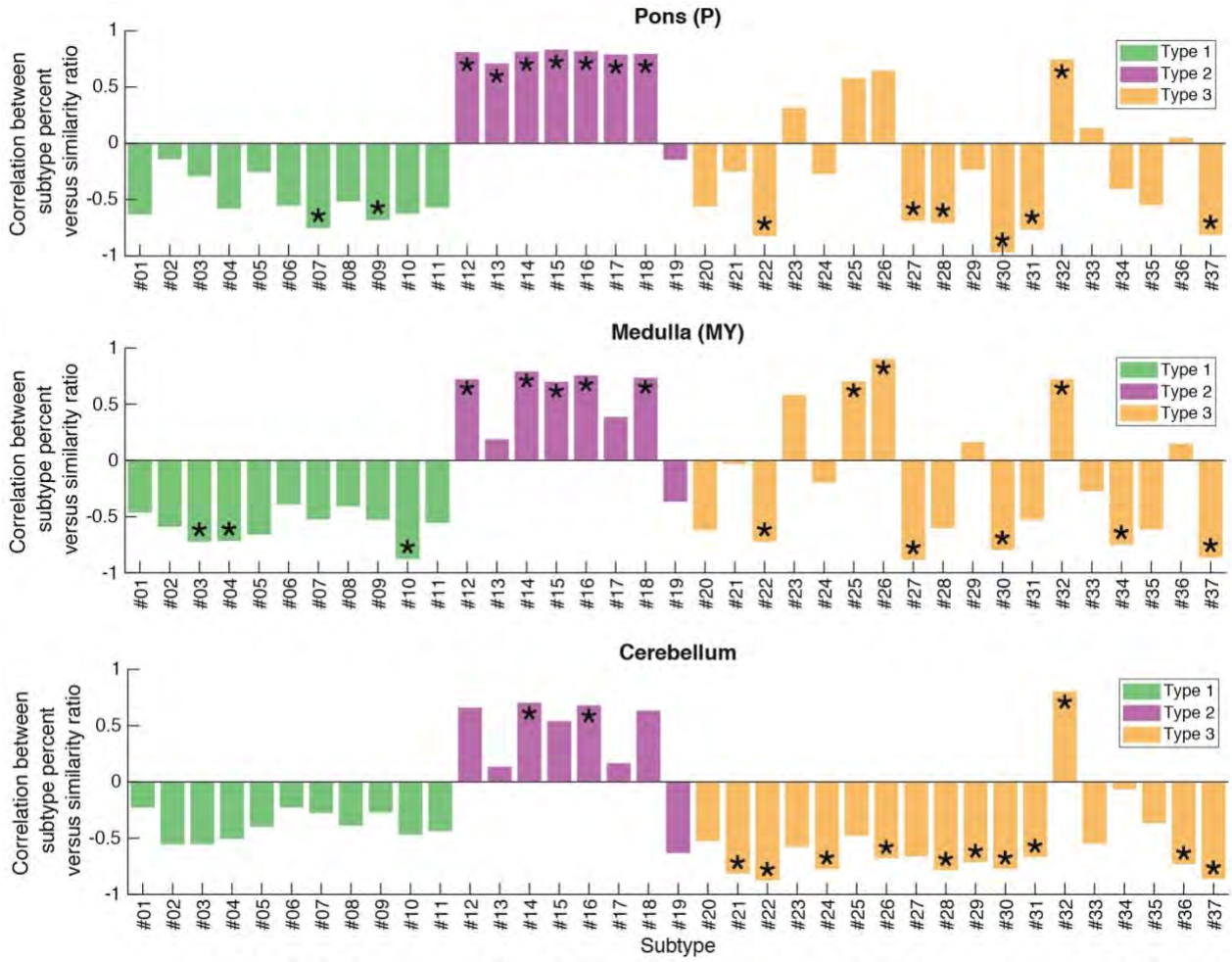

Fig. S20: Correlation between lifespan trajectories of synapse subtype percentage and similarity ratio in brain regions

Each panel represents a brain region and each bar in the region is the Pearson correlation coefficient between lifespan trajectories of a synapse subtype percentage and the similarity ratio in the same region (Fig. S17). Statistical significance was calculated using the Mantel test with Benjamini-Hochberg multiple comparison correction: $*P < 0.05$. Synapse types 1, 2 and 3 are color coded.

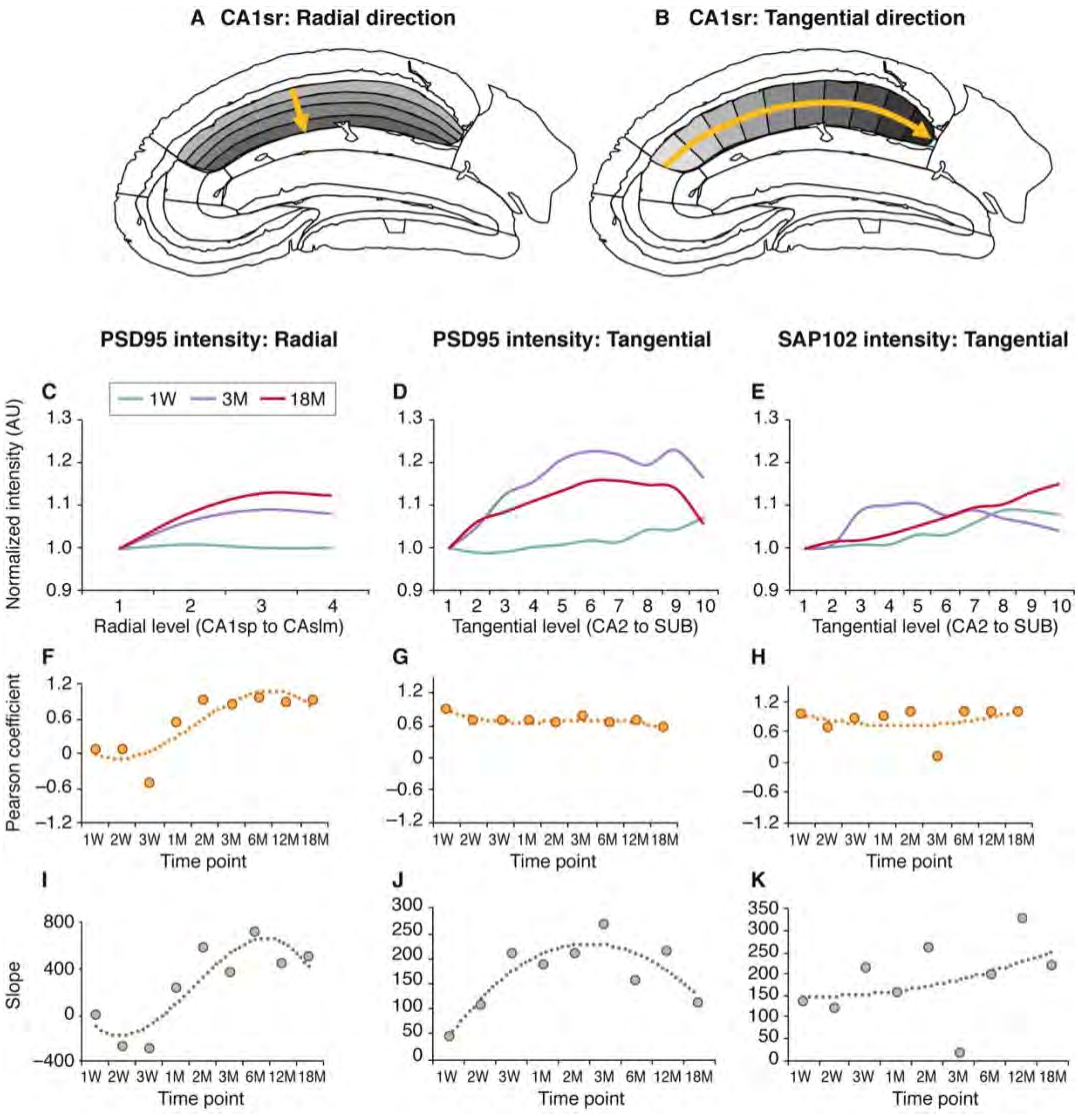

Fig. S21: Lifespan trajectories of hippocampal gradients

(A, B) Schematics showing the subdelineations of CA1sr in the radial (A) and tangential (B) directions used for hippocampal gradient analysis.

(C) Smoothed curves showing the PSD95 intensity values (normalized to the value in level 1 for each time-point) along the radial direction of CA1sr (4 levels, CA1sp to CA1slm) at 1W, 3M and 18M (arbitrary units, AU).

(D, E) Smoothed curves of PSD95 (D) and SAP102 (E) intensity values (normalized to the value in level 1 for each time-point) along the tangential direction of CA1sr (10 levels, CA2 to subiculum (SUB)) at 1W, 3M and 18M.

(F-H) Pearson coefficient of intensity values versus gradient levels across the lifespan for PSD95 intensity in the radial (F) and tangential (G) directions and for SAP102 intensity in the tangential direction (H). Dashed lines show the polynomial regression curve fitting. (F) We observe no PSD95 radial gradient during the first 3 weeks (Pearson ≈ 0 from 1W-2W). At 1M, a weak gradient appears (Pearson = 0.55), becomes fully established by 2M and is maintained during all mouse adult life (Pearson > 0.8, 2M-18M). (G) PSD95 intensity shows a tangential gradient as early as 1W (Pearson = 0.91), which is maintained throughout the lifespan (Pearson > 0.5, 1W-18M). (H) SAP102 intensity tangential gradient has a high Pearson coefficient from 1W and remains high throughout life.

(I-K) Slope value of the linear regression curve of intensity values versus gradient levels across the lifespan for PSD95 intensity in the radial (I) and tangential (J) directions and for SAP102 intensity in the tangential direction (K). Dotted lines show the polynomial regression curve fitting. (I) The slope of PSD95 intensity radial gradient follows a similar trajectory to its Pearson coefficient (slope $\approx$ 0 from 1W-2W, slope = 235 at 1M, slope > 350 from 2M-18M). (J) The slope of PSD95 intensity tangential gradient has a different trajectory to that of the radial gradient: it starts low at 1W and progressively increases, peaks at 3M and then gradually decreases 3M-18M. (K) SAP102 intensity tangential gradient has a high slope value from 1W and remains high throughout life.

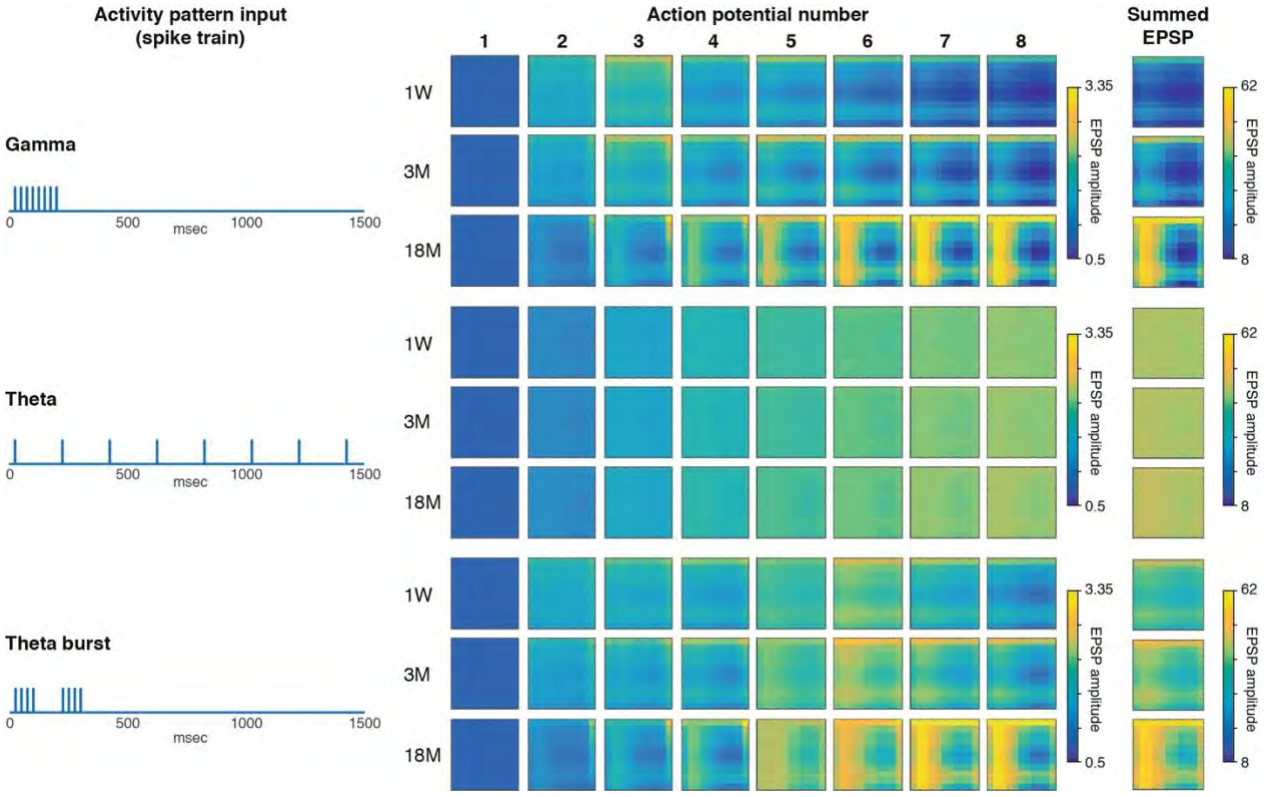

Fig. S22: Patterned neuronal activity produces distinct functional outputs from the synaptome of CA1 pyramidal neurons at different ages

The response (EPSP amplitude) to three patterns (gamma, theta, theta-burst) of 1-8 action potentials and summed response to 20 action potentials (summed EPSP) of the 11 x 11 matrix of hippocampus synapses at three ages.

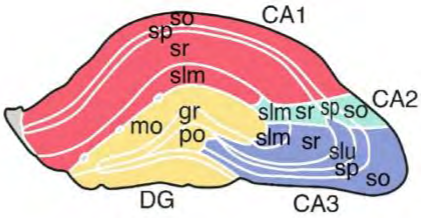

Dentate gyrus

DGgrInf | DGgrSup | DGmoInf | DGmoSup | DGpo

CA3

CA3so | CA3sp | CA3sr | CA3slm | CA3slu

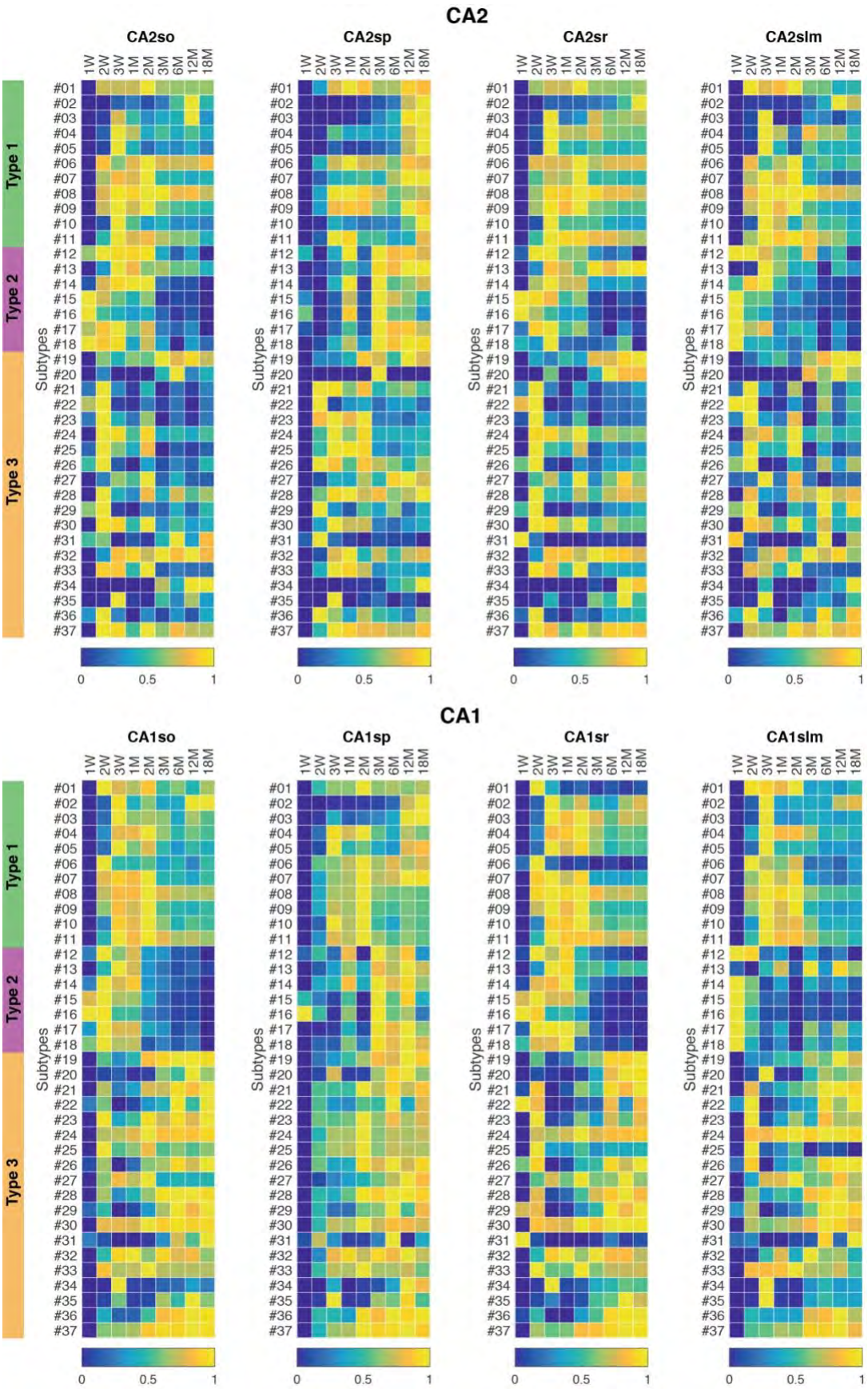
CA2
CA2so
CA2sp
CA2sr
CA2slm
CA1
CA1so
CA1sp
CA1sr
CA1slm
Type 1
Type 2
Type 3
Subtypes
1W
2W
3W
1M
2M
3M
6M
12M
18M
0
0.5
1

Fig. S23: Lifespan trajectories of synapse subtype density in hippocampal subregions

The normalized density of 37 synapse subtypes in subregions of the dentate gyrus, CA3, CA2 and CA1 subregions are shown. Subtype density of each subtype is min-max normalized (0-1) by row to its minimal and maximal density across the lifespan. Color scale bar indicates the normalized subtype densities ranging from 0 (blue) to 1 (yellow). DG, dentate gyrus; DGgrInf, DG granular layer, inferior blade; DGgrSup, DG granular layer, superior blade; DGmoInf, DG molecular layer, inferior blade; DGmoSup, DG molecular layer, superior blade; DGpo, DG polymorphic cell layer. CA3, cornu ammonis 3; CA3so, CA3 stratum oriens; CA3sp, CA3 stratum pyramidale; CA3slu, CA3 stratum lucidum; CA3 stratum radiatum; CA3slm, CA3 stratum lacunosum-moleculare; CA2, cornu ammonis 2; CA1so, CA2 stratum oriens; CA2sp, CA2 stratum pyramidale; CA2sr, CA2 stratum radiatum; CA2slm, CA2 stratum lacunosum-moleculare; CA1, cornu ammonis 1; CA1so, CA1 stratum oriens; CA1sp, CA1 stratum pyramidale; CA1sr, CA1 stratum radiatum; CA1slm, CA1 stratum lacunosum-moleculare;

Table S1: Names of brain regions and subregions in heatmaps

The identification of 109 subregions and their order used in heatmaps, histograms and similarity matrices.